ANL-8119

ANL-8119

IRRADIATION BEHAVIOR OF UNENCAPSULATED EBR-II MARK-II DRIVER FUEL TO A MAXIMUM BURNUP OF 6 at. %

by

G. L. Hofman, W. N. Beck, R. V. Strain,
G. O. Hayner, and C. M. Walter

U of C-AUA-USERDA

ARGONNE NATIONAL LABORATORY, ARGONNE, ILLINOIS

Prepared for the U. S. ENERGY RESEARCH AND DEVELOPMENT ADMINISTRATION under Contract W-31-109-Eng-38

Printed in the United States of America
Available from
U. S. Energy Research and Development Administration
Technical Information Center
P. O. Box 62
Oak Ridge, Tennessee 37830
Price: Printed Copy $5.00

ANL-8119
LMFBR Fuels and Materials
Engineering and Development
(UC-79b)

ARGONNE NATIONAL LABORATORY
9700 South Cass Avenue
Argonne, Illinois 60439

IRRADIATION BEHAVIOR OF UNENCAPSULATED EBR-II MARK-II DRIVER FUEL TO A MAXIMUM BURNUP OF 6 at. %

by

G. L. Hofman, W. N. Beck, R. V. Strain,*
G. O. Hayner,** and C. M. Walter

EBR-II Project

February 1976

*Materials Science Division
**Argonne-West

TABLE OF CONTENTS

	Page
ABSTRACT	11
I. INTRODUCTION	11
II. ELEMENT DESIGN AND TEST CONDITIONS	13
A. Design of Unencapsulated Mark-II Driver Elements	13
B. Irradiation History	13
C. Irradiation Conditions	16
III. IRRADIATION PERFORMANCE	19
A. Fuel	19
B. Cladding	27
1. Overall External Appearance of Elements	28
2. Diameter Increase	28
3. Metallography	32
IV. CONCLUSIONS	40
APPENDIXES	
A. Physical Measurements	41
B. Metallography	59
1. Subassembly C-2201S; ~2 at. % Burnup	59
2. Subassembly C-2203S; ~3 at. % Burnup	64
3. Subassembly C-2234S; ~4 at. % Burnup	68
4. Subassembly C-2236S; ~6 at. % Burnup	74
ACKNOWLEDGMENTS	79
REFERENCES	80

LIST OF FIGURES

No.	Title	Page
1.	Design of Mark-II Driver Element	14
2.	Horizontal Section of Mark-II Driver Element	14
3.	Irradiation History of Unencapsulated Mark-II Fuel Elements	15
4.	Gamma-activity and Burnup Profiles along Mark-II Elements	17
5.	Comparison of Commonly Used and Actually Measured Burnup Profiles along Mark-II Elements and of the Resulting Average Cladding-midwall Temperatures Calculated from Them	17
6.	Temperature Distributions along Hottest Mark-II Element in Subassembly C-2236S	18
7.	Volume Increase of Mark-II Fuel Pins	19
8.	Typical Length Increase with Burnup of Mark-II Pins	20
9.	Axial Cross Section of Top of Irradiated Mark-II Fuel Pin	21
10.	Release of Generated Fission Gas from Mark-II Fuel as a Function of Burnup	21
11.	Plenum Pressure in Mark-II Elements at Operating Temperature	22
12.	Sodium and Cesium in Top Transverse Section of High-burnup Mark-II Element E-18 from Subassembly C-2236S	23
13.	Transverse Sections of High-burnup Mark-II Element E-18 from Subassembly C-2236S, Showing Presence of Sodium in Highly Porous Regions in the Fuel	24
14.	Radial Distribution of Porosity in Transverse Sections of Fuel of Element E-18	25
15.	Interaction Band in Fuel at Interface of Fuel and Type 304L Stainless Steel Cladding	26
16.	Neutron Radiographs Showing Liftoff of Mark-II Fuel Pins	26
17.	Axial Cross Section of Bottom of Mark-II Fuel Pin That Lifted Off	27
18.	Diameter Changes along 304L-clad Mark-II Elements at Three Burnup Levels	28
19.	Diameter Changes along 316-clad Mark-II Elements at Three Burnup Levels	29
20.	Peak Diameter Change and Swelling of Cladding of Mark-II Elements as a Function of Burnup	30

LIST OF FIGURES

No.	Title	Page
21.	Density Change of Type 304L Stainless Steel Mark-II Cladding at Four Burnup Levels	30
22.	Density Change of Type 316 Stainless Steel Mark-II Cladding at Four Burnup Levels	31
23.	Temperature Dependence of Swelling of Cladding Materials	31
24.	Length Increase due to Swelling of Mark-II Elements	32
25.	Diameter Profiles of 304L-clad Mark-II Element Measured 90° from Each Other Showing Ovality Caused by Interaction with Spacer Wires	33
26.	Schematic View of Mechanical Interaction of Spacer Wire and Cladding That Causes Cladding Ovality	33
27.	Diameter Profiles of 316-clad Mark-II Element Measured 90° from Each Other Showing Little Interaction with Spacer Wires	34
28.	Type 304L Stainless Steel Cladding from Mark-II Elements after Oxalic Acid Etch	35
29.	TEM Micrographs of Types 304L and 316 Stainless Steel Mark-II Cladding, Showing Voids and Precipitates	37
30.	Axial Microhardness Profile of Type 316 Stainless Steel Cladding of Mark-II Elements with 6 at. % Peak Burnup	38
31.	Width of Ferritic Zone at Mark-II Cladding Inner Surface as a Function of Time at Power Since Fuel/Cladding Contact: Core Midplane, T = 520-570°C	38
A.1.	General Loading Diagrams for the Mark-II Subassemblies	42
A.2.	Gamma-activity Scans of Element E-18, Subassembly C-2236S, at ~6 at. % Burnup	47
A.3.	Diameter Profiles of Elements E-24 and -33, from Subassembly C-2201S, at ~2 at. % Burnup	49
A.4.	Diameter Profiles of Elements E-24, -64, -33, and -73, from Subassembly C-2203S, at ~3 at. % Burnup	50
A.5.	Diameter Profiles of Elements E-64, -74, -1, and -28, from Subassembly C-2234S, at ~4 at. % Burnup	52
A.6.	Diameter Profiles of Elements E-19, -59, -18, -33, -68, and -67, from Subassembly C-2236S, at ~6 at. % Burnup	54
A.7.	Radial Microprobe Traces of Element E-18, from Subassembly C-2236S, at ~6 at. % Burnup	57

LIST OF FIGURES

No.	Title	Page
B.1.	Cross Section of Element E-24, Subassembly C-2201S: 1 in. from Bottom of Fuel; ~2 at. % Burnup	59
B.2.	Cross Section of Element E-24, Subassembly C-2201S: 7 in. from Bottom of Fuel; ~2 at. % Burnup	59
B.3.	Cross Section of Element E-24, Subassembly C-2201S: 14 in. from Bottom of Fuel; ~2 at. % Burnup	60
B.4.	Micrographs of Fuel of Element E-24, Subassembly C-2201S: 3 in. from Bottom of Fuel; ~2 at. % Burnup	60
B.5.	Micrographs of Fuel of Element E-24, Subassembly C-2201S: 7 in. from Bottom of Fuel; ~2 at. % Burnup	60
B.6.	Micrographs of Fuel of Element E-24, Subassembly C-2201S: 11 in. from Bottom of Fuel; ~2 at. % Burnup.	61
B.7.	Cross Section of Element E-33, Subassembly C-2201S: 1 in. from Bottom of Fuel; ~2 at. % Burnup	61
B.8.	Cross Section of Element E-33, Subassembly C-2201S: 7 in. from Bottom of Fuel; ~2 at. % Burnup	61
B.9.	Cross Section of Element E-33, Subassembly C-2201S: 14 in. from Bottom of Fuel; ~2 at. % Burnup	62
B.10.	Micrographs of Fuel of Element E-33, Subassembly C-2201S: 3 in. from Bottom of Fuel; ~2 at. % Burnup	62
B.11.	Micrographs of Fuel of Element E-33, Subassembly C-2201S: 7 in. from Bottom of Fuel; ~2 at. % Burnup	63
B.12.	Micrographs of Fuel of Element E-33, Subassembly C-2201S: 11 in. from Bottom of Fuel; ~2 at. % Burnup.	63
B.13.	Cladding of Elements E-24 and -33, Subassembly C-2201S: 7 in. from Bottom of Fuel; ~2 at. % Burnup	63
B.14.	Cross Sections of Element E-46, Subassembly C-2203S, at 1/2, 3, $6\frac{3}{4}$, and 10 in. from Bottom of Fuel; ~3 at. % Burnup	64
B.15.	Cross Sections of Element E-73, Subassembly C-2203S, at 1/2, 3, $6\frac{3}{4}$, and 10 in. from Bottom of Fuel; ~3 at. % Burnup	65
B.16.	Microstructure of Fuel at Various Elevations near the Centerline of Fuel Pin in Element E-46, Subassembly C-2203S; ~3 at. % Burnup.	66
B.17.	Microstructure at Various Elevations of Fuel/Cladding Interface of Element E-46, Subassembly C-2203S; ~3 at. % Burnup	66

LIST OF FIGURES

No.	Title	Page
B.18.	Microstructure of Fuel at Fuel Centerline, Half the Fuel Radius, and at Fuel/Cladding Interface for Sample $6\frac{3}{4}$ in. from Bottom of Fuel of Element E-46, Subassembly C-2203S; ~3 at. % Burnup.	66
B.19.	Microstructure of Fuel at Fuel Centerline and Fuel/Cladding Interface for Sample 10 in. from Bottom of Fuel of Element E-73, Subassembly C-2203S; ~3 at. % Burnup	67
B.20.	Microstructure of Type 316 Stainless Steel Cladding from High-fluence Region of Element E-46, Subassembly C-2203S; ~3 at. % Burnup.	67
B.21.	Micrographs of Typical Areas at Outer Surface of Cladding of Element E-46, Subassembly C-2203S, 15 and 17 in. from Bottom of Fuel; ~3 at. % Burnup.	68
B.22.	Cross Sections of Element E-1, Subassembly C-2234S, at 1/2, 8, and 14 in. above Bottom of Fuel; ~4 at. % Burnup.	68
B.23.	Cross Sections of Element E-28, Subassembly C-2234S, at 1/2, 8, and 14 in. above Bottom of Fuel; ~4 at. % Burnup.	69
B.24.	Cross Sections of Element E-64, Subassembly C-2234S, at 1/2, 8, and 14 in. above Bottom of Fuel; ~4 at. % Burnup.	69
B.25.	Cross Sections of Element E-74, Subassembly C-2234S, at 1/2, 8, and 14 in. above Bottom of Fuel; ~4 at. % Burnup.	69
B.26.	Typical Areas of Fuel/Cladding Interface at 1/2 and 8 in. above Bottom of Fuel in Element E-1, Subassembly C-2234S; ~4 at. % Burnup.	70
B.27.	Typical Areas of Fuel/Cladding Interface at 1/2, 8, and 14 in. above Bottom of Fuel in Element E-28, Subassembly C-2234S; ~4 at. % Burnup.	70
B.28.	Typical Areas of Fuel/Cladding Interface at 1/2, 8, and 14 in. above Bottom of Fuel in Element E-64, Subassembly C-2234S; ~4 at. % Burnup.	70
B.29.	Typical Areas of Fuel/Cladding Interface at 1/2, 8, and 14 in. above Bottom of Fuel in Element E-74, Subassembly C-2234S; ~4 at. % Burnup.	71
B.30.	Typical Areas near Centerline of Fuel Pin at 1/2, 8, and 14 in. above Bottom of Pin in Element E-1, Subassembly C-2234S; ~4 at. % Burnup.	71

LIST OF FIGURES

No.	Title	Page
B.31.	Typical Areas near Centerline of Fuel Pin at 1/2, 8, and 14 in. above Bottom of Pin in Element E-28, Subassembly C-2234S; ~4 at. % Burnup.	71
B.32.	Typical Areas near Centerline of Fuel Pin at 1/2, 8, and 14 in. above Bottom of Pin in Element E-64, Subassembly C-2234S; ~4 at. % Burnup.	72
B.33.	Typical Areas at Center of the Fuel Pin at 1/2, 8, and 14 in. above Bottom of Pin in Element E-74, Subassembly C-2234S; ~4 at. % Burnup.	72
B.34.	Typical Cross Sections of Cladding at 1/2, 8, and 14 in. above Bottom of Fuel in Element E-1, Subassembly C-2234S; ~4 at. % Burnup.	72
B.35.	Typical Cross Sections of Cladding at 1/2, 8, and 14 in. above Bottom of Fuel in Element E-28, Subassembly C-2234S; ~4 at. % Burnup.	73
B.36.	Typical Cross Sections of Cladding at 1/2, 8, and 14 in. above Bottom of Fuel in Element E-64, Subassembly C-2234S; ~4 at. % Burnup.	73
B.37.	Typical Cross Sections of Cladding at 1/2, 8, and 14 in. above Bottom of Fuel in Element E-74, Subassembly C-2234S; ~4 at. % Burnup.	73
B.38.	Cross Section of Element E-18, Subassembly C-2236S: 1 in. from Bottom of Fuel; ~6 at. % Burnup	74
B.39.	Cross Section of Element E-18, Subassembly C-2236S: 7 in. from Bottom of Fuel; ~6 at. % Burnup	74
B.40.	Cross Section of Element E-18, Subassembly C-2236S: 14 in. from Bottom of Fuel; ~6 at. % Burnup	74
B.41.	Microstructure at OD of Fuel in Element E-18, Subassembly C-2236S: 1 in. from Bottom of Fuel; ~6 at. % Burnup	75
B.42.	Microstructure at Center of Fuel in Element E-18, Subassembly C-2236S: 1 in. from Bottom of Fuel; ~6 at. % Burnup	75
B.43.	Microstructure at OD of Fuel in Element E-18, Subassembly C-2236S: 7 in. from Bottom of Fuel; ~6 at. % Burnup	76
B.44.	Microstructure at Center of Fuel and at Half the Fuel Radius in Element E-18, Subassembly C-2236S: 7 in. from Bottom of Fuel; ~6 at. % Burnup	76

LIST OF FIGURES

No.	Title	Page
B.45.	Micrographs at Cladding ID of Element E-18, Subassembly C-2236S: 7 in. from Bottom of Fuel; ~ 6 at. % Burnup.	77
B.46.	Microstructure at OD of Fuel in Element E-18, Subassembly C-2236S: 14 in. from Bottom of Fuel; ~6 at. % Burnup	77
B.47.	Microstructure at Center of Fuel and at Half the Fuel Radius in Element E-18, Subassembly C-2236S: 14 in. from Bottom of Fuel; ~6 at. % Burnup	77
B.48.	Cross Sections at Bottom, Midplane, and Top of Element E-24, Subassembly C-2236S; ~6 at. % Burnup	78
B.49.	Microstructure of Cladding of Element E-24, Subassembly C-2236S, at Bottom, Midplane, and Top of Fuel; ~6 at. % Burnup.	78

LIST OF TABLES

No.	Title	Page
I.	Design Parameters for Mark-II Fuel Element	13
II.	Maximum Normal Operating Conditions for Unencapsulated Mark-II Elements	16
III.	Reactivity Changes due to Liftoff of Mark II Fuel	27
A.1.	Composition of Mark-II Cladding Material	43
A.2.	Specified Fuel Composition	43
A.3.	Summary of Results of Fission-gas Analyses	44
A.4.	Summary of Burnups Obtained by Chemical Analysis	44
A.5.	Summary of Cladding Immersion-density Measurements	45

IRRADIATION BEHAVIOR OF UNENCAPSULATED EBR-II MARK-II DRIVER FUEL TO A MAXIMUM BURNUP OF 6 at. %

by

G. L. Hofman, W. N. Beck, R. V. Strain,
G. O. Hayner, and C. M. Walter

ABSTRACT

An advanced driver-fuel design (Mark II) for Experimental Breeder Reactor No. II (EBR-II) has been tested in EBR-II to a peak burnup of 6 at. %. All the approximately 550 elements used in this test contained as fuel an alloy of metallic uranium, enriched to 64% in ^{235}U, and 5 wt % of stable metallic fission products (called "fissium"). About half the elements were clad with annealed Type 304L stainless steel, and half with annealed Type 316 stainless steel. All were unencapsulated. The irradiation conditions for the test were similar to those envisioned for production driver elements. No cladding failures or abnormal behavior of the elements were experienced, and the design, in general, behaved as predicted. The elements using Type 316 stainless steel as cladding were judged superior based on greater dimensional stability and lower chemical interaction of fuel and cladding.

I. INTRODUCTION

The design of the EBR-II Mark-II driver fuel has evolved over the past several years, and the experimental-irradiation program for this fuel has reflected this evolution. The program began with irradiation of encapsulated elements in December 1967 and is still continuing. These encapsulated elements represent a fairly large number of design variables, viz., element length, fuel enrichment, type and location of fuel-pin restrainer, and bond-sodium level above the fuel pin. The encapsulated elements were clad with either annealed Type 304L stainless steel or annealed Type 316 stainless steel.

In June 1969, experimental irradiation of six subassemblies, each containing 91 unencapsulated Mark-II driver elements, began. The length, enrichment, sodium level, and type of restrainer were the same for all these elements, but the restrainer locations were different. The discovery that the irradiation-induced swelling characteristics of Type 316 stainless steel were better than those of Type 304L led to the decision to clad about half the elements with annealed Type 316. This experiment was terminated when all six subassemblies had reached a maximum burnup of about 6 at. %.

Irradiation of the approximately 550 unencapsulated Mark-II driver elements is the principal subject of this report. However, some results from the irradiation of encapsulated Mark-II elements are included where they may help clarify trends and facilitate interpretation of the irradiation behavior of the unencapsulated elements. The report is organized into two main sections: (1) a description of the unencapsulated Mark-II driver fuel, its irradiation history, and its irradiation conditions; (2) a discussion of the irradiation behavior of the element, fuel, and cladding. A final brief section summarizes the conclusions reached on the basis of the experimental results.

II. ELEMENT DESIGN AND TEST CONDITIONS

A. Design of Unencapsulated Mark-II Driver Elements

The Mark-II driver elements were designed to achieve a higher burnup than the currently used Mark-IA driver elements. The capability for high burnup was accomplished by providing for more fuel swelling and a higher plenum inventory of fission-product gas. The radial dimension of the Mark-II element is such that the fuel can swell to 133% of its original volume before it contacts the cladding. At that point, the pores of the fuel interlink, and the fission-product gases vent from the fuel into the plenum above the bond sodium.[1] The larger plenum keeps the pressure of this accumulated fission-product gas low; this, combined with a thicker cladding wall, reduces cladding stresses.

Table I lists the design data, and Figs. 1 and 2 show the element and a cross section of it. Details of the cladding and fuel material are given in Tables A.1 and A.2 of Appendix A.

TABLE I. Design Parameters for Mark-II Fuel Element

Fuel	U-5 wt % Fs[a]
Fuel enrichment, at. % ^{235}U	64.0
Fuel-pin weight, g	54.5
Fuel-pin length, in.	14.2
Fuel-pin diameter, in.	0.130
Fuel/Cladding bond	Sodium
Fuel/Cladding radial gap, in.	0.010
Cladding wall thickness, in.	0.012
Cladding outside diameter, in.	0.174
Element length, in.	26
Restrainer height above fuel, in.	0.5, 1.0, no restrainer
Sodium level above fuel, in.	1.50
Plenum volume, $in.^3$	0.170
Plenum gas	Argon
Cladding material	Annealed 316 SS and annealed 304L SS (Welded Tubing)
Spacer-wire diameter, in.	0.049
Spacer-wire material	Annealed 304L SS

[a] Fs stands for fissium, an equilibrium concentration of fission-product elements left by the pyrometallurgical reprocessing cycle designed for EBR-II. It consists of molybdenum, ruthenium, rhodium, palladium, zirconium, niobium, and technetium in relatively fixed proportions. (See Table A.2, Appendix A.)

B. Irradiation History

Figure 3 charts the irradiation history of the unencapsulated Mark-II elements. The first three subassemblies (C-2201S, -2203S, and -2205S) were inserted at the start of reactor run 36, and the remaining three during reactor run 38. All six subassemblies started their irradiation in row-3 positions. With run 46, the reactor power was increased from 50 to 62.5 MWt, and all six subassemblies were moved to a row-5 position to keep them at a flux level

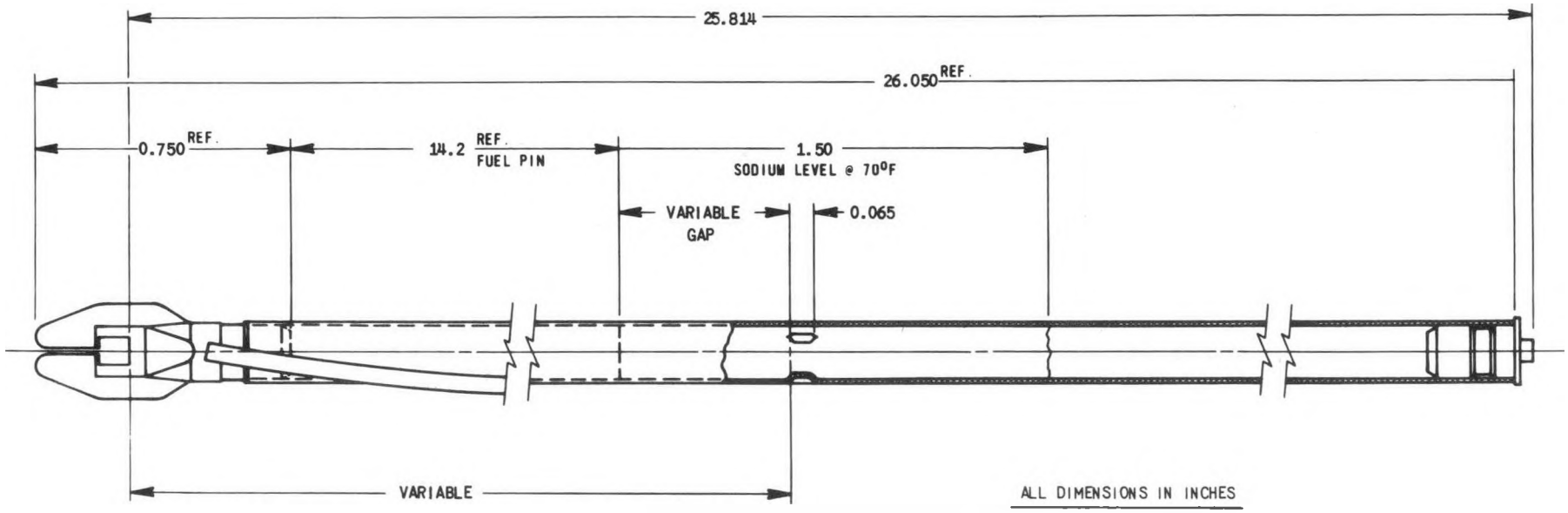

Fig. 1. Design of Mark-II Driver Element. ANL Neg. No. 103-Q5840 Revised.

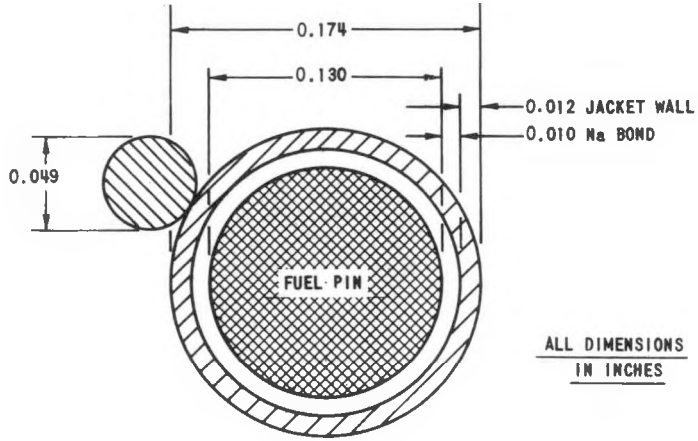

Fig. 2

Horizontal Section of Mark-II Driver Element.
ANL Neg. No. 103-Q5841 Revised.

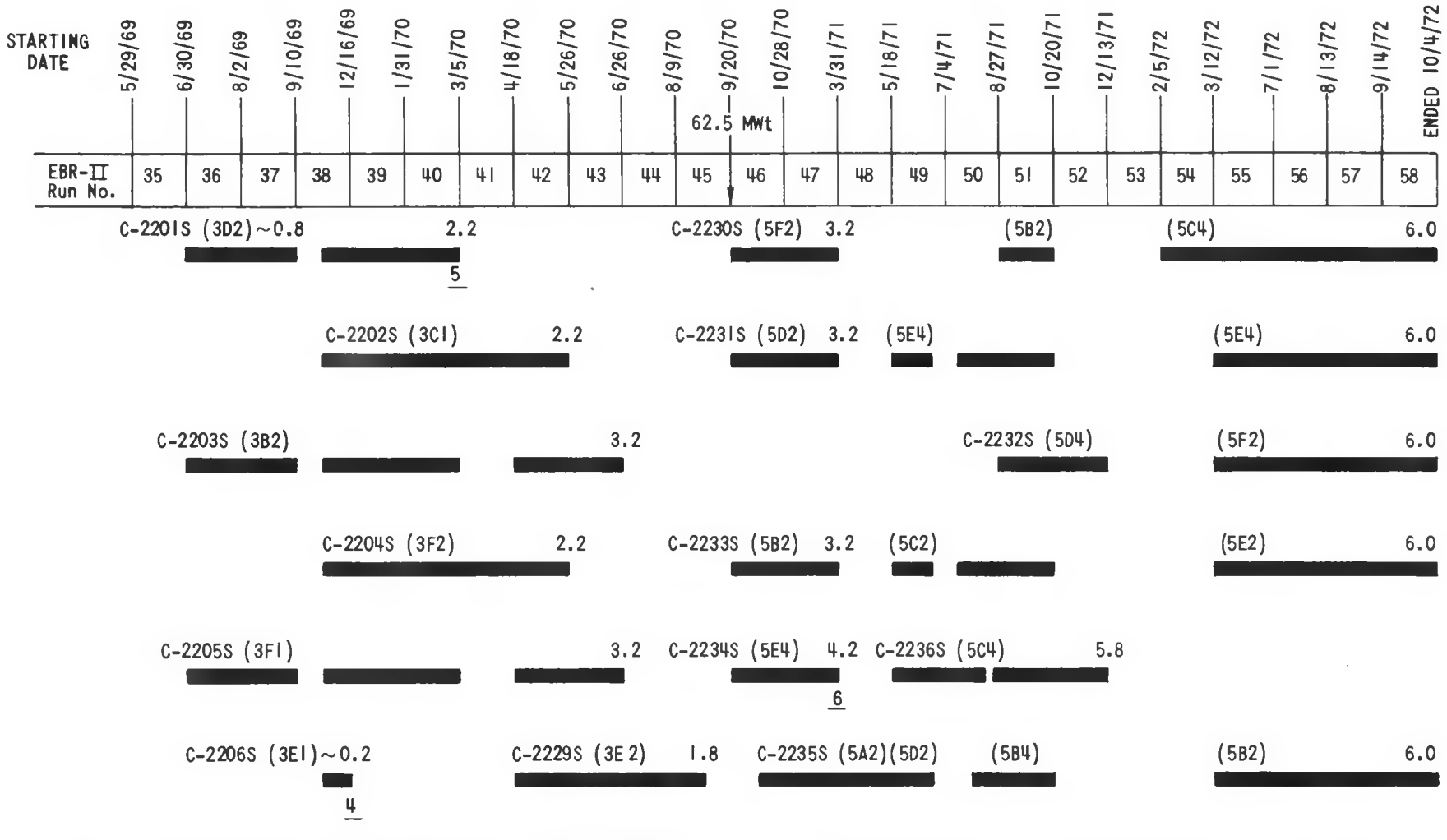

[a]Legend:

-- In Reactor

C-2201S -- Subassembly No.

(3D2) -- Position in Reactor

2.2 -- Maximum Burnup, at. %

5 -- Number of Elements Replaced Upon Examination of Subassembly

Fig. 3. Irradiation History of Unencapsulated Mark-II Fuel Elements

equivalent to that in row 3 before the power change. This move required reconstitution of the subassemblies to keep the element temperatures close to what they were before the change in power. When a subassembly is reconstituted (i.e., equipped with new subassembly hardware), it is given a new number. A subassembly is always reconstituted after an interim examination.

Interim examinations were performed on the elements at several burnup levels, as follows:

Subassembly No.	Maximum Burnup, at. %	At End of Run
C-2206S	~0.2	38
C-2201S	2.2	40
C-2203S	3.2	43
C-2234S	4.2	47
C-2236S	5.8	52

C. Irradiation Conditions

Table II gives the operating conditions for this experiment. These conditions are representative for all but the outermost row of the element cluster; that row operates at a slightly lower temperature. Figures 4-6 give more-detailed information in the form of axial distributions. Figure 4 shows a normalized axial burnup profile, obtained from the results of burnup analyses tabulated in Table A.4 of Appendix A, as well as axial gamma-activity profiles for radioactive fission products in the fuel and activation products in the cladding. The burnup profile agrees well with the gamma scans for the fission products. We conclude, therefore, that such scans can be used to obtain axial burnup profiles, provided that a chemical analysis for burnup is also made somewhere along the element. The burnup profile also coincides with the power-production profile and should be used for temperature calculations. Figure 5 compares the results of HECTIC[2] calculations for cladding-midwall temperature based on the burnup profile from this experiment and on the widely used profile recommended by the EBR-II Project. The temperature profiles do not differ significantly from each other. Figure 6 shows in more detail the HECTIC-calculated thermal conditions along a selected element.

TABLE II. Maximum Normal Operating Conditions for Unencapsulated Mark-II Elements

Flow rate through subassembly, gpm	87
Maximum coolant temperature, °F	1020
Maximum cladding temperature, °F	1075
Maximum temperature at fuel center, °F	1250
Peak element power, kW/ft avg	8
Peak ^{235}U fission rate, fissions/g-sec	0.967×10^{13}
Peak neutron-flux density ($E > 0.1$ MeV), 1/sec-cm^2	2.0×10^{15}

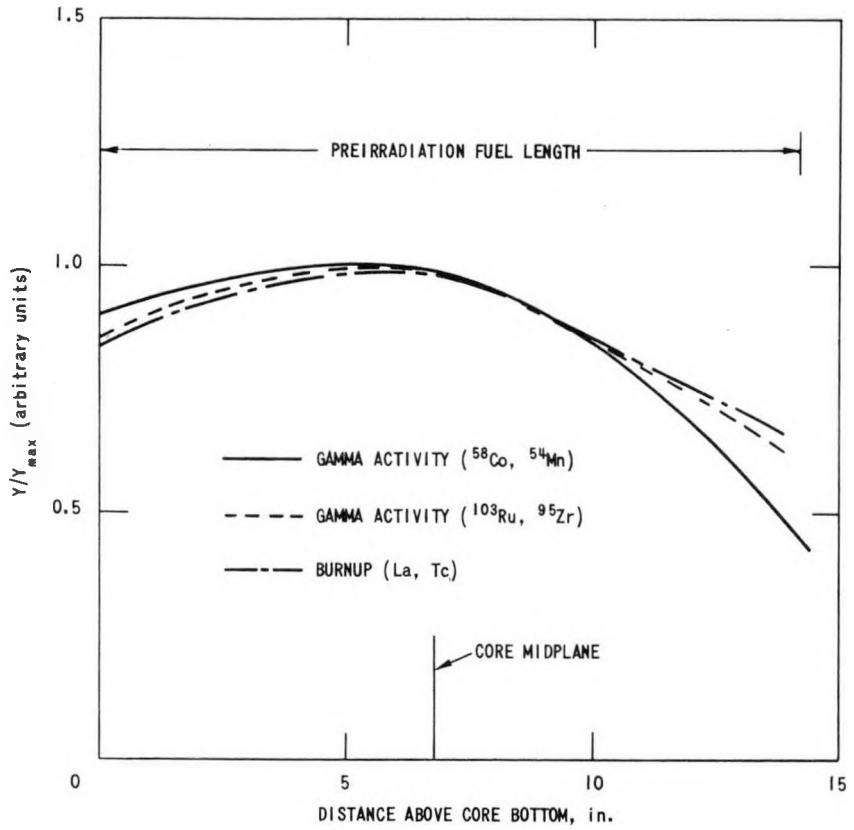

Fig. 4. Gamma-activity and Burnup Profiles along Mark-II Elements

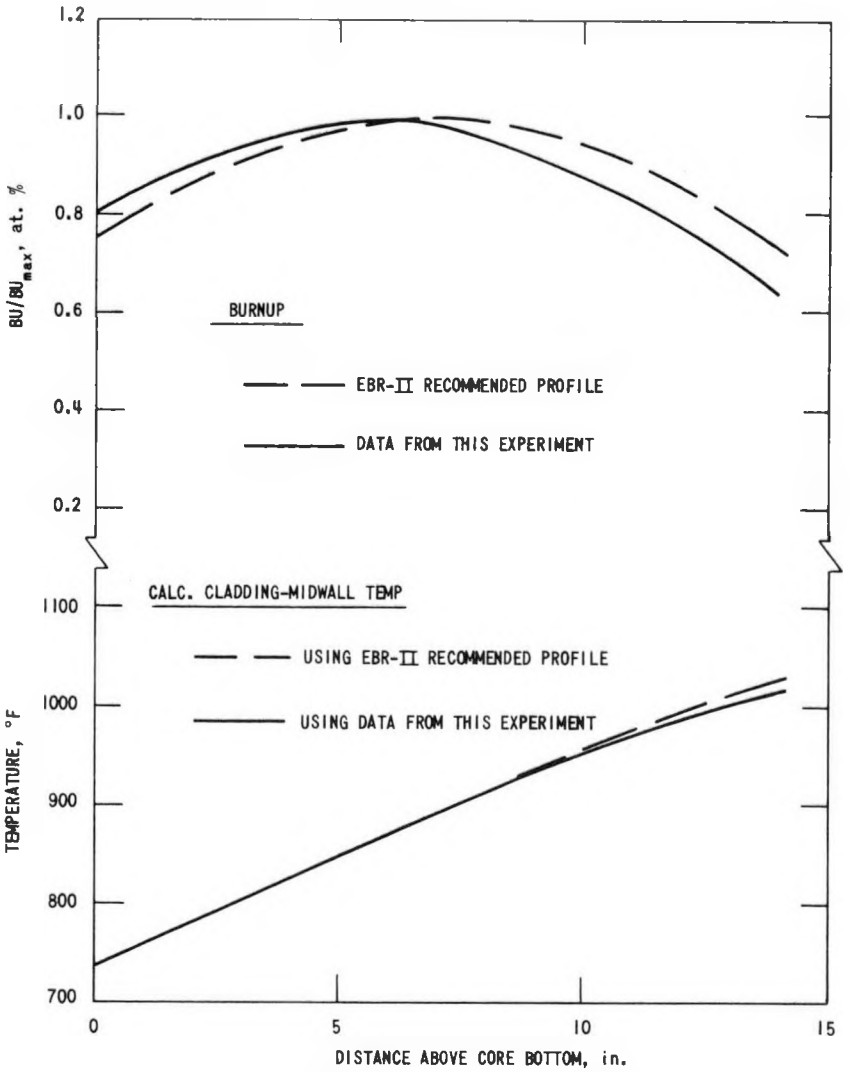

Fig. 5. Comparison of Commonly Used and Actually Measured Burnup Profiles along Mark-II Elements (top) and of the Resulting Average Cladding-midwall Temperatures Calculated from Them

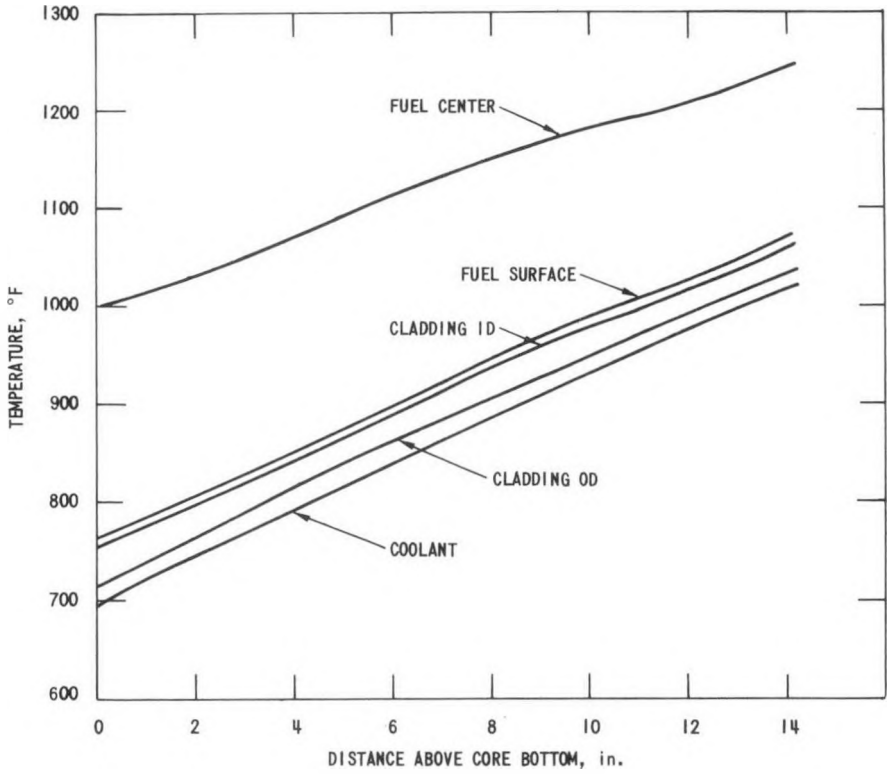

Fig. 6. Temperature Distributions along Hottest Mark-II Element in Subassembly C-2236S

The flux-density profile, which is used to correlate such phenomena as irradiation-induced swelling and creep, is also different from that recommended by the EBR-II Project. It seems that the higher energy part of the neutron spectrum is affected most, as evidenced by the more pronounced skewness (see Fig. 4) of the gamma-activity profile of the two detectors with high-energy thresholds in the cladding: $^{58}Mn(n,\gamma)^{58}Co$ and $^{54}Fe(n,\gamma)^{54}Mn$. We believe that the effect on the profiles is due to the difference between the material densities below the core and above the core. Mark-II elements have a large (~10-in.-long) gas plenum above the fuel; below the fuel, stainless steel and coolant sodium are the primary materials.

III. IRRADIATION PERFORMANCE

A. Fuel

Fission-induced swelling of U-5% Fs fuel at EBR-II operating temperatures proceeds initially at a constant, moderate rate of about 4% volume increase per at. % burnup. The swelling is characterized by the formation of (a) relatively small, virtually incompressible tears and bubbles that contain gaseous fission products and (b) solid fission products that are either in solution or in the various precipitated uranium-fissium phases.

At about 1 at. % burnup, the fuel exhibits a rapid acceleration in swelling rate.[3] As the fuel approaches a 33% expansion in volume, the pores become interconnected, and the fuel pin begins to release fission gas. This rapid swelling, termed breakaway swelling, would persist to high burnup values if it were not for the restraining presence of the element jacket (see Fig. 7). By 3 at. % burnup, the swelling rate begins to decrease as the fuel pin contacts the cladding; swelling beyond this burnup is controlled by the change in cladding inside diameter. Actually, some fuel pins exhibit a very low swelling rate at their lower ends, where pin temperature is the lowest, so the lower section of a particular fuel pin may not be in contact with the cladding at peak burnups as high as 4 at. % (see Appendix B). The bottom inch or so of production-type fuel pins has been found to have a grain size different from that in the rest of the pin and also to have some texture and/or residual stress

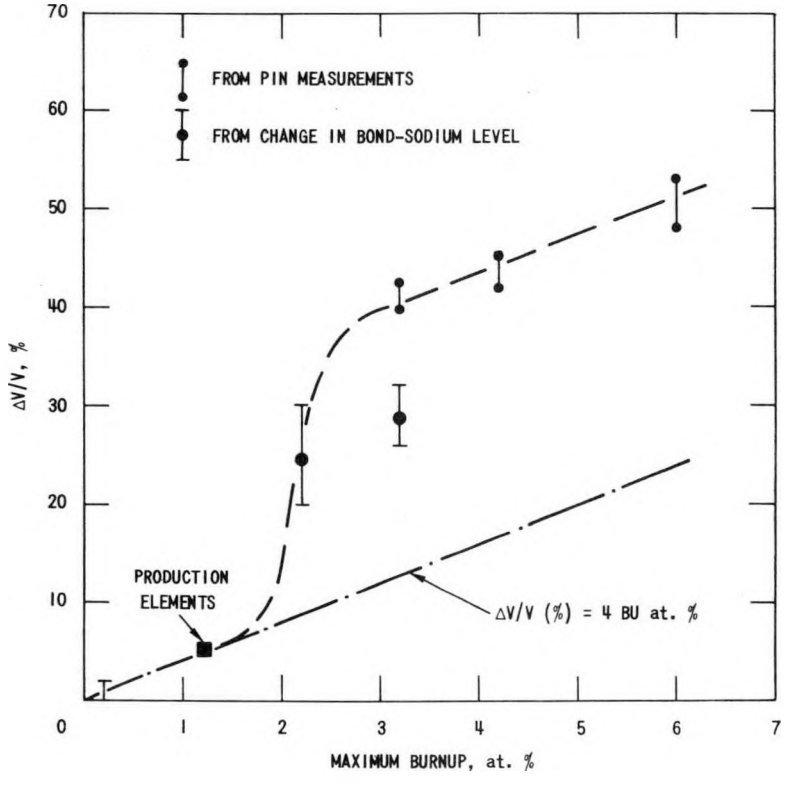

Fig. 7. Volume Increase of Mark-II Fuel Pins

as a result of the casting and bonding treatment.[4] This nonuniformity in the fuel structure contributes somewhat to a reduction in swelling, but the lower temperatures are probably the major factor.

That breakaway swelling is arrested after fuel/cladding contact is made and is not translated into accelerated axial growth indicates that the fuel pin has considerable mechanical strength and is not a viscous, easy-flowing slug. In this irradiation experiment, initial fuel swelling was determined by measuring the increase in bond-sodium level above the fuel pin (see Fig. 7). Swelling cannot be determined that way, however, after the fuel pores become interconnected, because the sodium then penetrates the fuel pin, thereby causing a noticeable drop in the sodium level. (Observations of sodium penetration are described later in this section.) At the higher swelling values, the best methods to measure fuel swelling are metallography and eddy-current measurements of bond level to determine the extent of fuel/cladding contact.

Figure 8 shows the typical axial growth with burnup of Mark-II fuel pins. As indicated before, the fuel pin seems to possess sufficient mechanical strength to restrain breakaway swelling in the axial direction after fuel/cladding contact has been established. The axial growth beyond 3 at. % burnup is primarily due to increased porosity in the extreme top section of the fuel pin (see Fig. 9). Axial growth proceeds linearly with burnup until the fuel meets the restrainer, when the growth is greatly slowed.

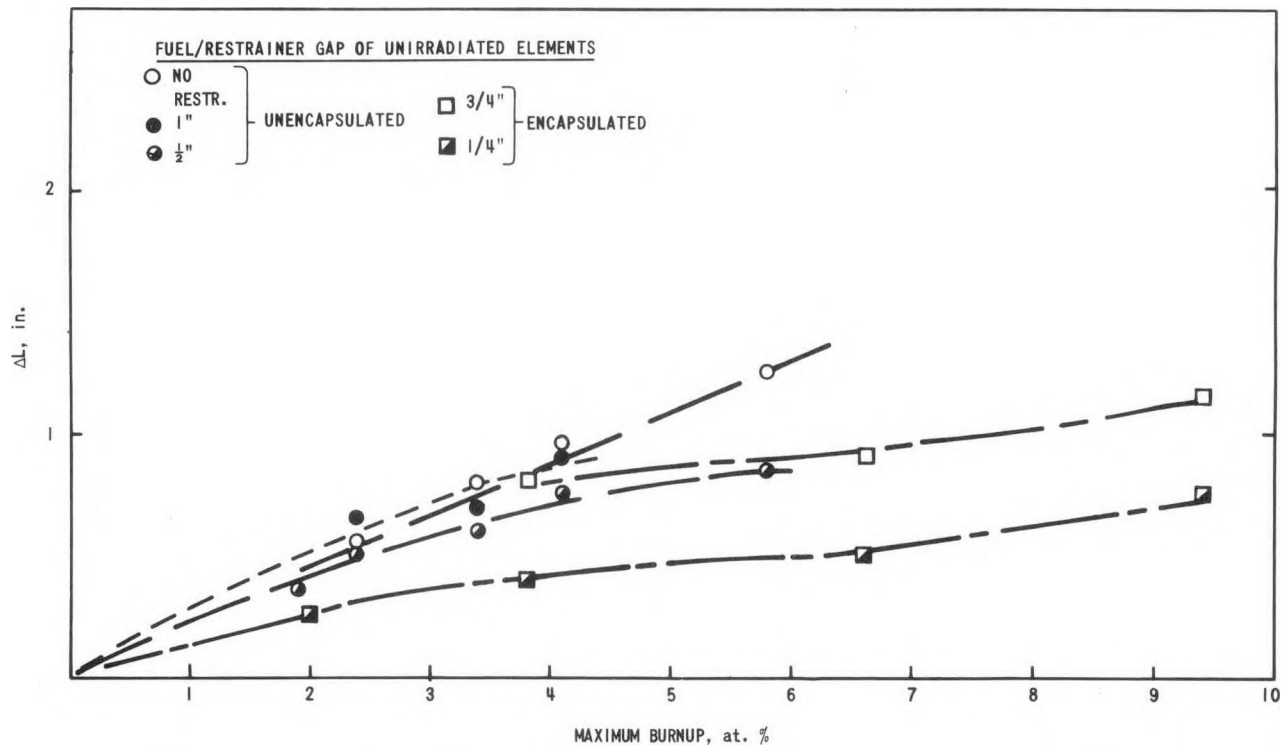

Fig. 8. Typical Length Increase with Burnup of Mark-II Pins. ANL Neg. No. 103-Q5844.

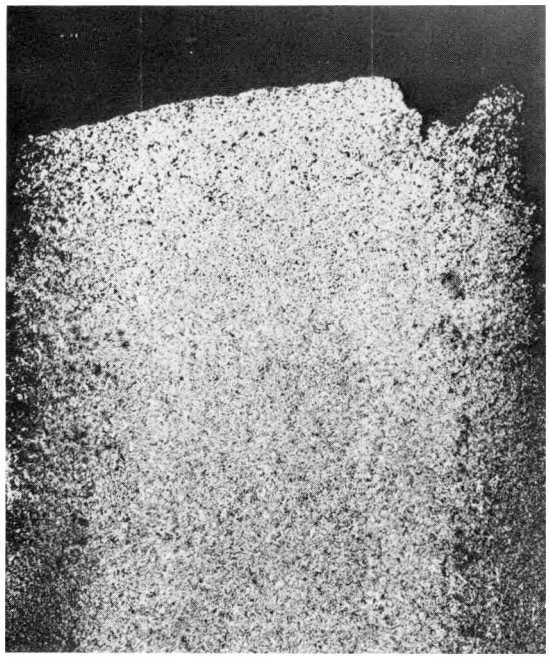

Fig. 9. Axial Cross Section of Top of Irradiated Mark-II Fuel Pin. Mag. 18X. Neg. No. MSD-163605.

The analyses of the fission gas collected from punctured element plenums are summarized in Table A.3 (Appendix A). These data and calculated fission-yield data for gaseous fission products were used to determine the fraction of fission gas released from the fuel as a function of burnup. Figure 10 is a plot of this relationship. It shows that, before the fuel pores become interconnected (at about 2 at. % burnup), fission-gas release is negligible. (Figure 7 shows this interconnecting to begin as fuel-volume expansion approaches 33%.)

As part of the plenum-gas sampling, the plenum pressures are measured. The data points in Fig. 11 show these pressure data, corrected to operating temperature, for unencapsulated and encapsulated Mark-II elements. (The calculated coolant temperature at the top of the fuel pin is taken as the plenum temperature.) The measured plenum pressures compare well with the pressures calculated with the BEMOD code[5] and plotted as lines in Fig. 11.

The question of whether and to what extent bond sodium could penetrate the substantially interconnected pores in high-burnup Mark-II fuel arose during the examination of the unencapsulated Mark-II driver elements at 6 at. % peak burnup. As mentioned before, at burnup levels exceeding 3 at. %, the fuel in Mark-II elements is almost entirely in contact with the cladding. Consequently, the bond sodium initially present in the annulus between the fuel pin and the cladding would be expected to be forced into the plenum of the element. In all, about 1.40 cm^3 of sodium should be present in the plenums of the high-burnup elements. Neutron radiographs of those elements, however, indicated about 0.25 cm^3 less than that amount in the

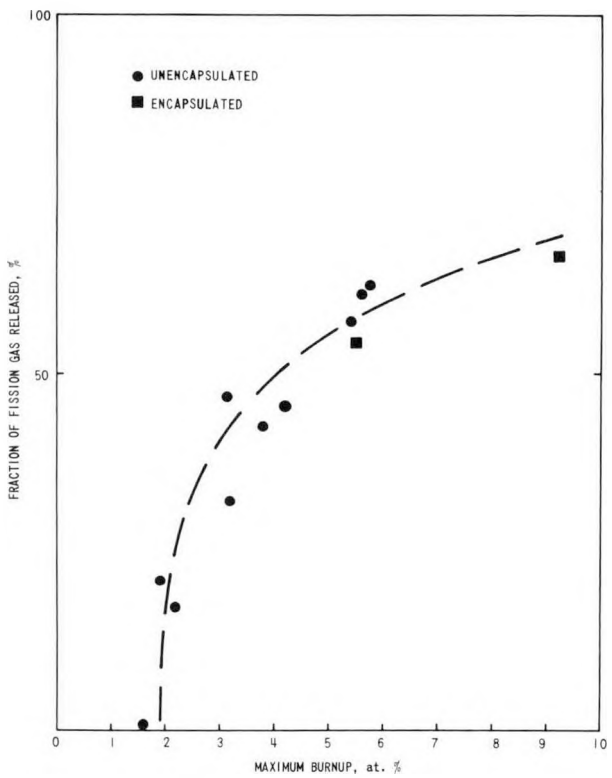

Fig. 10. Release of Generated Fission Gas from Mark-II Fuel as a Function of Burnup. ANL Neg. No. 103-Q5847.

plenums. Apparently, about 16% of the bond sodium seemed to reside in the fuel pores. The pore volume at 6 at. % burnup is about 1.25 cm^3; thus, on the average, the pores were about one-fifth filled with sodium.

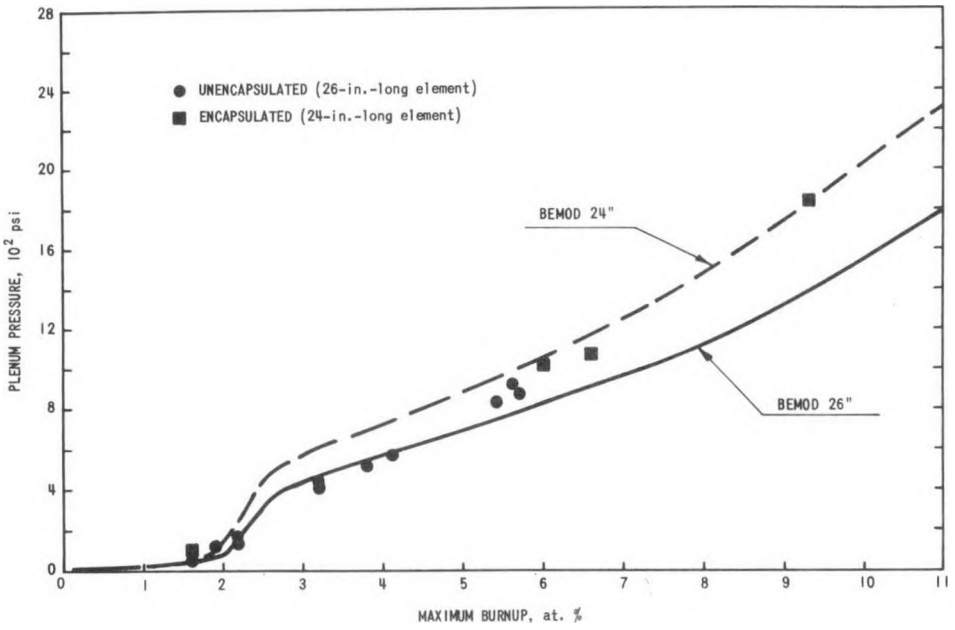

Fig. 11. Plenum Pressure in Mark-II Elements at Operating Temperature. ANL Neg. No. 103-Q5848.

A simple test was performed to determine how far down the sodium penetrated the fuel. Cuts were made at intervals through the cladding wall of one of the elements with 6 at. % burnup. The cuts were made at 1-in. intervals starting at the bottom of the element. After each cut was made, the element was heated to 900°F for 1 hr. No sign of sodium was found until a cut at 4 in. above the bottom of the element was made. A large amount of sodium was expelled through this cut. It was concluded that, although sodium may penetrate to the bottom of the fuel pin in the axial center region of the pin, it does not extend radially to the cladding in the lower 4 in. of the pin.

Subsequent metallography and electron-microprobe analysis substantiate this conclusion, as shown by Fig. 12. The presence of sodium in the large (interconnected) pores in the fuel is clearly revealed. Cesium, a fission product, seems to concentrate in the sodium present in these large pores. Figure 13, consisting of oblique exposures taken of transverse metallographic sections after a small amount of oxidizing atmosphere had been admitted to the metallograph, shows the distribution of sodium (the black areas on the cross sections of Fig. 12) and cesium. This distribution coincides with the nature of the porosity. Quantitative metallography shows the sodium-containing areas to have a porosity exceeding 33% (see Fig. 14). It is at this porosity value that the pores become largely interconnected. (The porosities as shown in Fig. 14 are somewhat higher than they actually are, because the interaction of sodium with the cell atmosphere makes voids appear slightly larger.)

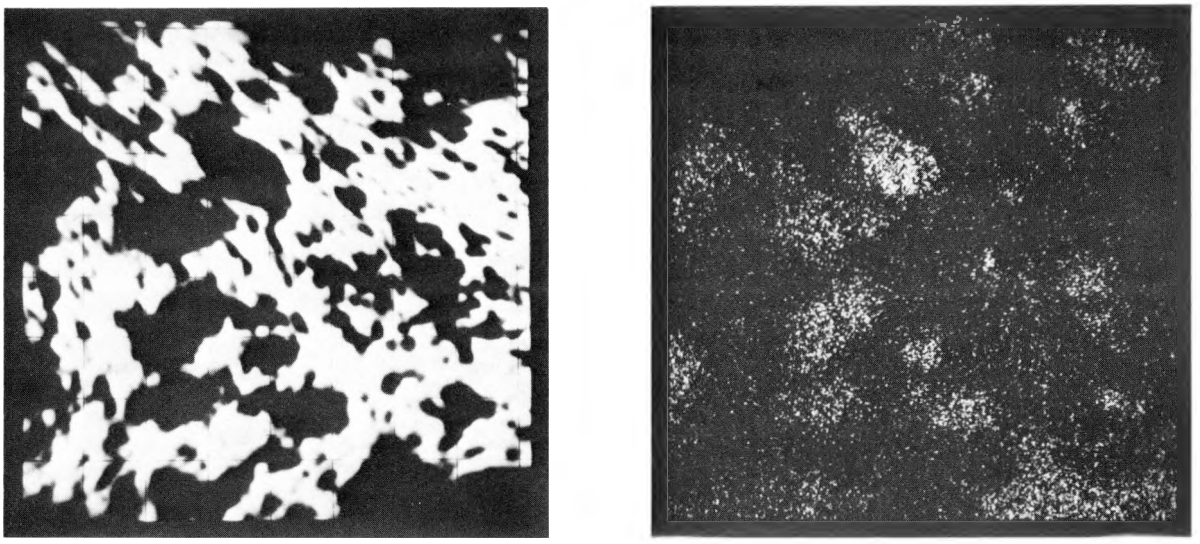

a) Specimen current and cesium X-ray image of an area near the cladding illustrating that cesium is concentrated in the larger voids.

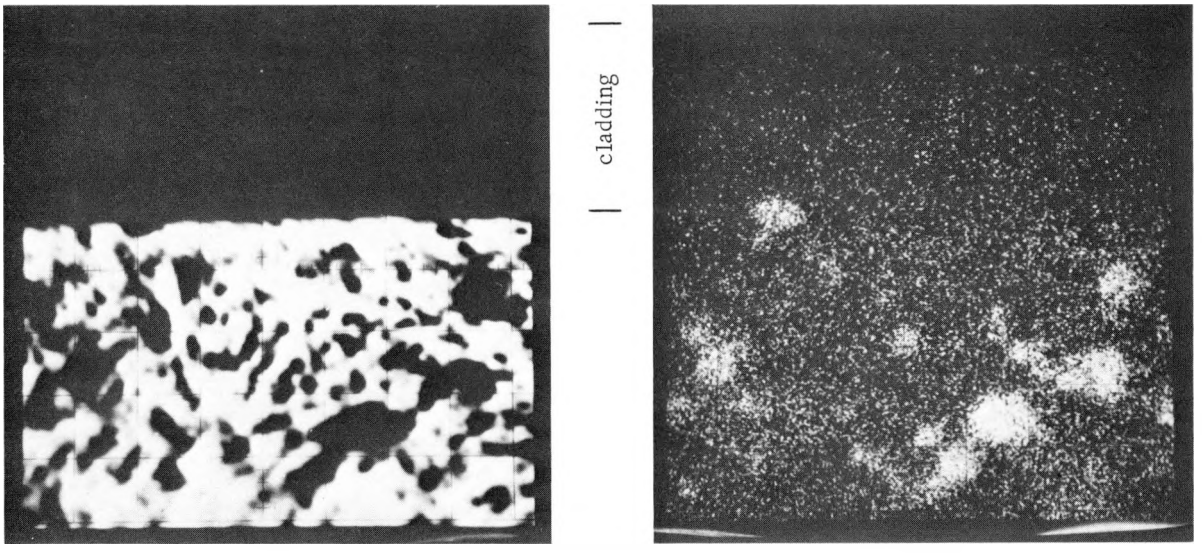

b) Specimen current and sodium X-ray image of the fuel-cladding interface illustrating that sodium is present in the larger voids.

Fig. 12. Sodium and Cesium in Top Transverse Section of High-burnup Mark-II Element E-18 from Subassembly C-2236S. Neg. No. MSD-163612.

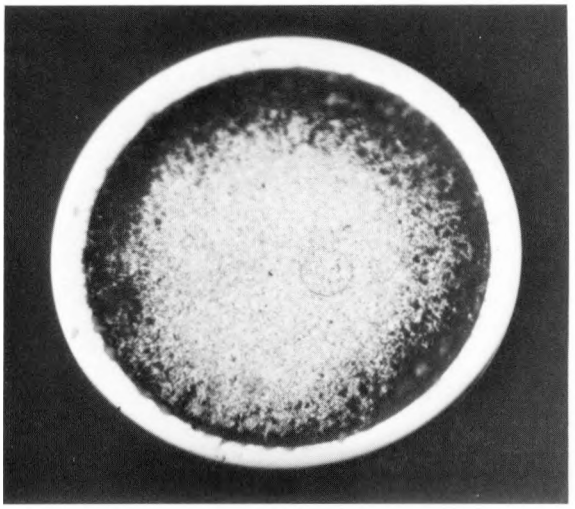

TOP OF PIN

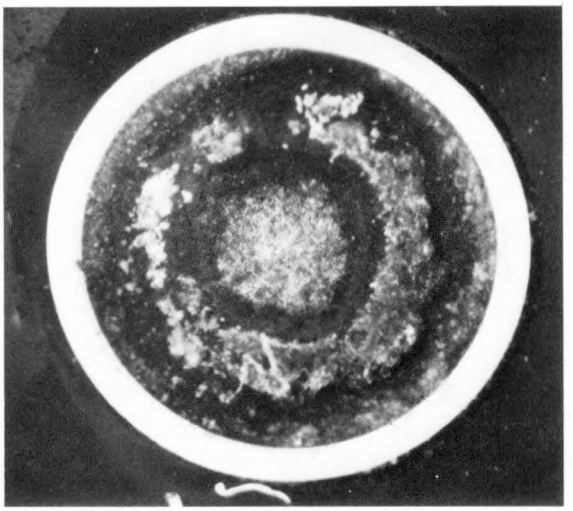

CORE MIDPLANE

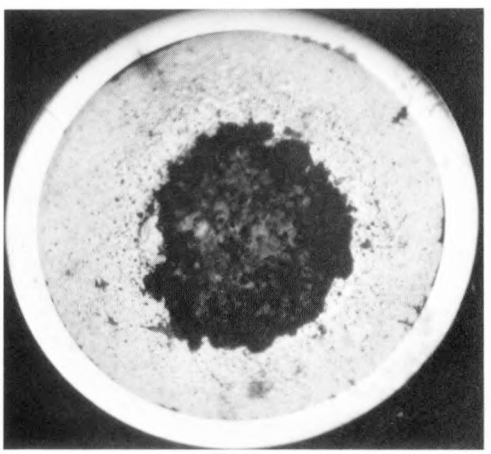

BOTTOM OF PIN

Fig. 13. Transverse Sections of High-burnup Mark-II Element E-18 from Subassembly C-2236S, Showing Presence of Sodium (Dark areas) in Highly Porous Regions in the Fuel

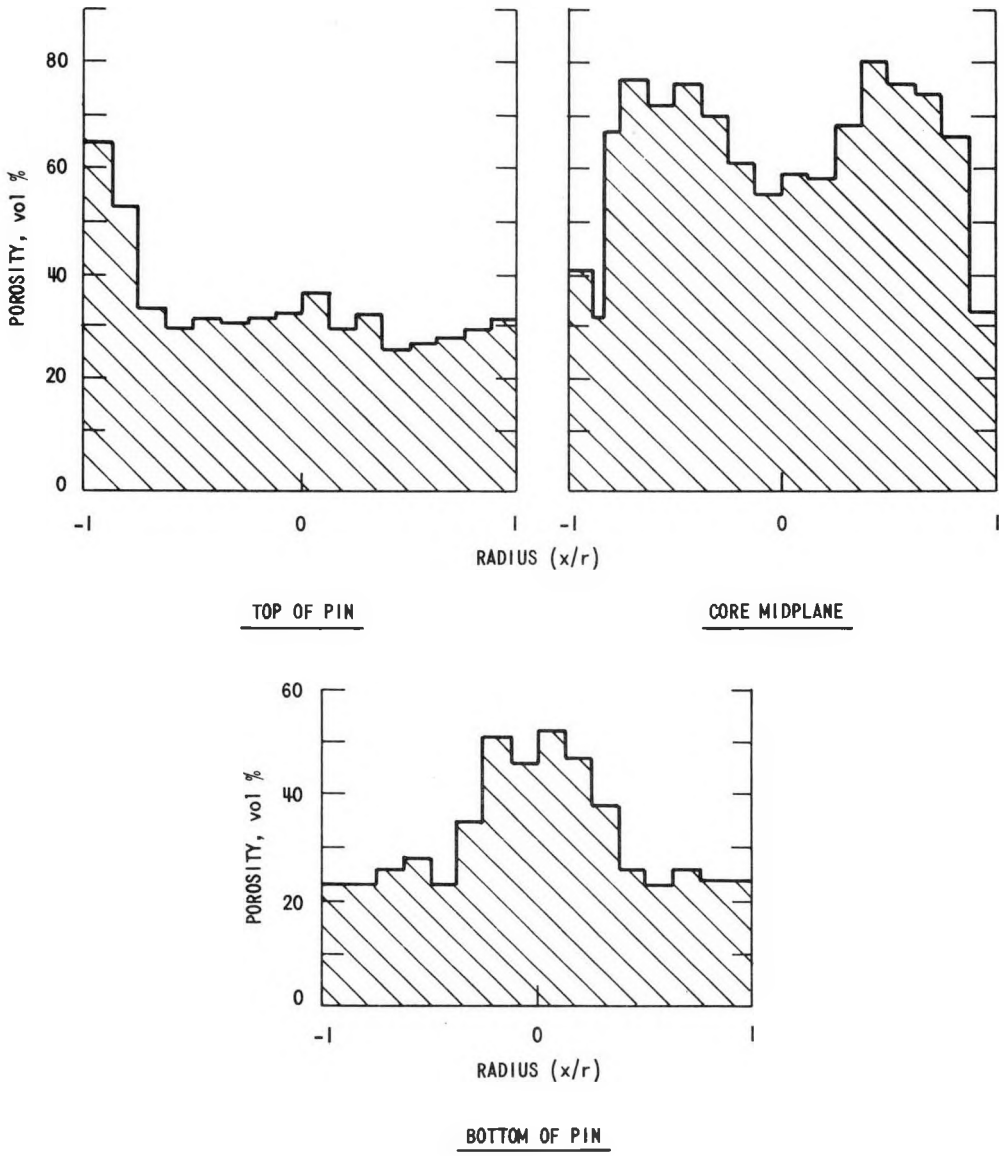

Fig. 14. Radial Distribution of Porosity in Transverse Sections of Fuel of Element E-18

Radial electron-microprobe scans for molybdenum and ruthenium (the two major fission products) were taken across the fuel of bottom, midplane, and top sections of a high-burnup (6 at. %) Mark-II element to determine the distribution of the two products. (See Fig. A.7, Appendix A.) Both scans are concentrated in large, widely spaced particles in the bottom and midplane sections and in small, closely spaced particles in the top section. In each section, however, the average concentration of the products appears to be uniform radially (see Appendix B). This would indicate that no detectable thermomigration of these fission products takes place. Therefore, redistribution of these products need not be taken into account when interpreting axial gamma scans. (See Sec. II.C above.)

Another noteworthy feature observed in the metallographic examination of the fuel in the midplane and top sections of most high-burnup (4.2 and 6 at. %) elements examined is the rather high-density band in the fuel at the fuel/cladding interface (see Fig. 15). Detailed examination of this band in encapsulated elements with even higher burnup showed it to contain nickel and to have a microhardness comparable to that of the cladding, viz., much higher than the hardness of the rest of the fuel. The presence of this band could have a significant effect on the mechanical loading experienced by the cladding.

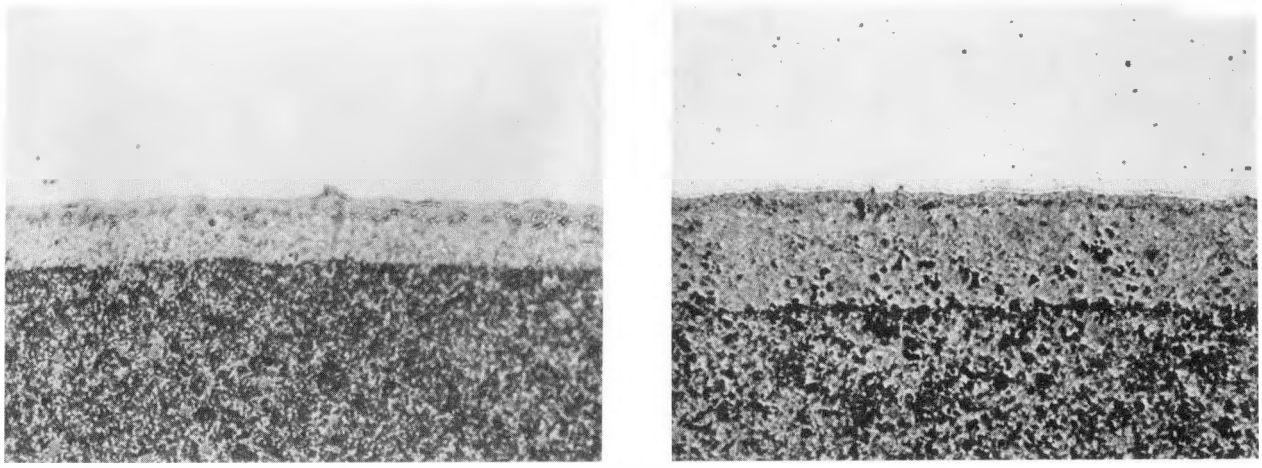

ELEMENT E-74, S/A C-2234S: 4.2 at. % BU

ELEMENT E-24, S/A C-2236S: 5.8 at. % BU

Fig. 15. Interaction Band in Fuel at Interface of Fuel and Type 304L Stainless Steel Cladding. Mag. 340X. HFEF Met. Lab. Neg. Nos. 38D3-3 and 89E4-3.

A slight liftoff of the fuel pin from the jacket bottom is common in Mark-II fuel elements. Examples of this phenomenon are shown in the neutron radiographs of elements at 3.2 and 4.2 at. % peak burnup in Fig. 16. A maximum

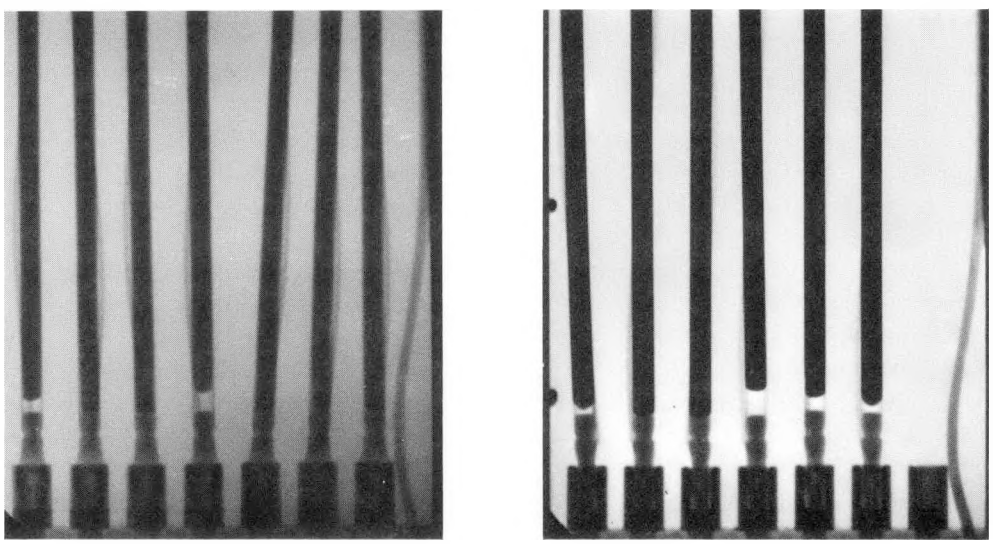

Fig. 16. Neutron Radiographs Showing Liftoff of Mark-II Fuel Pins. Left: subassembly C-2234S, 4.2 at. % burnup; right: subassembly C-2203S, 3.2 at. % burnup.

liftoff of about 1/4 in. has been observed in a Mark-II element. More typically (in 20-30% of the examined elements), the liftoff is around 1/16 in.

Table III summarizes the results of a calculation on the effect of liftoff on reactivity. The calculation was based on a 1/4-in. liftoff in one-eighth to one-quarter of the driver subassemblies in a core with a radial stainless steel reflector.

TABLE III. Reactivity Changes due to Liftoff of Mark-II Fuel[a]

Location of Fuel Liftoff	Number of Subassemblies with Liftoff	k_{eff}	Change in Reactivity	
			% $\Delta k/k$	Inhours
None	-	1.030496	-	-
Rows 1-2	4	1.030136	0.035	15
Rows 1-3	8	1.030136	0.035	15

[a]Calculated with CITATION code[6] in 2D RZ geometry.

These results agree with the observation that the last 1/4 in. of travel of 10 control rods corresponds to a reactivity change of about 28 inhours.

The high degree of porosity at the bottom of the lifted-off pins, obvious in Fig. 17, indicates that the bottom ends of these pins have swelled rather unrestrainedly. One may deduce from this that the pins lifted off early during their irradiation. Ratchetting of bowed fuel pins (pins often are bowed in one or more nodes by nonuniform swelling of the fuel) during shutdowns and startups probably is the mechanism by which liftoff occurs. Although a fuel pin could conceivably ratchet up until it is stopped by the restrainer, no evidence has been found for this in Mark-II elements having no restrainer (i.e., maximum liftoff was 1/4 in.).

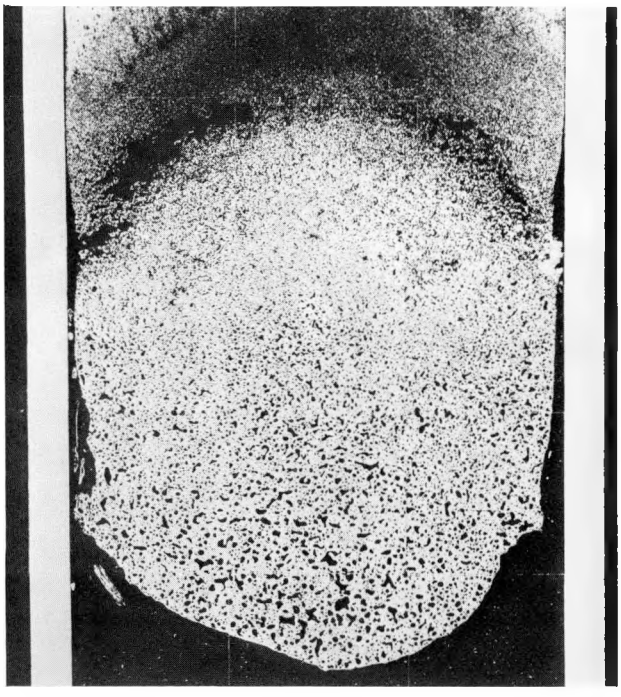

Fig. 17

Axial Cross Section of Bottom of Mark-II Fuel Pin That Lifted Off. Mag. 16.5X. Neg. No. MSD-163601.

B. Cladding

The combined effect of neutron exposure, temperature, and internally generated pressure demonstrates itself in dimensional and metallurgical changes of the cladding materials. In addition, interdiffusion between cladding and fuel occurs.

1. Overall External Appearance of Elements

Visual inspection of the elements showed them to be generally in good condition at all burnup levels.

During the examination of subassembly C-2203S at a burnup of 3.2 at. %, brown, rustlike discolorations were found in the core region of both the subassembly hexagonal can and the element cladding. These discolorations have been reproduced in the laboratory[7] by applying both concentrated (50%) and dilute (<1%) sodium hydroxide solutions to austenitic and ferritic stainless steel when the steel was heated to 300°F. No discoloration occurred, however, when the sodium hydroxide was applied at room temperature. The discolorations in subassembly C-2203S seem to have been caused by a combination of residual caustic solution from preexamination subassembly washing and decay heat.

The spacer wires remained rather tightly wrapped on Type 304L stainless-steel-clad elements at all burnup levels, but were somewhat loose on Type 316 stainless-steel-clad elements at higher burnup levels. This is consistent with the use of Type 304L stainless steel spacer wire for all elements.

2. Diameter Increase

Figures 18 and 19 show the measured diameter changes of 304L- and 316-clad elements at several burnup levels. The maximum diameter

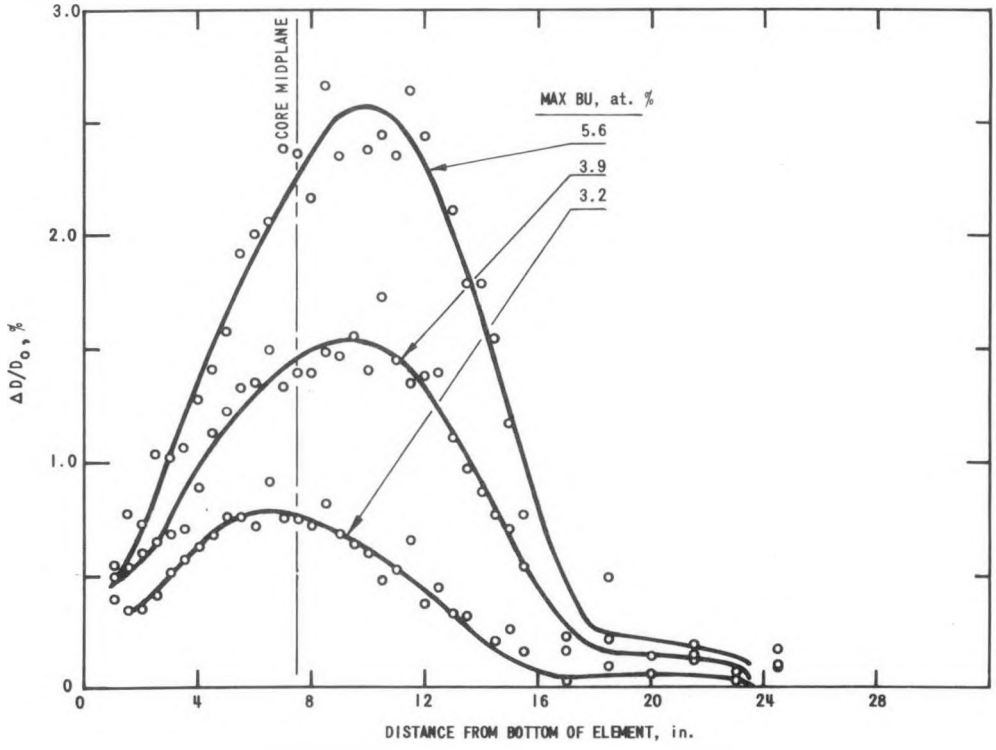

Fig. 18. Diameter Changes along 304L-clad Mark-II Elements at Three Burnup Levels. ANL Neg. No. 103-Q5850.

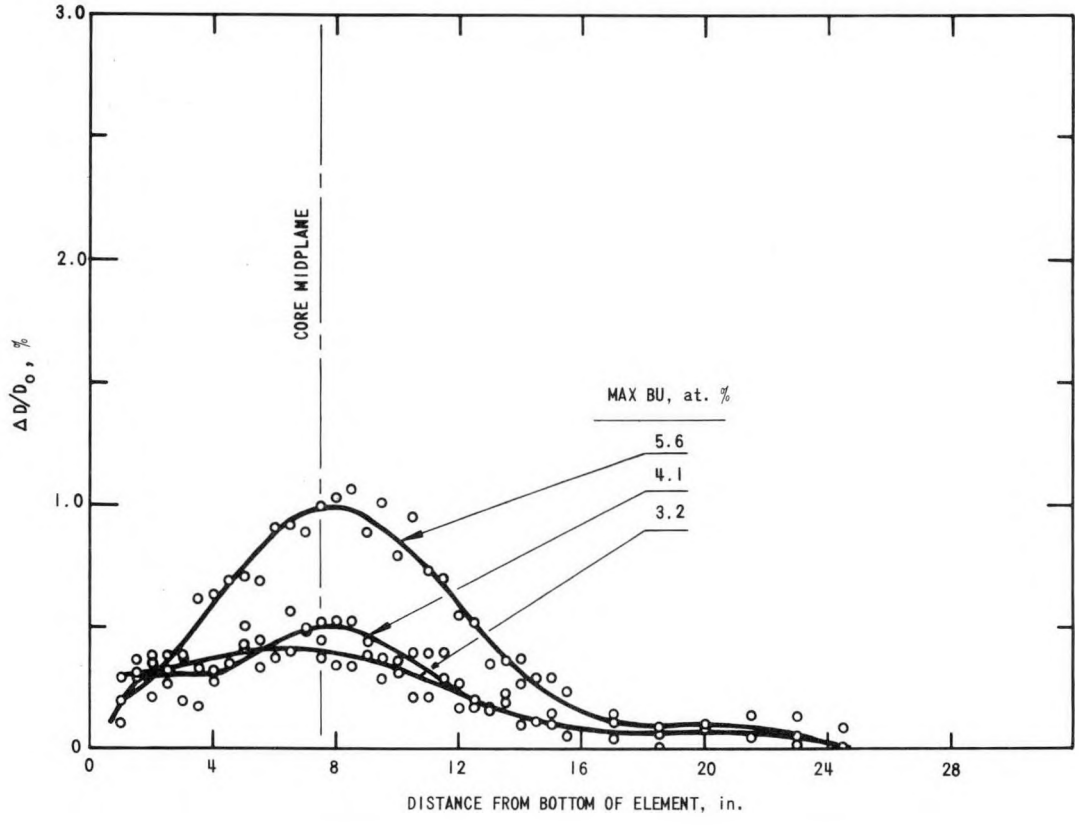

Fig. 19. Diameter Changes along 316-clad Mark-II Elements at Three Burnup Levels. ANL Neg. No. 103-Q5851.

change appears to occur around the core midplane. For the 304L-clad elements, however, the point of maximum diameter change shifts toward the top of the element with increasing burnup. Figure 20 plots maximum diameter change and swelling as a function of burnup for many of the elements. Clearly, the diameter changes of the 304L-clad elements are significantly greater (by about a factor of three) than those of the 316-clad elements. Swelling of the stainless steel is the major cause of diameter increase in both cladding materials. This fact was determined by immersion-density measurements of the cladding samples of selected elements (see Figs. 21 and 22). The difference between total diameter change and the change due to swelling only is irradiation-induced creep. As with the swelling rate, the creep rate seems to be smaller for the Type 316 stainless steel cladding. This observation agrees with published data for solution-annealed steel.[8-10] As shown in Fig. 23, however, our observed swelling of the Type 304L cladding has a different temperature dependence than reported in those references. We speculate that the difference results from stress due to pressures exerted by the plenum gas and swelling fuel. The shift of the peak swelling rate to a higher temperature in stressed Type 304L stainless steel is consistent with the shift of the peak diameter change toward the top (i.e., toward a high temperature) of 304L-clad elements after 2-3 at. % burnup. As stated earlier, before that burnup level is reached, no significant pressure is generated in Mark-II elements.

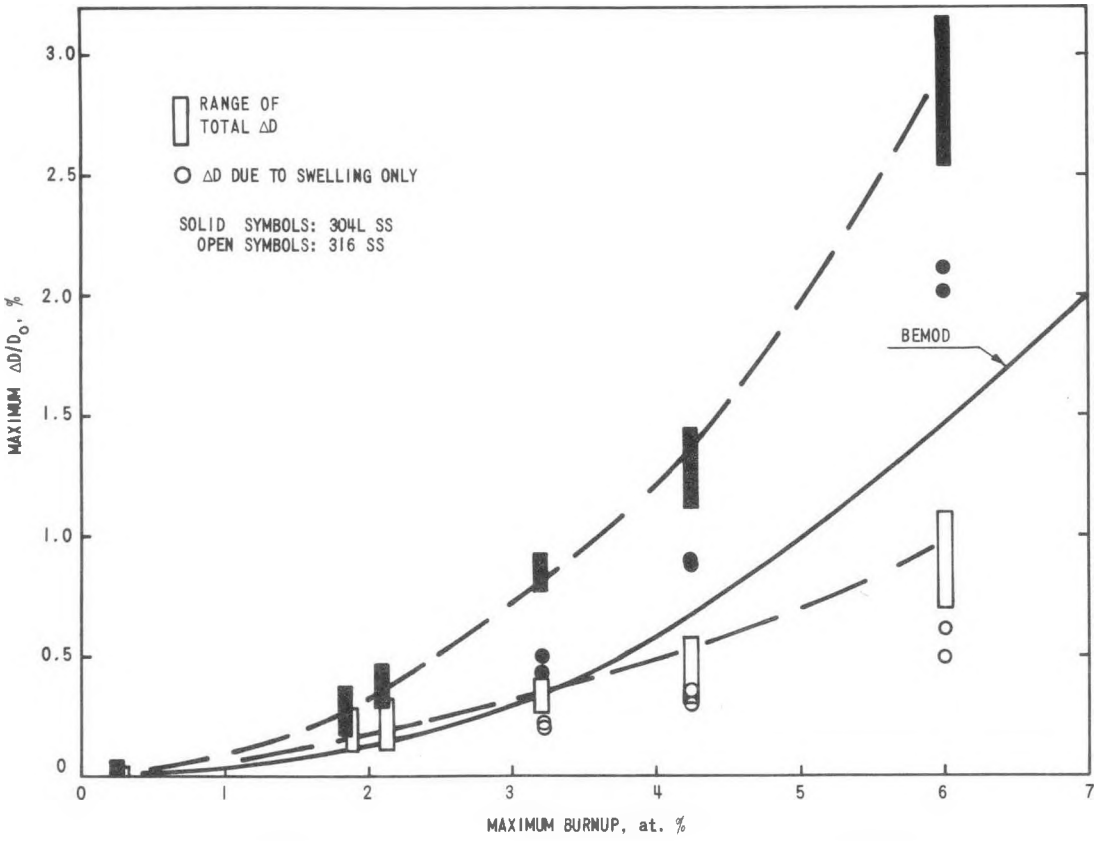

Fig. 20. Peak Diameter Change and Swelling of Cladding of Mark-II Elements as a Function of Burnup. ANL Neg. No. 103-Q5849.

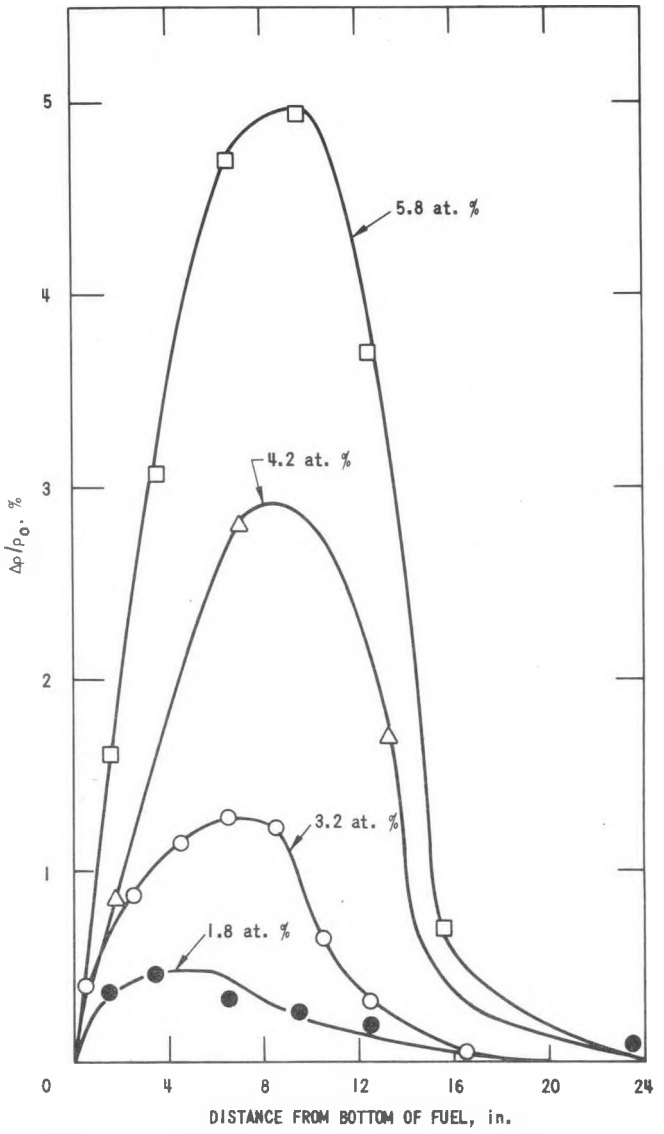

Fig. 21. Density Change of Type 304L Stainless Steel Mark-II Cladding at Four Burnup Levels

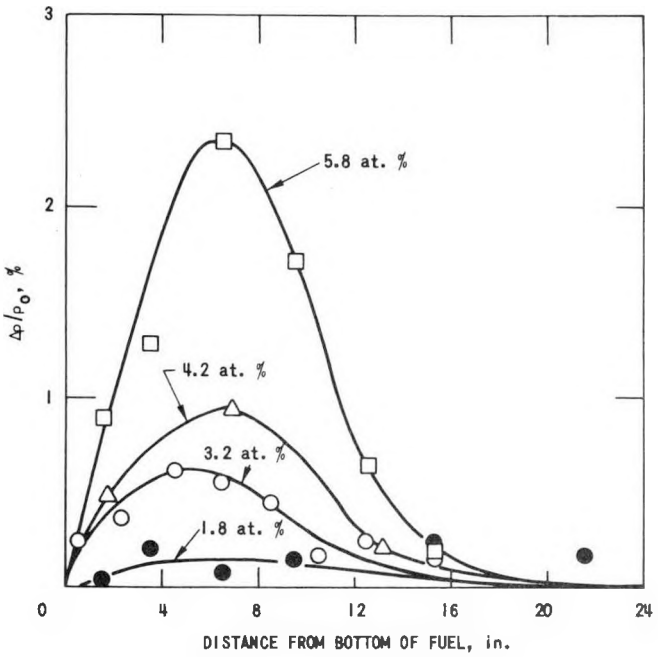

Fig. 22

Density Change of Type 316 Stainless Steel Mark-II Cladding at Four Burnup Levels

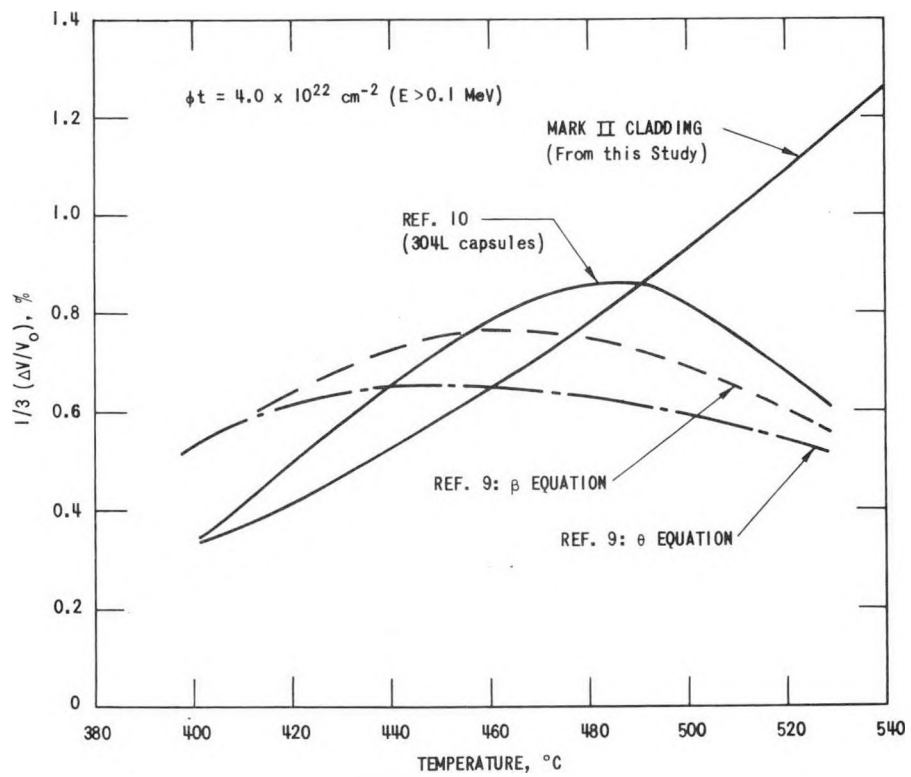

Fig. 23. Temperature Dependence of Swelling of Cladding Materials

All immersion densities of cladding measured in this experiment are given in Table A.5, Appendix A.

Isotropic swelling of the cladding material not only increases the cladding diameter, but also the cladding-wall thickness and the element length. Increase of the cladding-wall thickness adds to the diameter change, but this contribution becomes significant only at relatively high swelling values.

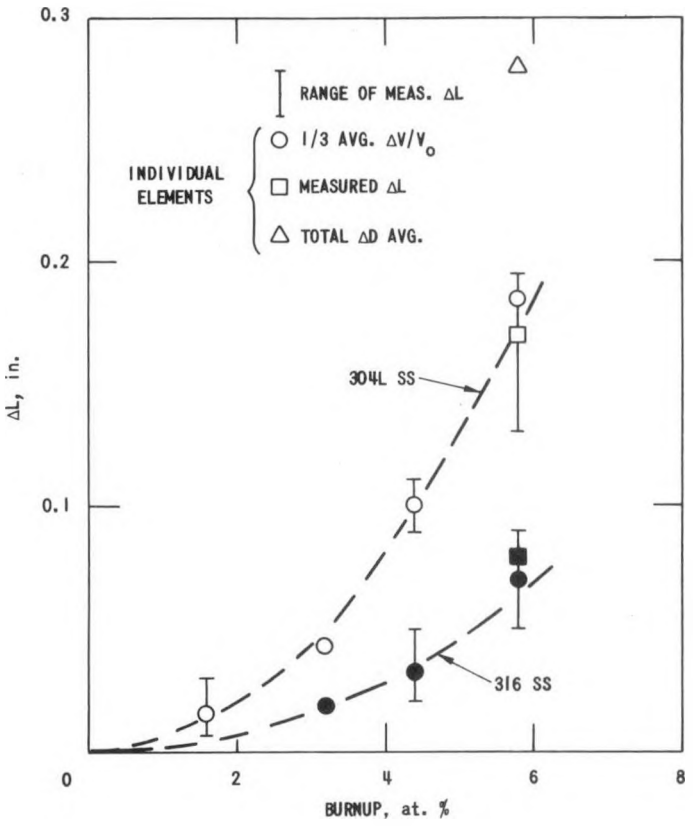

Fig. 24. Length Increase due to Swelling of Mark-II Elements

The swelling profiles shown in Figs. 21 and 22 were integrated to obtain the element-length increases due to swelling. The results are shown by the two curves in Fig. 24. The figure shows the actual measured length changes of the elements at 6 at. % burnup as well as the entire range of length changes measured on all elements. In addition, the integrated total diameter change for the high-burnup 304L-clad element that has a measured cladding-immersion-density profile is included in Fig. 24.

It can be concluded that the length increase is entirely due to swelling and that axial mechanical strain, if present at all, is very small. As would be expected, the axial stress in the cladding is apparently much smaller than the hoop stress.

Within the confines of the hexagonal subassembly, the large diameter changes of 304L-clad elements at high burnup levels can result in clearly visible mechanical interaction between adjacent elements. Figure 25 shows an example of this. The traces in this figure are taken 90° apart (azimuthally) and show both the deep depressions, where the spacer wire, which has a 12-in. pitch, contacts the cladding and the consequent bulges 90° from the spacer-wire location, where no restraint is present. The situation is shown schematically in Fig. 26. The 316-clad elements (see Fig. 27) show much less interaction, owing to their smaller diameter increase.

3. Metallography

Metallographic examination of the cladding shows that extensive sensitization (grain-boundary precipitation) occurs during irradiation. Figure 28 shows samples from Type 304L stainless steel cladding examined at 4.2 and 6 at. % burnup. The sensitization is least pronounced at the bottom of the elements, and becomes rather heavy toward the hotter top of the elements.

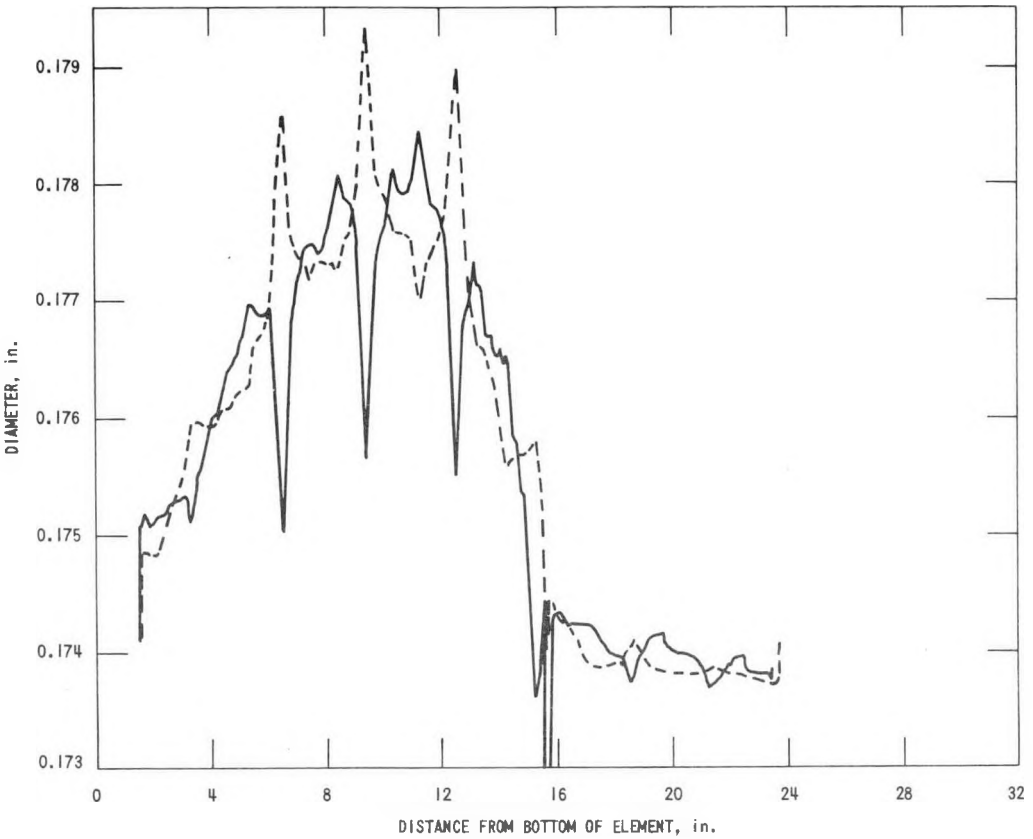

Fig. 25. Diameter Profiles of 304L-clad Mark-II Element Measured 90° from Each Other Showing Ovality Caused by Interaction with Spacer Wires (Element E-67, subassembly C-2236S)

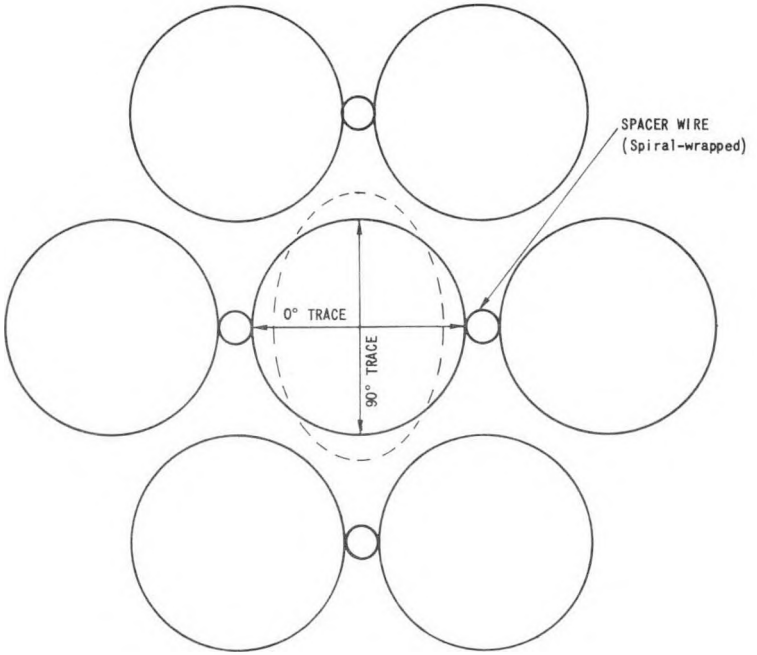

Fig. 26. Schematic View of Mechanical Interaction of Spacer Wire and Cladding That Causes Cladding Ovality

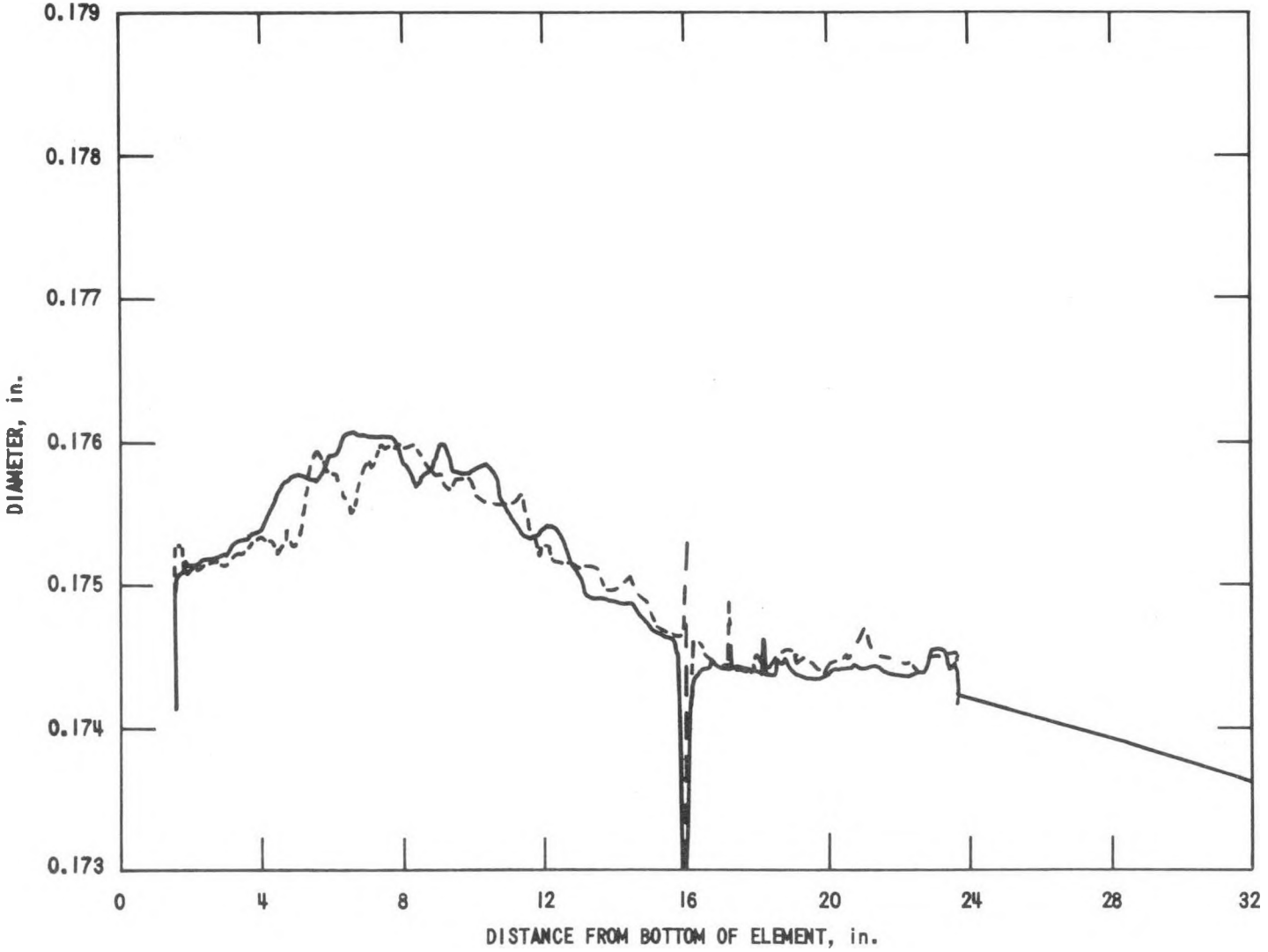

Fig. 27. Diameter Profiles of 316-clad Mark-II Element Measured 90° from Each Other Showing Little Interaction with Spacer Wires (Element E-18, subassembly C-2236S)

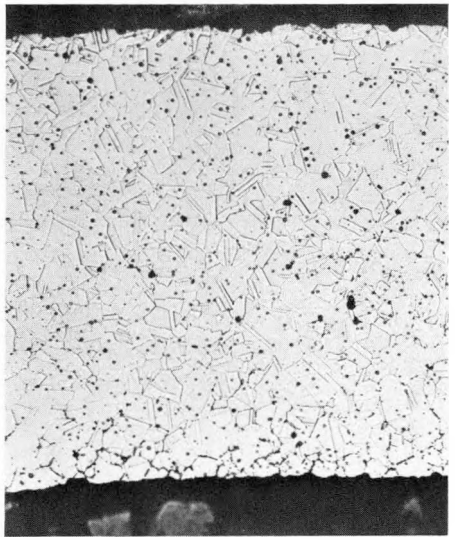

1/2 in. above Bottom of Fuel. HFEF Met. Lab. Neg. No. 44D2-3.

8 in. above Bottom of Fuel. HFEF Met. Lab. Neg. No. 44D3-2.

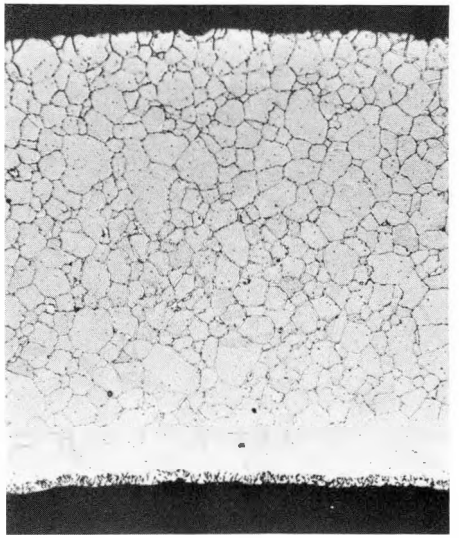

14 in. above Bottom of Fuel. No Neg. No.

1/2 in. above Bottom of Fuel. HFEF Met. Lab. Neg. No. 89E3-3.

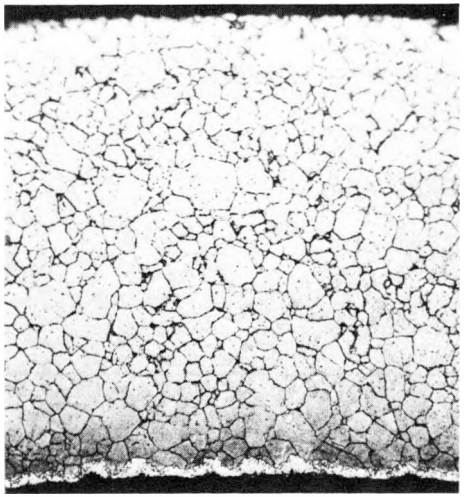

8 in. above Bottom of Fuel. HFEF Met. Lab. Neg. No. 89E4-4.

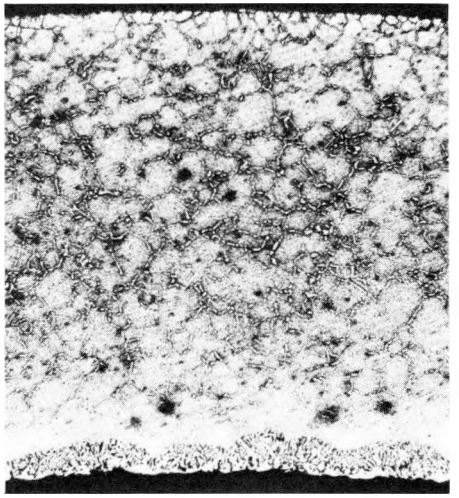

14 in. above Bottom of Fuel. HFEF Met. Lab. Neg. No. 89E5-3.

Fig. 28. Type 304L Stainless Steel Cladding from Mark-II Elements after Oxalic Acid Etch. Top row, 4.2 at. % burnup; bottom row, 6 at. %. Mag. 200X.

Examples of the precipitates are shown in the TEM micrographs of the Type 304L stainless steel cladding in Fig. 29. The precipitates, which have been identified to be composed of both $M_{23}C_6$ and sigma phase, often exhibit a strung-out pattern along grain boundaries. This feature of the precipitates may become significant in the propagation of eventual cladding failures at higher burnups. Figure 29 also shows the effect of temperature on the irradiation damage in general. The void morphology changes drastically going from the bottom to the top of the elements. The voids are small and densely spaced at the bottom, but become progressively larger and more widely spaced at the top of the elements.

The Type 316 stainless steel cladding exhibits a smaller void size throughout the element as compared with the Type 304L stainless steel cladding. This is reflected in the lower swelling rate of the Type 316 material. The size and density distribution of the irradiation-induced defects is also reflected in the mechanical properties of the cladding; for example, see the microhardness profile in Fig. 30.

Referring again to Fig. 28, one can observe a distinct interaction band on the inner surface of the Type 304L stainless steel cladding. There is a faint but inconclusive indication that such an interaction also may have occurred in the 316-clad element with the highest burnup. The interaction band in the Type 304L cladding is caused primarily by diffusion of nickel into the fuel, as determined by microprobe examination. The band is much harder than the original austenitic cladding and is believed to be ferritic. A strong temperature dependence of the rate of growth of the interaction band is reflected in the increase in bandwidth going from core midplane to element top.

A peculiar feature of this interaction band is its growth rate at any particular temperature. The relationship of the growth rate to time is nearly linear, rather than parabolic as would be expected for a diffusion-controlled process. Also, the rate itself is much higher than predicted from out-of-pile studies[11,12] (see Fig. 31). The linear growth rate of the interaction band suggests that the migration of the phase boundary controls the growth.

It can only be speculated at this point that enhancement of the nickel diffusion by radiation causes the normally faster phase-boundary migration to become the rate-controlling step in the interaction-band formation. Microprobe analyses of the Type 316 stainless steel cladding show no significant redistribution of cladding components, a finding consistent with the absence of a measurable interaction band. As mentioned before, the nickel that has diffused out of the cladding is associated with the relatively hard, dense band in the fuel adjacent to the cladding. This band is about three times as wide as the nickel-depleted zone in the cladding. At the likely burnup limit for Mark-II fuel elements (i.e., about 10 at. % burnup), the dense band in the fuel would be about 6 mils wide.

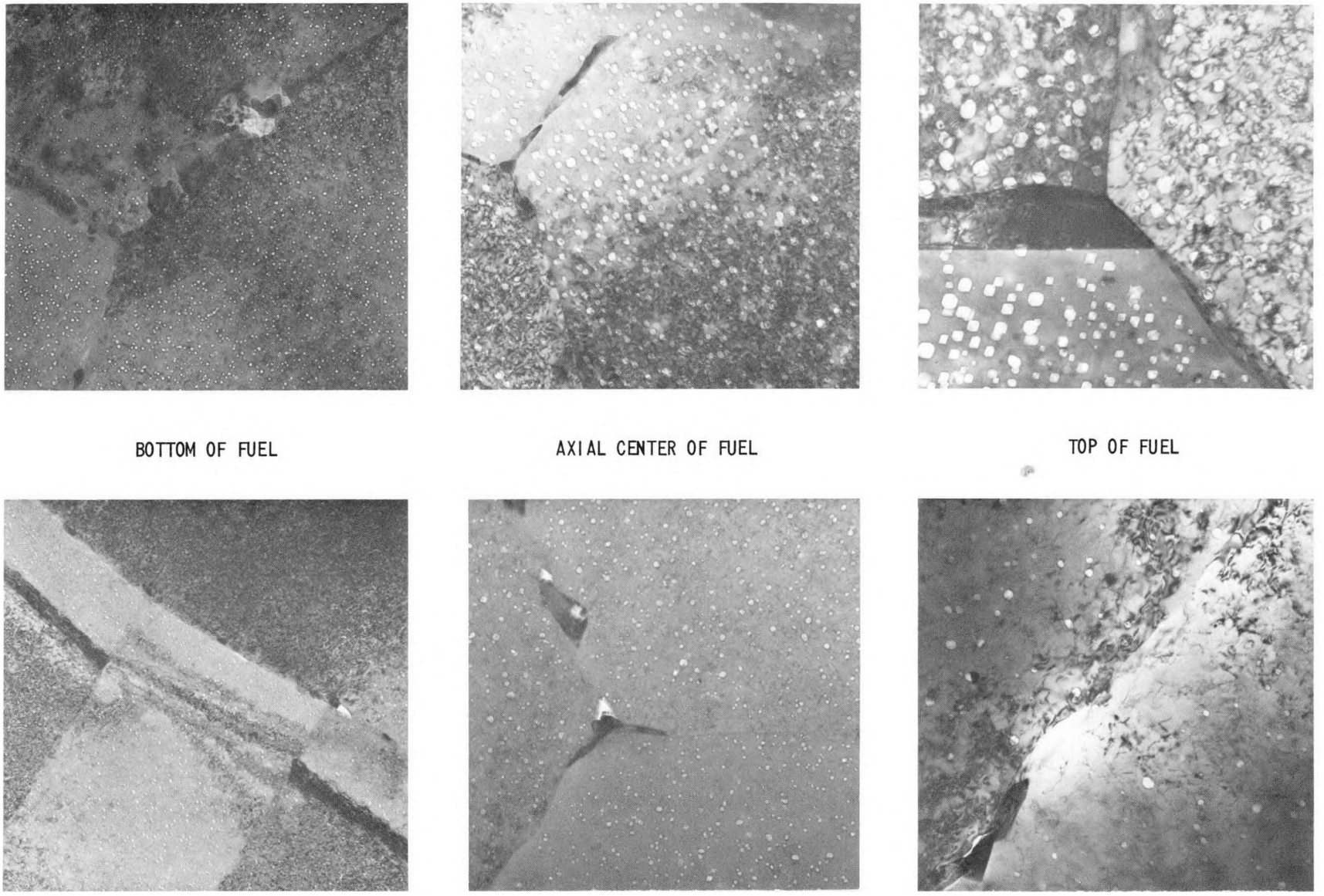

Fig. 29. TEM Micrographs of Types 304L (top) and 316 Stainless Steel (bottom) Mark-II Cladding, Showing Voids and Precipitates. Mag. 27,000X.

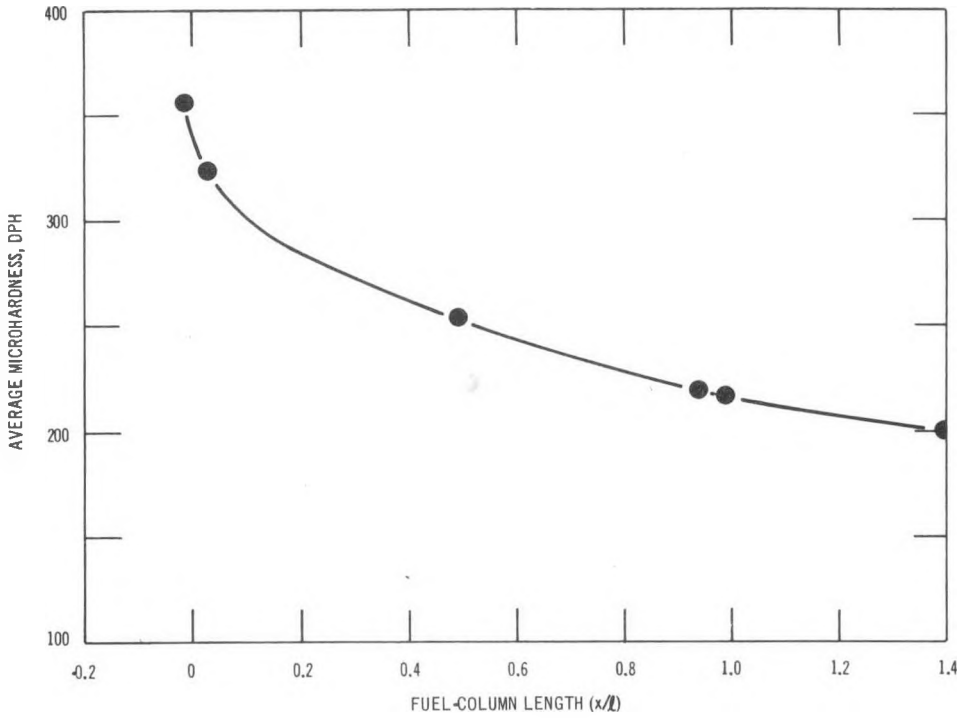

Fig. 30. Axial Microhardness Profile of Type 316 Stainless Steel Cladding of Mark-II Elements with 6 at. % Peak Burnup

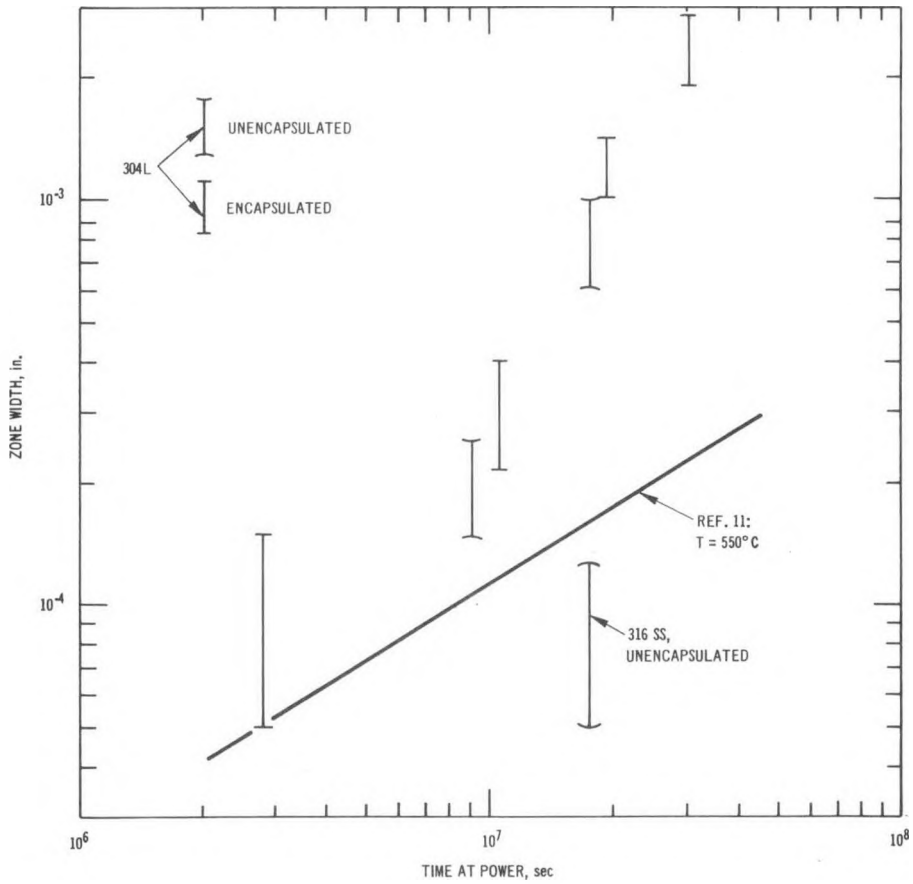

Fig. 31. Width of Ferritic Zone at Mark-II Cladding Inner Surface as a Function of Time at Power Since Fuel/Cladding Contact: Core Midplane, T = 520-570°C

Some relatively low-melting eutectic phases are present in these interaction zones. The formation of a liquid phase has been found to occur at 705 ± 5 and 715 ± 5°C, respectively, in 304L/U-Fs and 316/U-Fs couples.[11,12] These temperatures are well above the normal operating temperature of a fuel element. Only during abnormal operations, such as power transients and loss of flow, could temperatures reach 750 or 800°C and allow the low-melting eutectics to form. Fortunately, the growth rate of these eutectic zones, when formed, is slow (on the order of 0.6 mil/hr at 740°C and 50 mils/hr at 850°C).[13] Because of the short duration of possible abnormal operation, no catastrophic effects on the cladding are expected to occur as a result of cladding/fuel interaction.

IV. CONCLUSIONS

The Mark-II fuel element has been proved to operate successfully as EBR-II driver fuel to a peak burnup of about 6 at. %.

Of the two cladding materials used in this test (i.e., annealed Types 304L and 316 stainless steel), the Type 316 stainless steel appears to be the superior material at least up to 6 at. % burnup. Cladding of that material showed (1) a much smaller diameter increase than the Type 304L stainless steel cladding, (2) a fuel/cladding chemical interaction that was nearly negligible relative to that of the Type 304L cladding, and (3) at least an equality with Type 304L cladding in all other aspects of irradiation performance.

APPENDIX A

Physical Measurements

This appendix contains:

General loading diagram for the Mark-II subassemblies: Fig. A.1.

Representative composition of as-received cladding: Table A.1.

Specified composition of as-fabricated fuel: Table A.2.

Summary of the results of the fission-gas analyses: Table A.3.

Summary of burnups obtained by chemical analysis: Table A.4.

Summary of cladding immersion-density measurements: Table A.5.

Gamma-activity scans of an element at ~6 at. % burnup: Fig. A.2.

Representative diameter profiles of elements: Figs. A.3-A.6.

Radial microprobe traces of an element at ~6 at. % burnup: Fig. A.7.

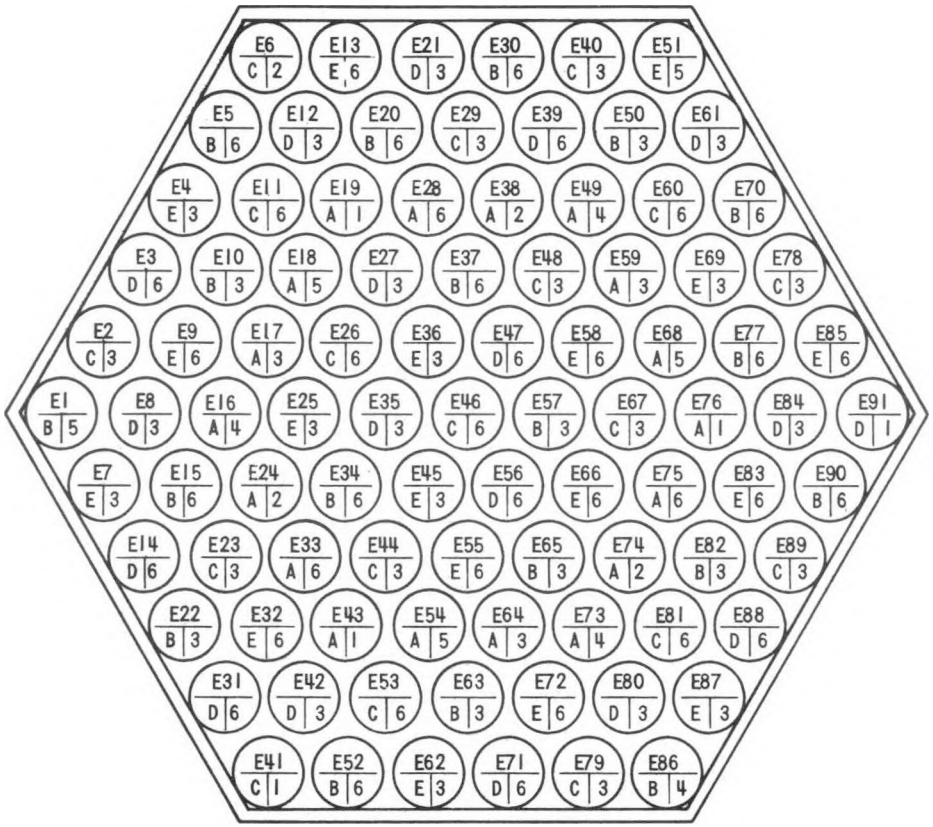

BATCH IDENTIFICATION (INDICATING CASTING BATCH NO.)

Number Elem.	Ident.	Subassembly No.					
		C-2201S	C-2202S	C-2203S	C-2204S	C-2205S	C-2206S
18	A	800	801	802	803	804	805
19	B	801	803	806	807	805	809
18	C	802	804	807	809	806	808
18	D	803	805	800	801	808	806
18	E	804	800	808	802	809	807

CLADDING AND RESTRAINER IDENTIFICATION

Number Elem.	Ident.	Clad	Restr. Height, in.
5	1	304L	No restr.
4	2	304L	1
37	3	304L	1/2
4	4	316	No restr.
5	5	316	1
36	6	316	1/2

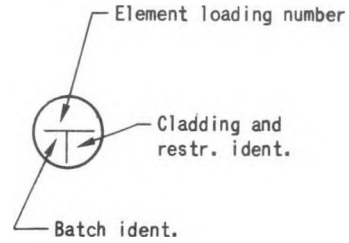

Fig. A.1. General Loading Diagrams for the Mark-II Subassemblies

TABLE A.1. Composition of Mark-II Cladding Material

Material	316 SS	304L SS	
Vendor	Wall Tube and Metal Products Company	Superior Tube Company	
Heat No.	51577	00465	27460
Quantity, ft	3260	2140	472
Date received	6/22/67	10/26/66	
Analysis, wt %			
C	0.035	0.017	0.030
Mn	1.53	1.54	1.66
P	0.020	0.008	0.016
S	0.007	0.010	0.014
Si	0.39	0.39	0.59
Ni	11.87	10.40	10.56
Cr	16.06	18.69	18.31
Cu	0.19	-	-
Mo	2.39	-	-
Co	0.06	-	-

TABLE A.2. Specified Fuel Composition

Element	wt %
Mo	2.46 ± 0.17
Ru	1.96 ± 0.16
Rh	0.28 ± 0.05
Pd	0.19 ± 0.04
Zr	0.10 ± 0.03
Nb	0.01 ± 0.006
U	95.00 ± 1.00
Impurities	2500 ppm (max)
Isotopic Uranium	
^{235}U	52.18 ± 0.50
^{234}U, ^{236}U, ^{238}U	47.82 ± 0.50
^{234}U, ^{236}U	< 1.0

Impurity Levels	ppm
Al	300
Be	100
B	100
C	400
Cr	200
Fe + Ni	600
N	200
O	200
Si	300
Th	100

TABLE A.3. Summary of Results of Fission-gas Analyses

S/A No.	Element No.	Max. Burnup, at. %	Fission Gas Recovered, ml	Plenum-gas Composition, mol %							Krypton and Xenon Isotopic Analysis, mol %								
				He	N_2	O_2	Ar	Misc.	Kr	Xe	^{83}Kr	^{84}Kr	^{85}Kr	^{86}Kr	^{130}Xe	^{131}Xe	^{132}Xe	^{134}Xe	^{136}Xe
C-2201S	E-46	2.11	10.76	0.20	ND[a]	ND	8.75	61.63	5.17	24.25	15.3	27.42	7.25	50.01	-	14.46	21.04	35.47	29.03
C-2201S	E-73	2.27	8.75	1.20	ND	ND	7.60	45.60	6.60	39.00	15.43	28.02	7.32	49.24	-	15.00	20.51	35.42	29.06
C-2203S	E-73	~3.3[b]	6.26	0.46	0.01	ND	0.49	88.7	0.54	9.76	15.70	26.72	7.20	50.38	0.009	14.67	21.22	34.75	29.35
C-2203S	E-46	2.86	16.74	0.45	0.07	0.04	1.01	83.3	1.51	13.62	15.53	27.23	7.00	50.24	0.01	14.78	21.19	34.67	29.35
C-2236S	E-24	5.41	35.57	0.44	0.27	0.03	0.04	0.57	10.88	87.80	-	-	-	-	0.0168	14.60	21.50	35.30	28.58
C-2236S	E-73	~5.5[b]	34.47	0.44	0.37	0.07	0.02	0.04	11.24	87.82	-	-	-	-	0.0185	14.76	21.63	35.30	28.28
C-2236S	E-59	~5.5[b]	34.47	0.39	0.34	0.05	3.71	0.53	10.71	84.27	-	-	-	-	0.0168	14.82	21.78	35.22	28.16
C-2236S	E-64	~5.5[b]	5.66	0.40	0.57	0.12	24.31	0.05	8.10	66.45	-	-	-	-	-	-	-	-	-
C-2236S	E-28	~5.5[b]	2.11	ND	0.74	0.31	98.29	0.14	ND	0.52	-	-	-	-	-	-	-	-	-
C-2232S	E-1	~6.0[b]	40.92	0.54	ND	ND	5.15	0.21	12.18	81.92	-	-	-	-	0.0198	14.35	21.56	35.23	28.83
C-2232S	E-2	~6.0[b]	42.05	0.54	ND	ND	3.79	0.36	12.11	83.20	-	-	-	-	0.0188	14.35	21.61	35.20	28.82
C-2232S	E-6	~3.0[b]	18.12	0.52	ND	ND	8.17	0.01	11.48	79.83	-	-	-	-	0.0095	14.20	21.15	35.54	29.09
C-2232S	E-35	~3.0[b]	17.45	0.65	ND	ND	4.54	0.26	12.07	82.48	-	-	-	-	0.0099	14.39	21.09	35.45	29.04
C-2232S	E-90	~3.7[b]	35.30	0.43	ND	ND	3.72	0.30	10.59	84.96	-	-	-	-	0.0179	14.45	21.44	35.22	28.87
C-2232S	E-91	~5.7[b]	35.35	0.66	ND	ND	4.47	0.28	6.83	87.76	-	-	-	-	0.0177	14.46	21.41	35.27	28.84
C-2230S	E-33	~3.7[b]	21.61	0.59	0.02	ND	7.04	0.20	11.77	80.38	-	-	-	-	0.0127	14.27	21.41	35.31	28.98
C-2230S	E-46	~3.7[b]	21.85	0.57	ND	ND	7.08	0.25	11.59	80.51	-	-	-	-	0.0127	14.37	21.47	35.27	28.87
C-2236S	E-2	~6.0[b]	34.60	0.6	0.4	0.01	7.9	0.36	12.43	78.3	15.61	27.16	6.11	50.92	ND	14.30	20.94	34.09	27.71
C-2236S	E-46	~6.0[b]	34.65	0.6	0.4	0.01	4.7	0.46	15.33	78.50	15.65	27.39	6.52	50.23	ND	14.77	21.52	35.16	28.53
C-2236S	E-67	~6.0[b]	34.48	0.6	0.3	0.01	5.5	0.26	15.30	78.0	15.03	27.45	6.53	50.98	ND	14.74	21.66	35.13	28.46
C-2236S	E-18	~5.5[b]	31.11	0.3	15.8	0.3	0.8	36.1	7.5	39.2	16.00	28.00	6.67	49.33	ND	14.80	21.94	34.44	28.32
C-2201S	E-24	2.03	11.04	0.6	0.4	0.02	18.1	0.68	10.9	69.3	15.6	27.5	7.3	49.5	ND	14.3	21.2	35.5	29.0
C-2201S	E-33	1.90	5.37	0.5	0.7	0.1	29.4	1.7	9.3	58.3	15.1	28.0	75.5	49.5	ND	14.4	21.2	35.4	28.9
C-2201S	E-54	1.80	11.54	0.6	0.6	0.02	16.4	0.68	11.0	70.7	15.4	27.3	7.2	50.0	ND	14.6	21.2	35.4	28.9

[a]ND = Not Detected.
[b]Calculated individual-pin burnups.

TABLE A.4. Summary of Burnups Obtained by Chemical Analysis

Subassembly No.	Element No.	Burnup, at. %			Distance from Core Midplane, in.				
		Nd	Tc	La	-6.5	-3.0	-0.5	+3.5	+7.0
C-2234S	E-74	-	3.49	3.82	-	-	x	-	-
C-2234S	E-64	-	3.77	3.77	-	-	x	-	-
C-2234S	E-1	-	3.81	4.15	-	-	x	-	-
C-2234S	E-28	-	3.84	3.94	-	-	x	-	-
C-2234S	E-28	-	-	4.33	-	-	x	-	-
C-2236S	E-24	4.96	-	5.41	-	-	x	-	-
C-2201S	E-46	-	1.8	-	-	-	-	-	x
C-2201S	E-46	-	2.06	-	-	-	-	x	-
C-2201S	E-46	-	2.11	-	-	-	x	-	-
C-2201S	E-46	-	1.76	-	-	x	-	-	-
C-2201S	E-46	-	1.50	-	x	-	-	-	-
C-2201S	E-73	-	1.93	-	-	-	-	-	x
C-2201S	E-73	-	2.02	-	-	-	-	x	-
C-2201S	E-73	-	2.27	-	-	-	x	-	-
C-2201S	E-73	-	1.91	-	-	x	-	-	-
C-2201S	E-73	-	1.55	-	x	-	-	-	-
C-2203S	E-46	-	2.46	-	-	-	-	-	x
C-2203S	E-46	-	2.67	-	-	-	-	x	-
C-2203S	E-46	-	2.86	-	-	-	x	-	-
C-2203S	E-46	-	2.32	-	-	x	-	-	-
C-2203S	E-24	-	-	3.04	-	-	x	-	-
C-2203S	E-24	-	-	2.10	x	-	-	-	-
C-2203S	E-33	-	-	3.08	-	-	x	-	-
C-2203S	E-33	-	-	2.20	x	-	-	-	-
C-2201S	E-24	-	2.03	-	-	-	x	-	-
C-2201S	E-33	-	1.90	-	-	-	x	-	-
C-2201S	E-54	-	1.80	-	x	-	-	-	-
C-2201S	E-54	-	1.66	-	-	-	x	-	-
C-2201S	E-54	-	1.32	-	-	-	-	-	x

TABLE A.5. Summary of Cladding Immersion-density Measurements

Subassembly No.	Element No.	Sample No.	d[a]	$\bar{\rho}$[b]	Type of SS
C-2234S	E-64	735	$1\frac{1}{4}$	7.8447	304L
		737	7	7.6918	304L
		740	$13\frac{1}{4}$	7.7878	304L
		746	$23\frac{1}{4}$	7.9161	304L
C-2234S	E-74	750	$1\frac{1}{4}$	7.8482	304L
		752	7	7.6877	304L
		755	$13\frac{1}{4}$	7.7705	304L
		769	$23\frac{1}{4}$	7.9084	304L
C-2234S	E-28	720	$1\frac{1}{4}$	7.9369	316
		722	7	7.9016	316
		725	$14\frac{3}{4}$	7.9635	316
		731	$23\frac{1}{4}$	7.9846	316
C-2234S	E-1	705	$1\frac{1}{4}$	7.9443	316
		707	7	7.9053	316
		710	$13\frac{1}{4}$	7.9602	316
		716	$23\frac{1}{4}$	7.9713	316
C-2203S	E-33	923	$1\frac{1}{4}$	7.9660	316
		925	$3\frac{1}{4}$	7.9571	316
		927	$5\frac{1}{4}$	7.9405	316
		929	$7\frac{1}{4}$	7.9417	316
		931	$9\frac{1}{4}$	7.9500	316
		933	$11\frac{1}{4}$	7.9713	316
		935	$13\frac{1}{4}$	7.9703	316
		939	$15\frac{1}{4}$	7.9760	316
		947	$25\frac{1}{2}$	7.9861	316
C-2203S	E-24	835	$1\frac{1}{4}$	7.8805	304L
		837	$3\frac{1}{4}$	7.8430	304L
		839	$5\frac{1}{4}$	7.8221	304L
		841	$7\frac{1}{4}$	7.8118	304L
		843	$9\frac{1}{4}$	7.8458	304L
		845	$11\frac{1}{4}$	7.8605	304L
		847	$13\frac{1}{4}$	7.8870	304L
		851	$17\frac{1}{4}$	7.9081	304L
		860	$24\frac{1}{2}$	7.8931	304L
C-2203S	E-54	605	$6\frac{1}{2}$	7.909	316
		606	$20\frac{1}{2}$	7.960	316
C-2203S	E-64	607	$6\frac{1}{2}$	7.772	304L
		608	$20\frac{1}{2}$	7.890	304L

TABLE A.5 (Contd.)

Subassembly No.	Element No.	Sample No.	d[a]	$\bar{\rho}$[b]	Type of SS
C-2236S	E-24	417	$1\frac{1}{4}$	7.7806	304L
		418	$3\frac{3}{4}$	7.6164	304L
		420	7	7.4910	304L
		424	$10\frac{1}{4}$	7.4674	304L
		436	16	7.8261	304L
		437	$22\frac{1}{4}$	7.9058	304L
C-2236S	E-28	361A	$1\frac{1}{2}$	7.9766	316
		363A	$3\frac{1}{2}$	7.9640	316
		367A	$6\frac{1}{2}$	7.9746	316
		370A	$9\frac{1}{2}$	7.9687	316
		373A	$12\frac{1}{2}$	7.9576	316
		376A	$15\frac{1}{2}$	7.9612	316
		385A	$24\frac{1}{2}$	7.9661	316
C-2236S	E-64	394A	$6\frac{1}{2}$	7.8831	304L
		397A	$9\frac{1}{2}$	7.8894	304L
		400A	$12\frac{1}{2}$	7.8950	304L
		403A	$15\frac{1}{2}$	7.9169	304L
		411A	$24\frac{1}{2}$	7.9026	304L
		388A	$1\frac{1}{2}$	7.8810	304L
		390A	$3\frac{1}{2}$	7.8736	304L
C-2236S	E-59	228A	$1\frac{1}{2}$	7.7824	304L
		252A	$3\frac{1}{2}$	7.6668	304L
		256A	$6\frac{1}{2}$	7.5370	304L
		259A	$9\frac{1}{2}$	7.5142	304L
		262A	$12\frac{1}{2}$	7.6173	304L
		265A	$15\frac{1}{2}$	7.8554	304L
		273A	$23\frac{1}{2}$	7.9064	304L
C-2236S	E-73	276A	$1\frac{1}{2}$	7.9093	316
		278A	$3\frac{1}{2}$	7.8782	316
		282A	$6\frac{1}{2}$	7.7929	316
		285A	$9\frac{1}{2}$	7.8431	316
		288A	$12\frac{1}{2}$	7.9285	316
		291A	$15\frac{1}{2}$	7.9647	316
		332A	$23\frac{1}{2}$	7.9799	316

[a]Distance up, in inches, from bottom of core.
[b]Average of three density measurements.

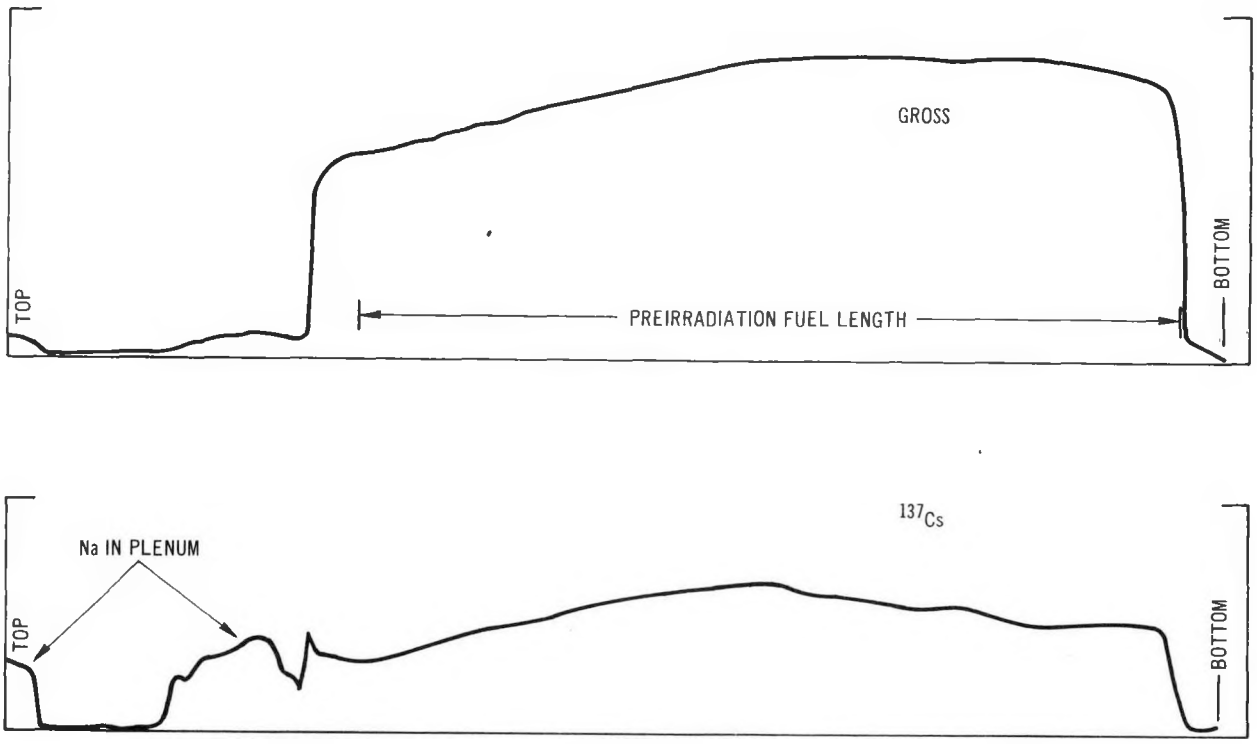

Fig. A.2. Gamma-activity Scans of Element E-18, Subassembly C-2236S, at ~6 at. % Burnup

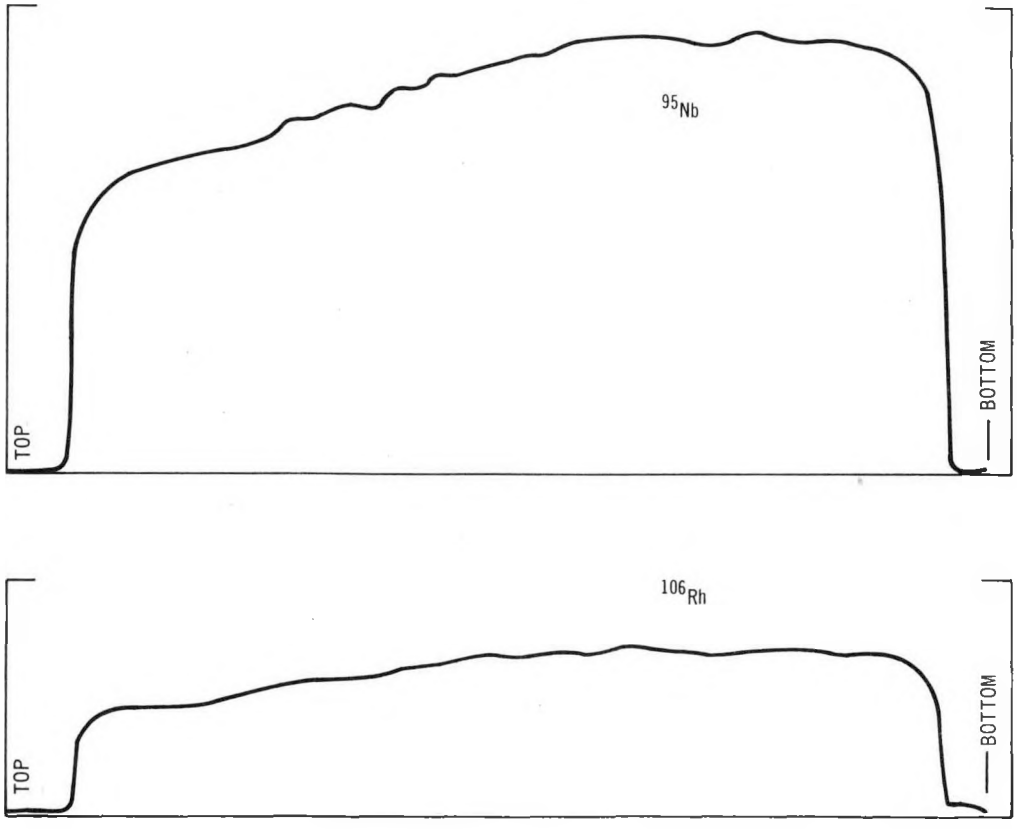

Fig. A.2 (Contd.)

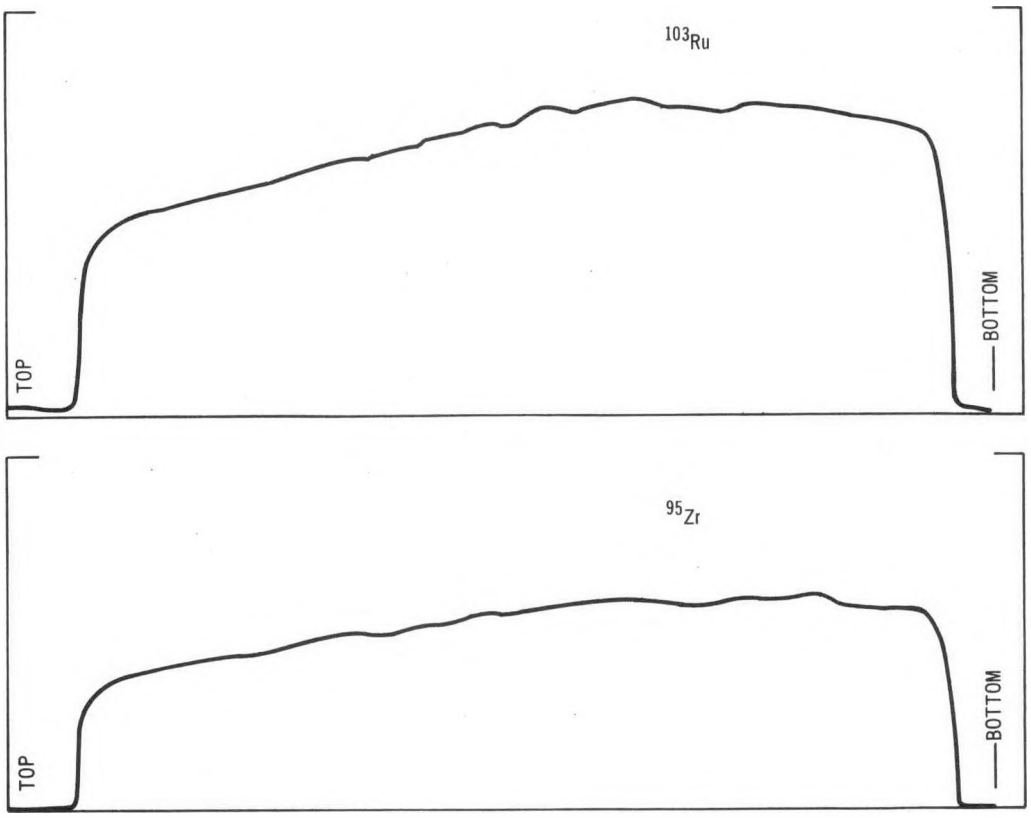

Fig. A.2 (Contd.)

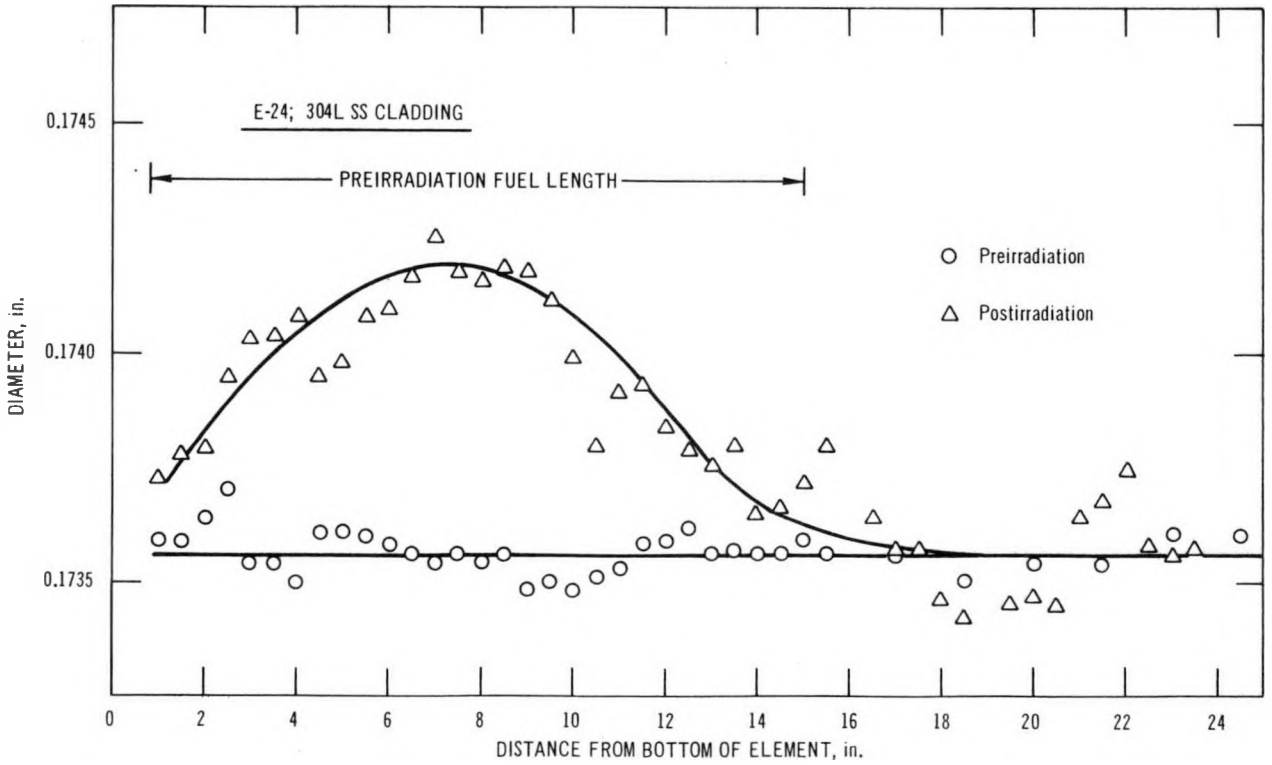

Fig. A.3. Diameter Profiles of Elements E-24 and -33, from Subassembly C-2201S, at ~2 at. % Burnup

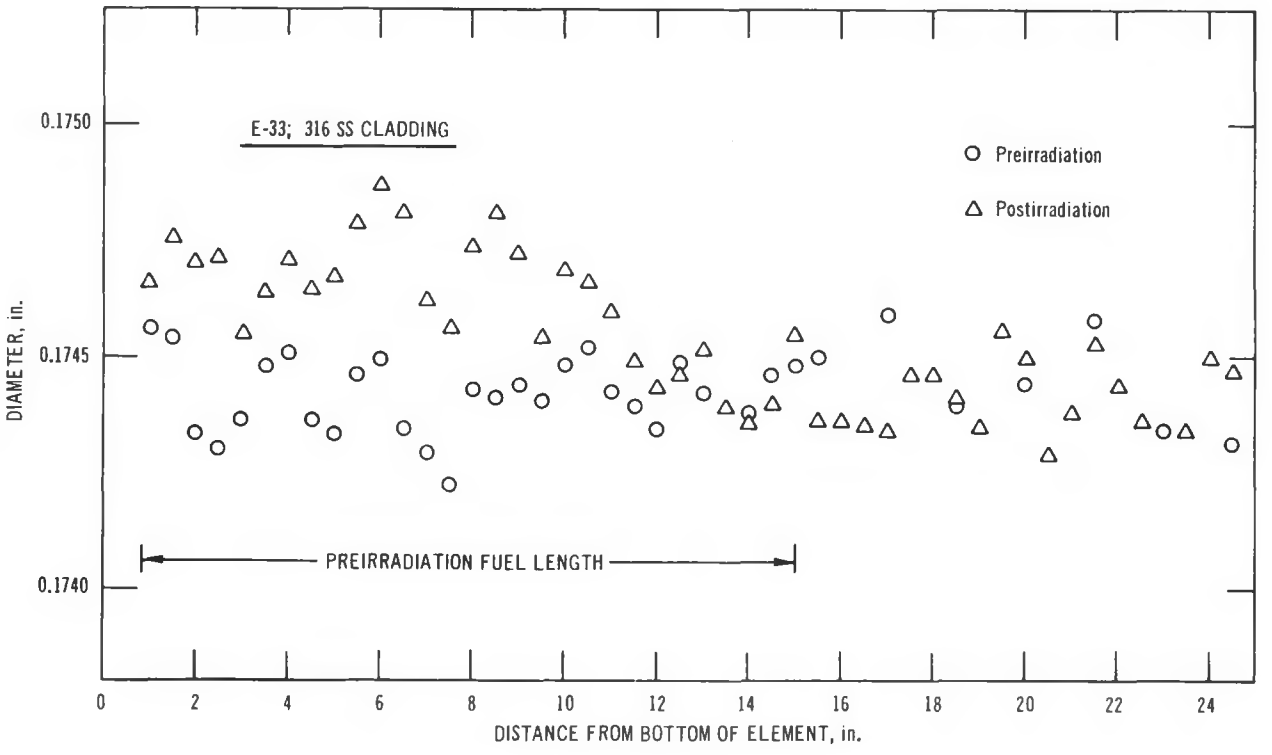

Fig. A.3 (Contd.)

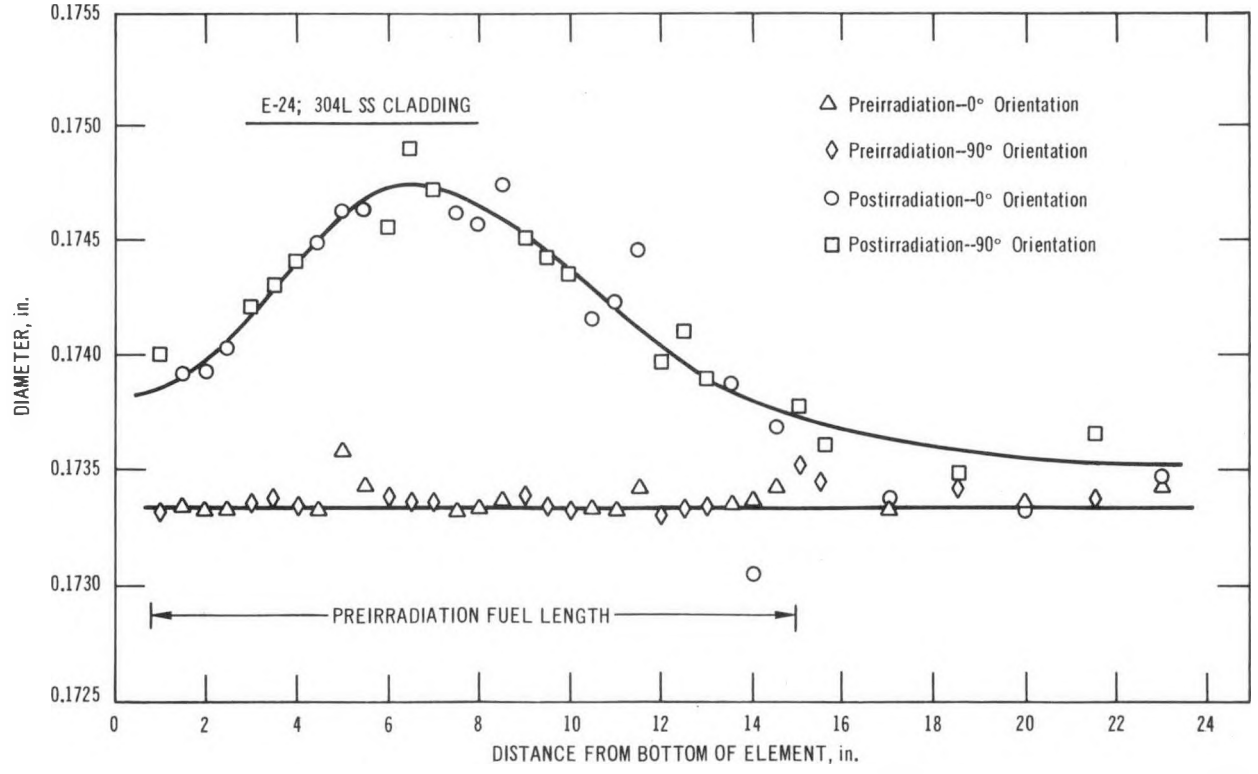

Fig. A.4. Diameter Profiles of Elements E-24, -64, -33, and -73, from Subassembly C-2203S, at ~3 at. % Burnup

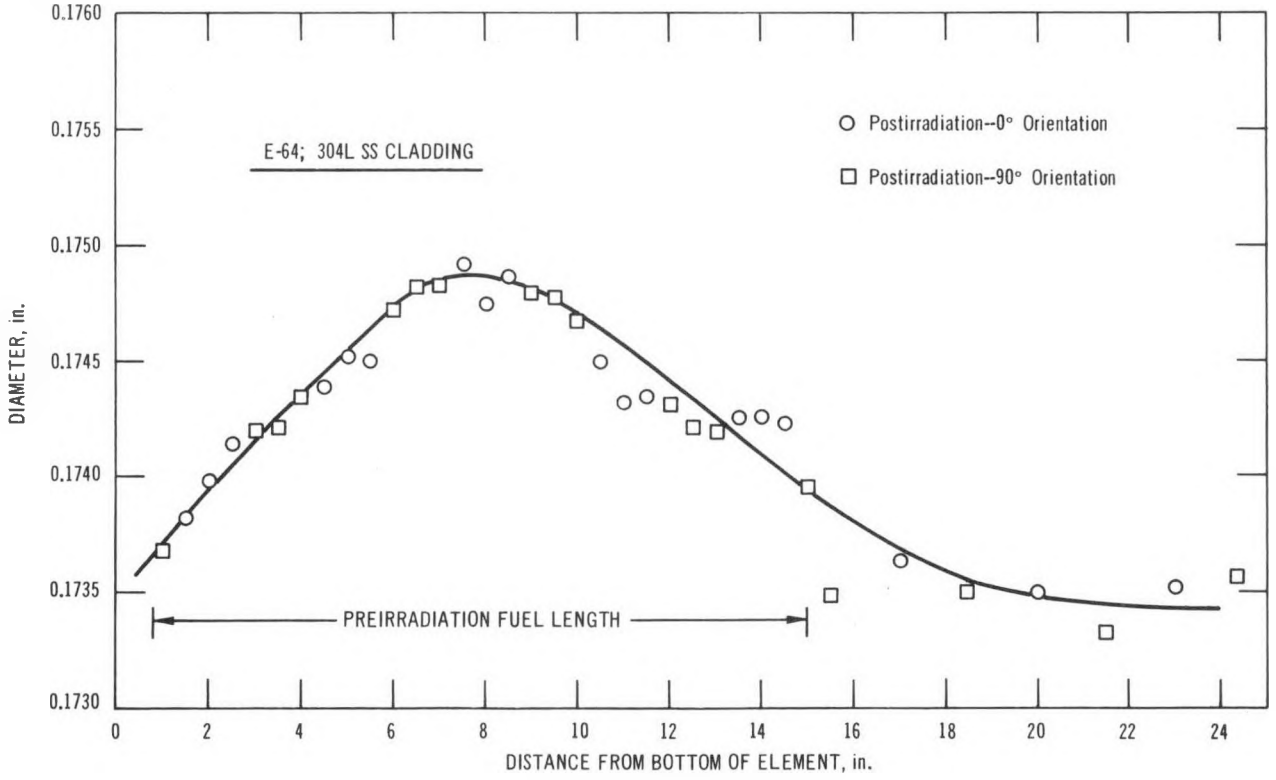

Fig. A.4 (Contd.)

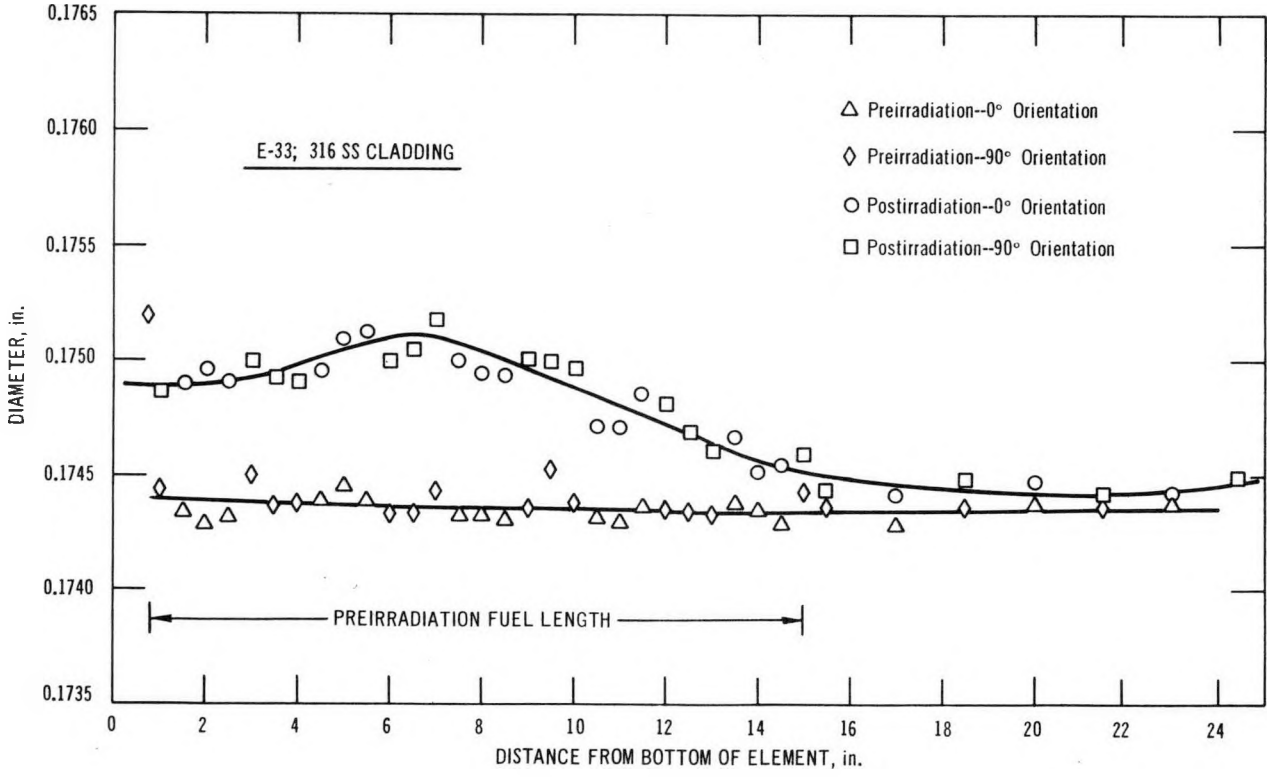

Fig. A.4 (Contd.)

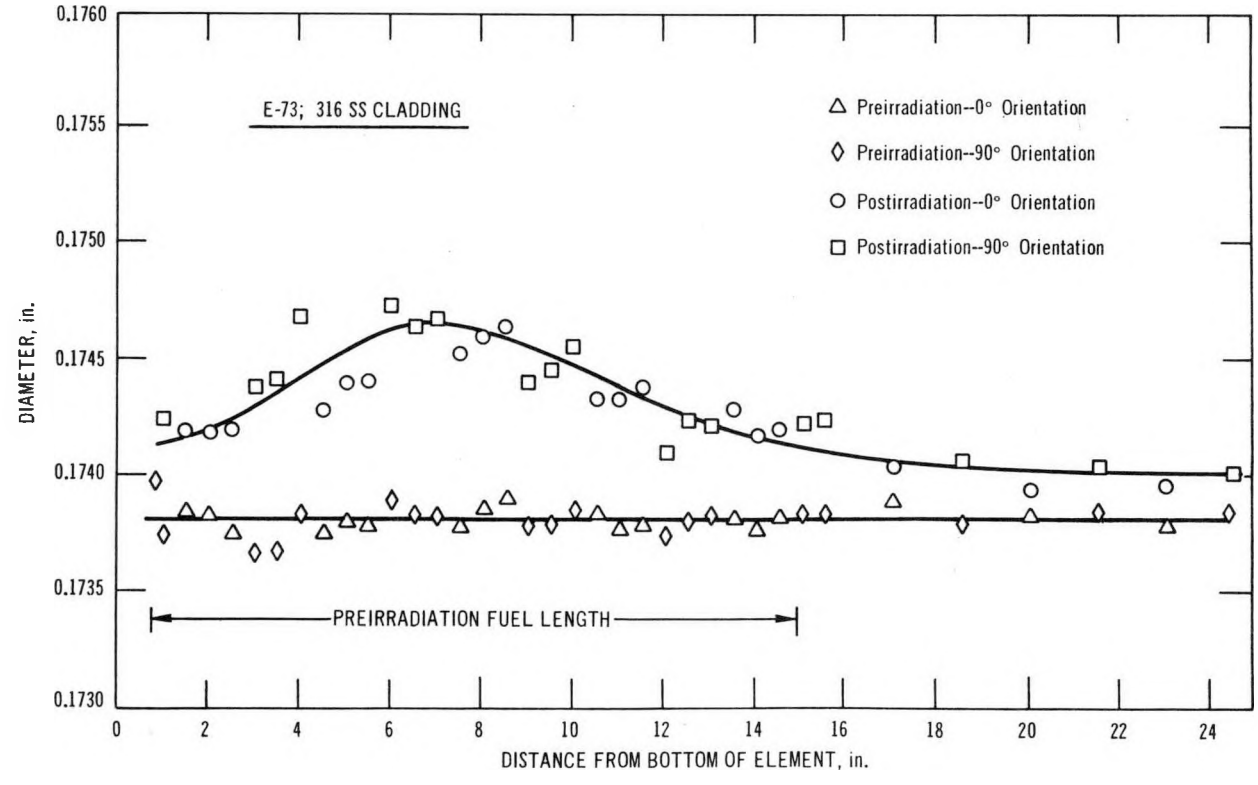

Fig. A.4 (Contd.)

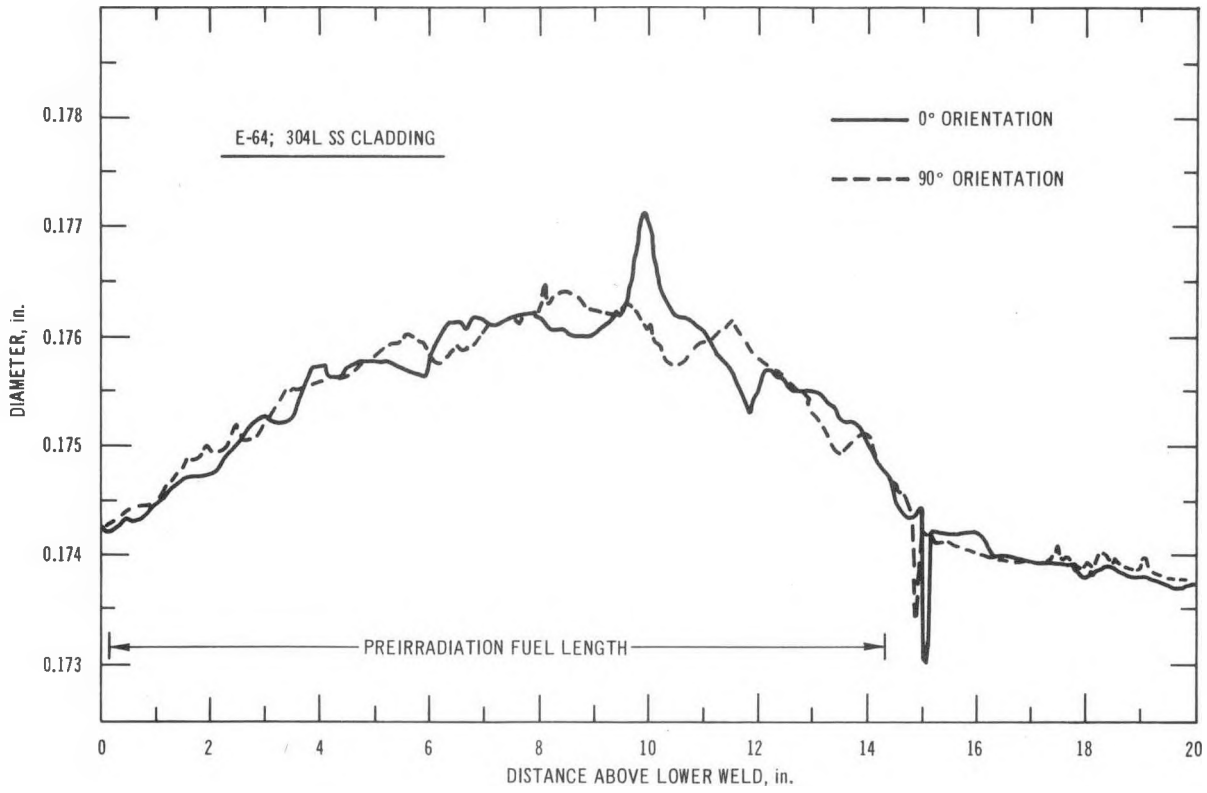

Fig. A.5. Diameter Profiles of Elements E-64, -74, -1, and -28, from Subassembly C-2234S, at ~4 at. % Burnup

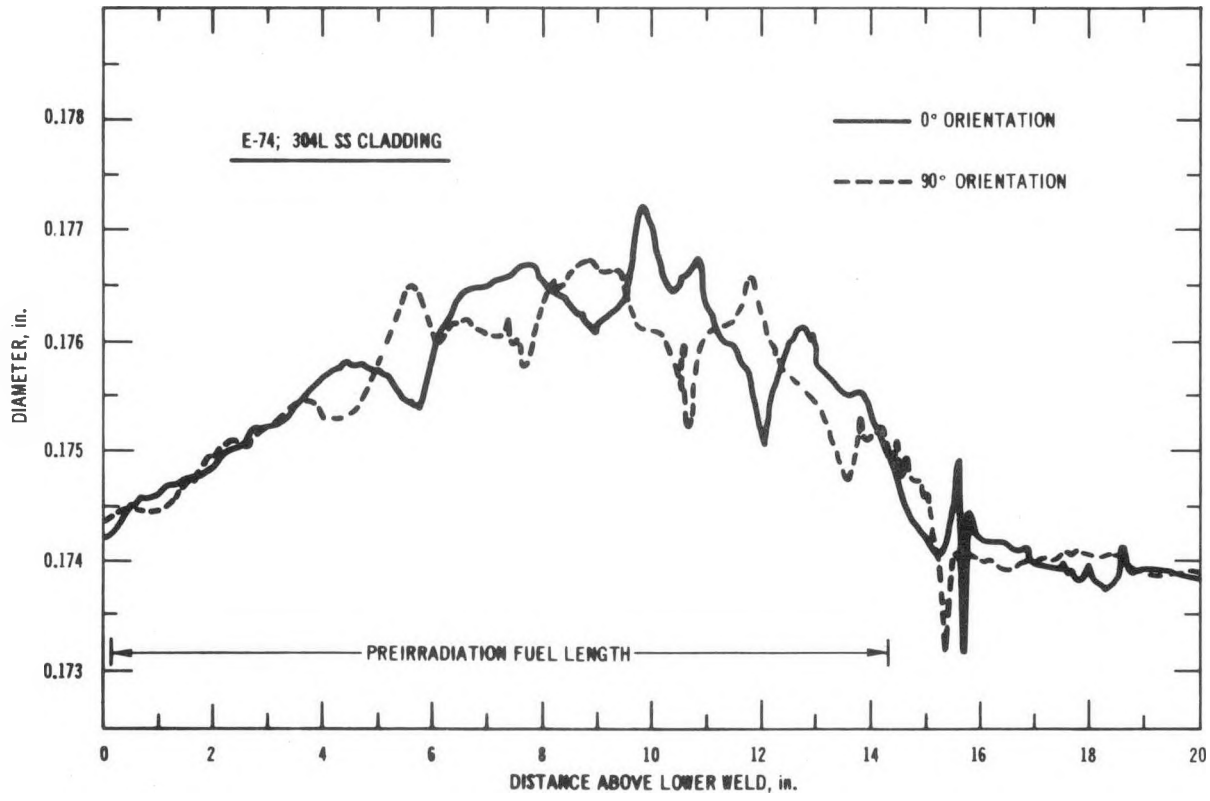

Fig. A.5 (Contd.)

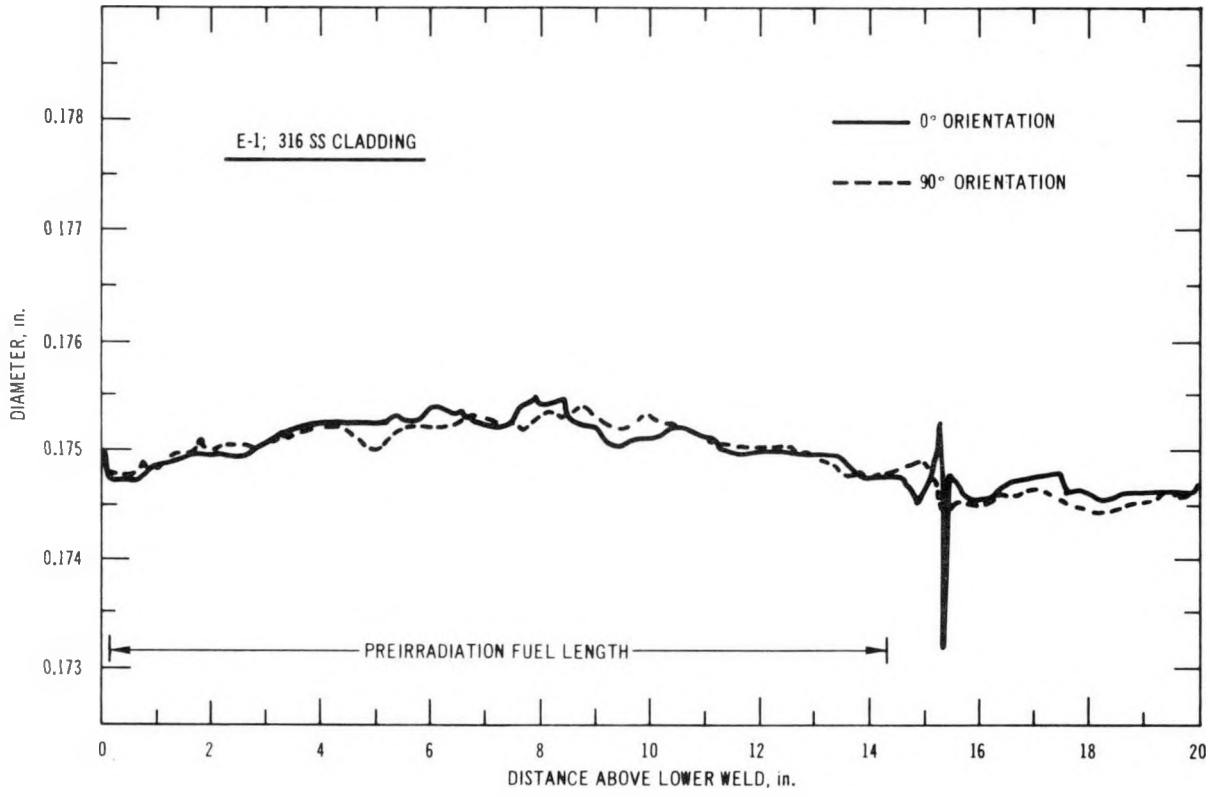

Fig. A.5 (Contd.)

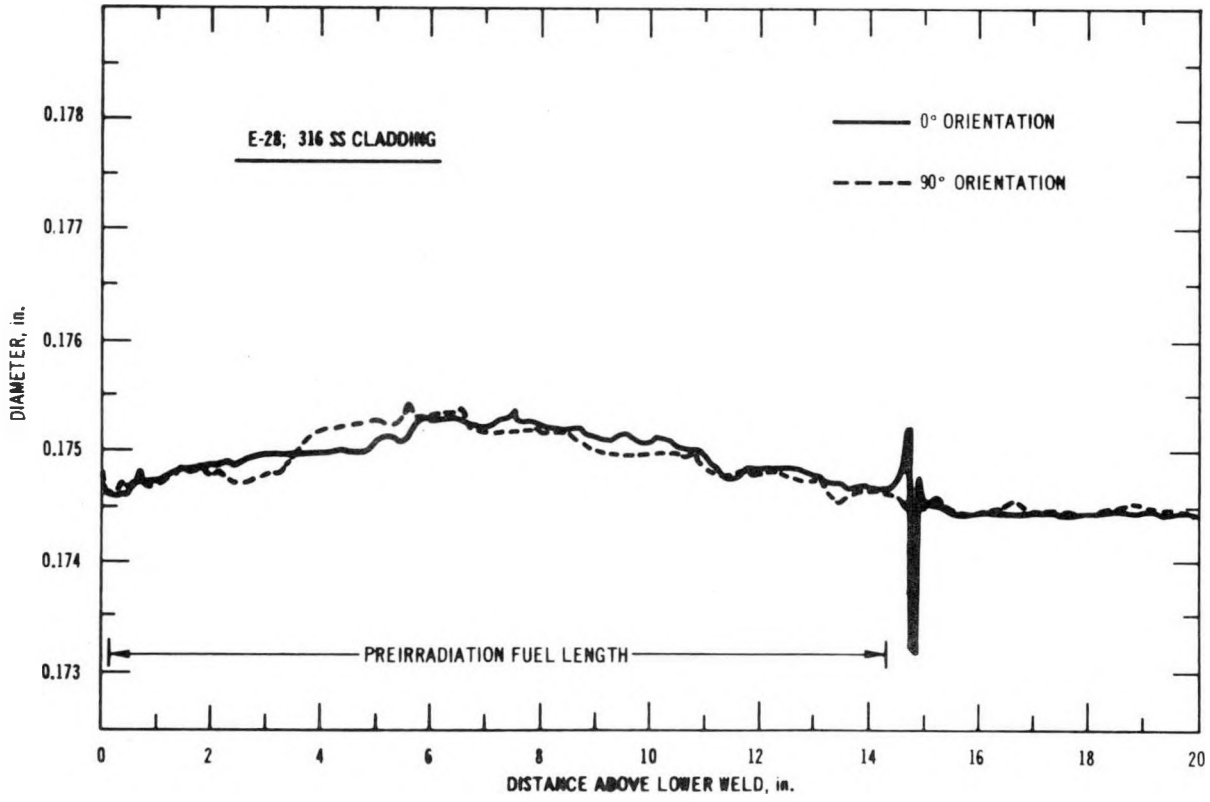

Fig. A.5 (Contd.)

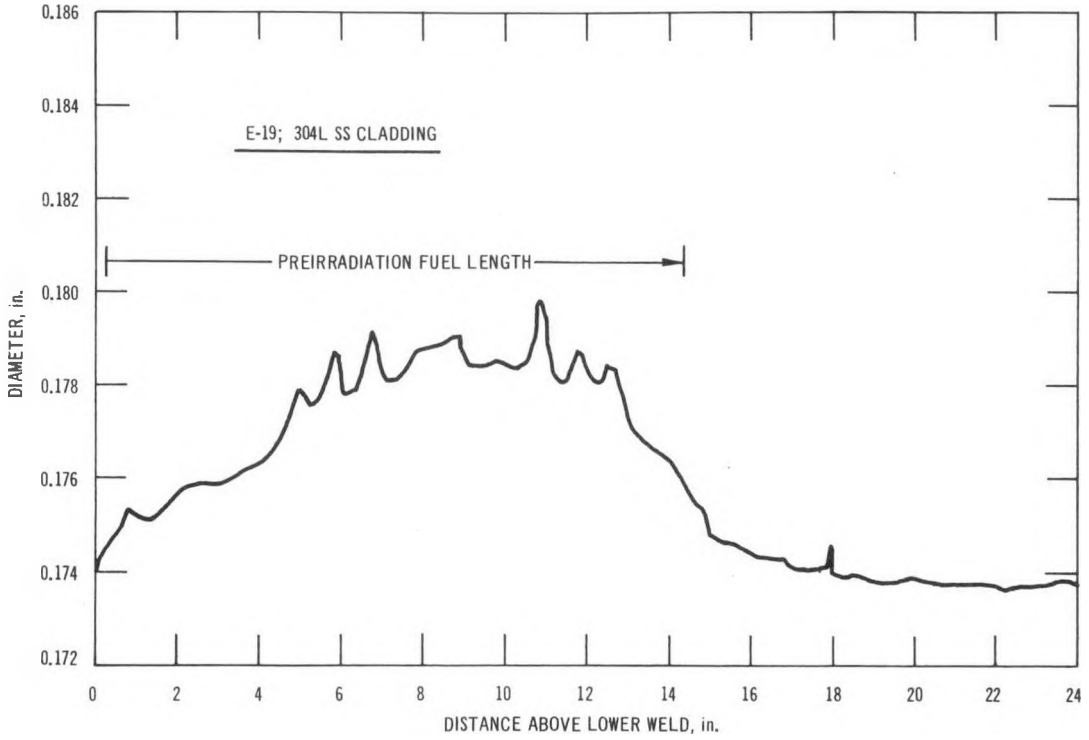

Fig. A.6. Diameter Profiles of Elements E-19, -59, -18, -33, -68, and -67, from Subassembly C-2236S, at ~6 at. % Burnup

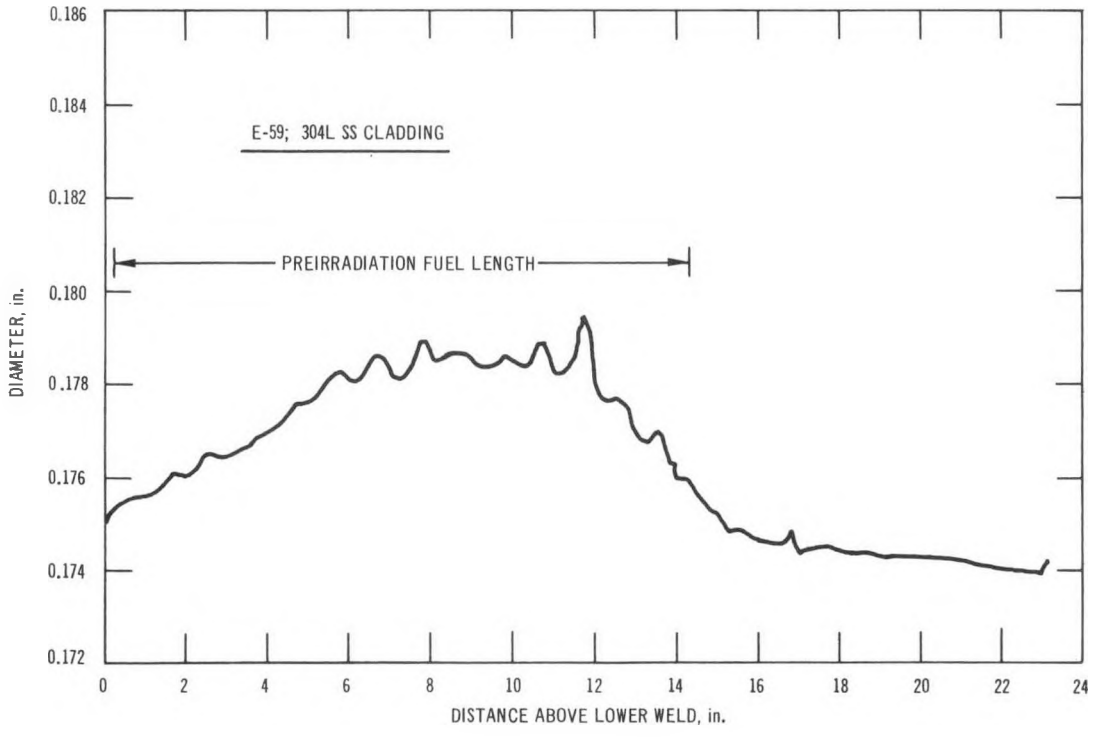

Fig. A.6 (Contd.)

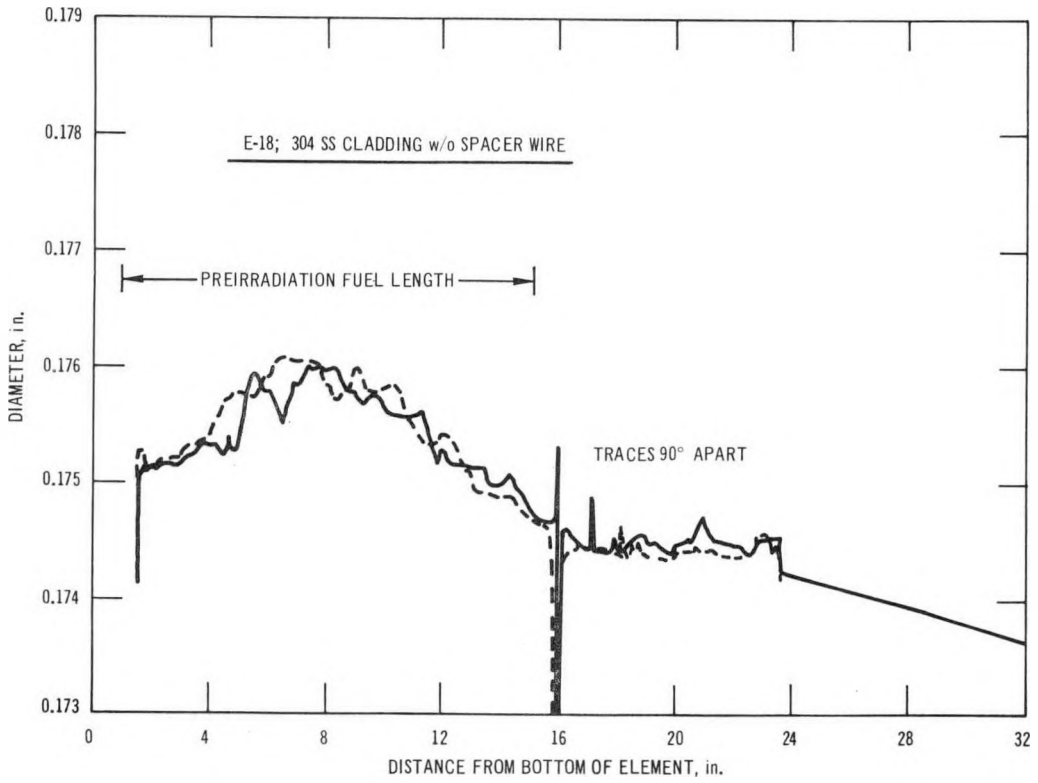

Fig. A.6 (Contd.)

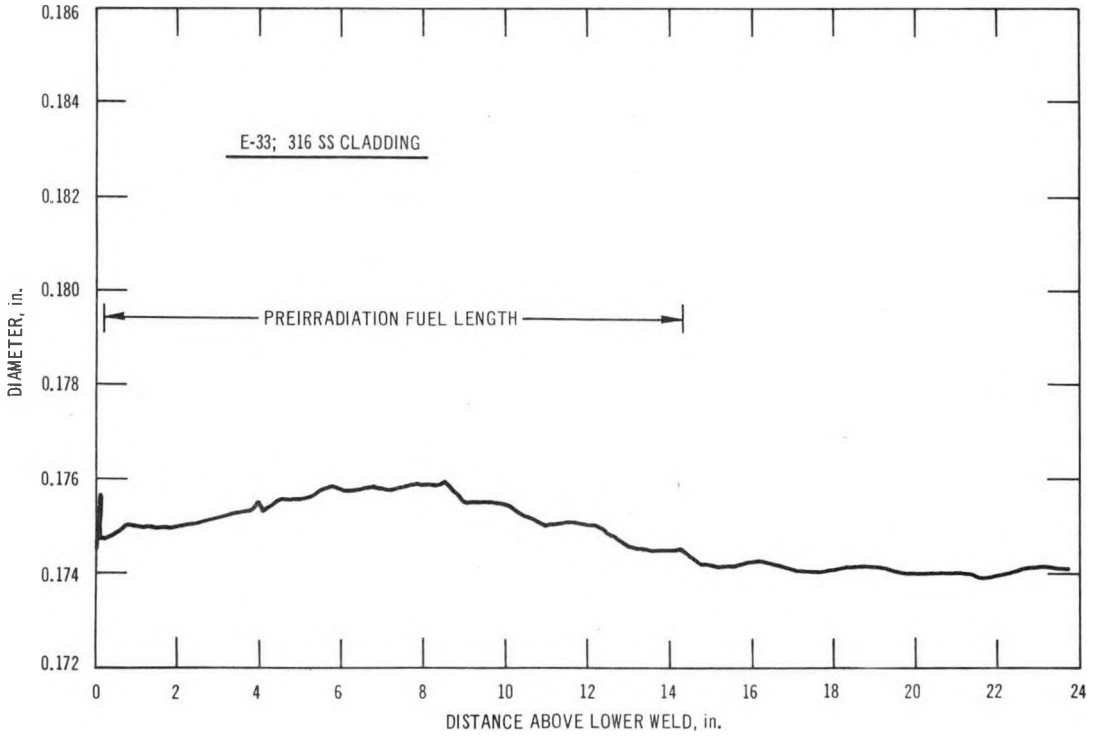

Fig. A.6 (Contd.)

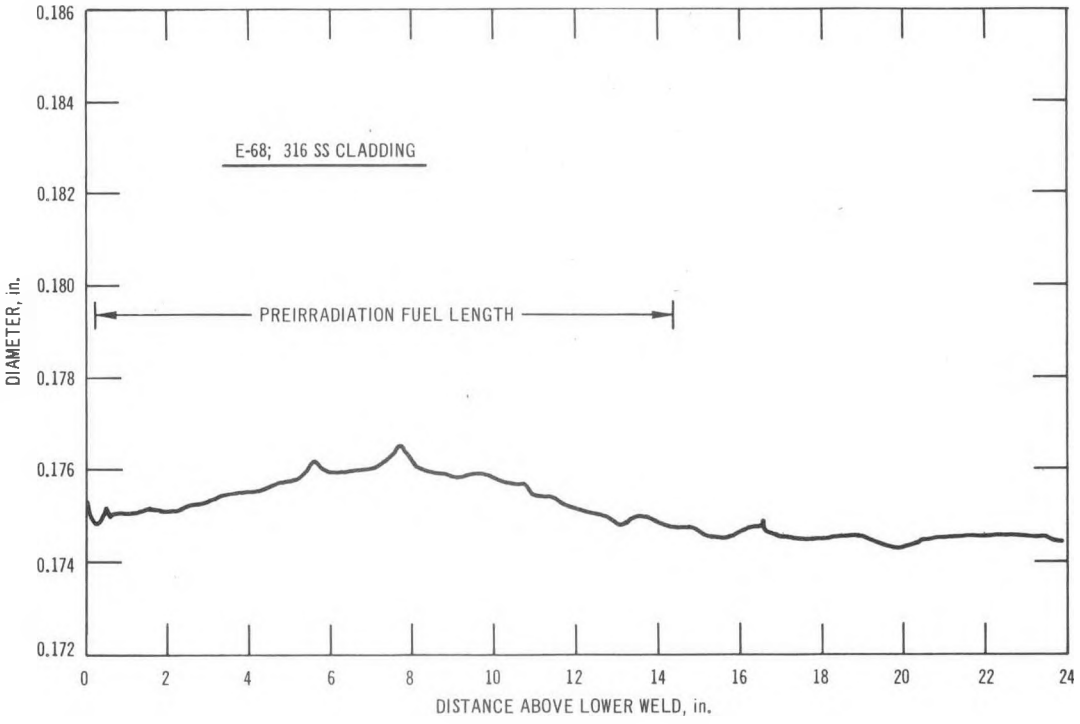

Fig. A.6 (Contd.)

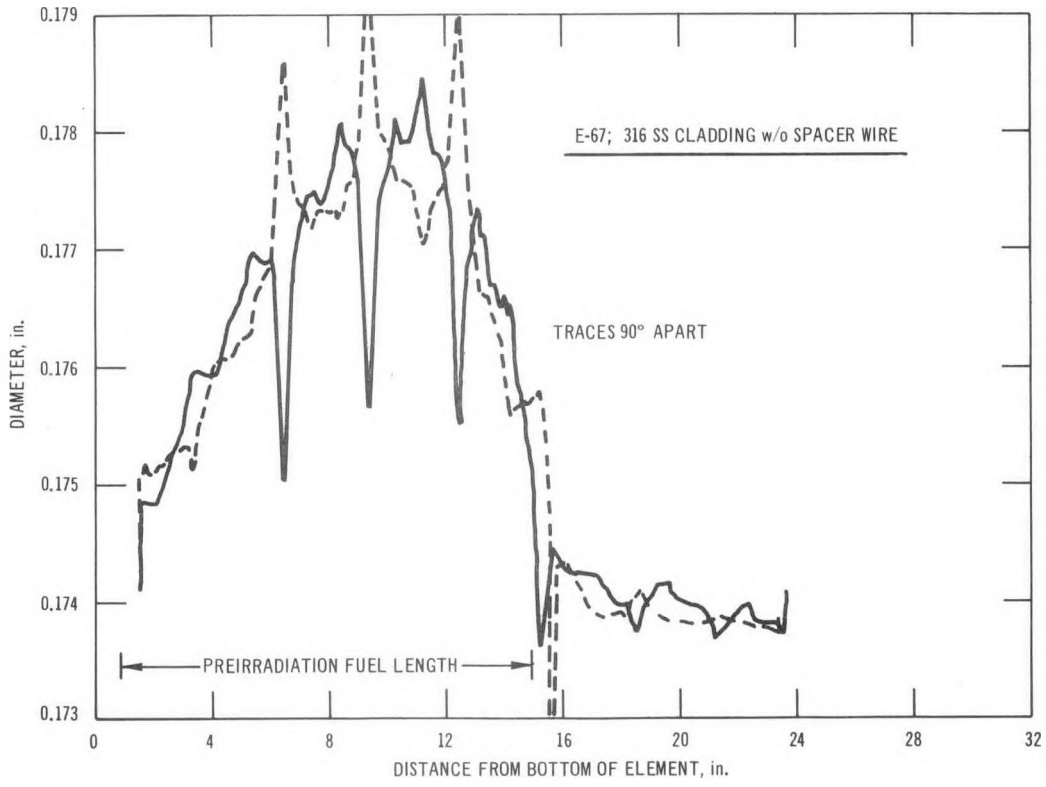

Fig. A.6 (Contd.)

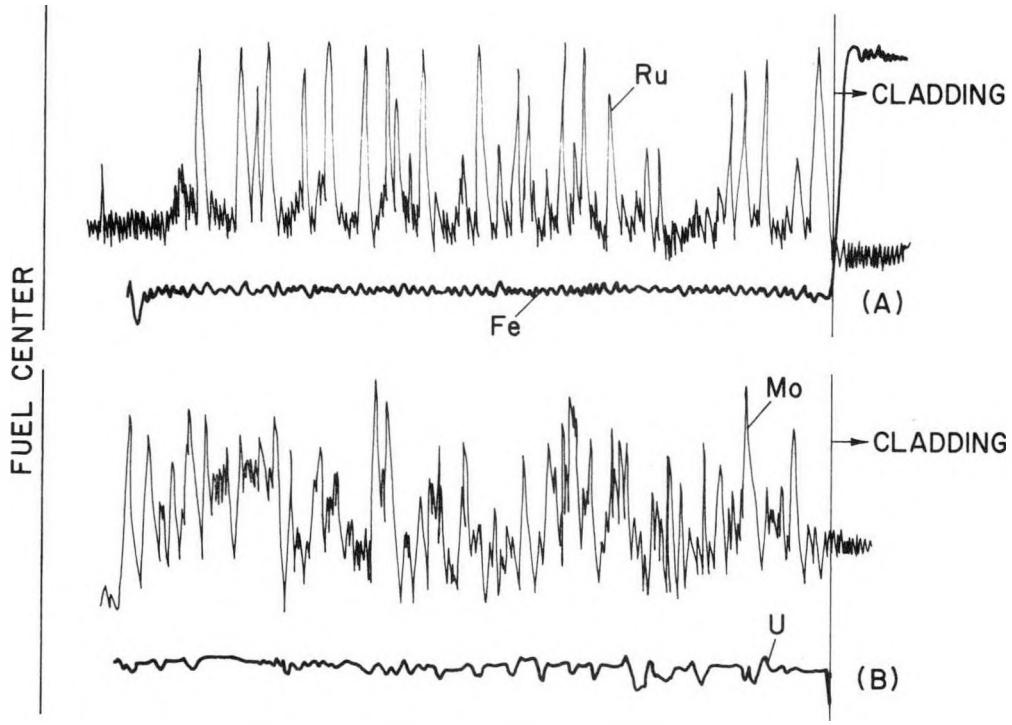

Fig. A.7. Radial Microprobe Traces of Element E-18, from Subassembly C-2236S, at ~6 at. % Burnup. (A) and (B): Top end of fuel column; (C) and (D): core-midplane location of fuel column; (E) and (F): bottom end of fuel column. (Amplitudes are in arbitrary units.)

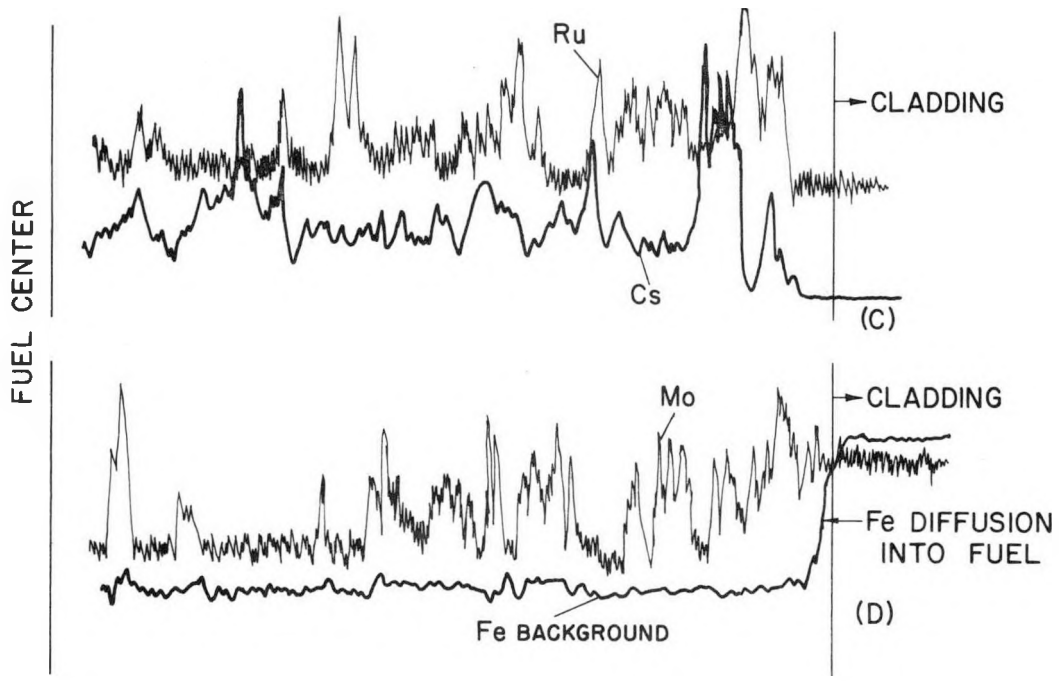

Fig. A.7 (Contd.)

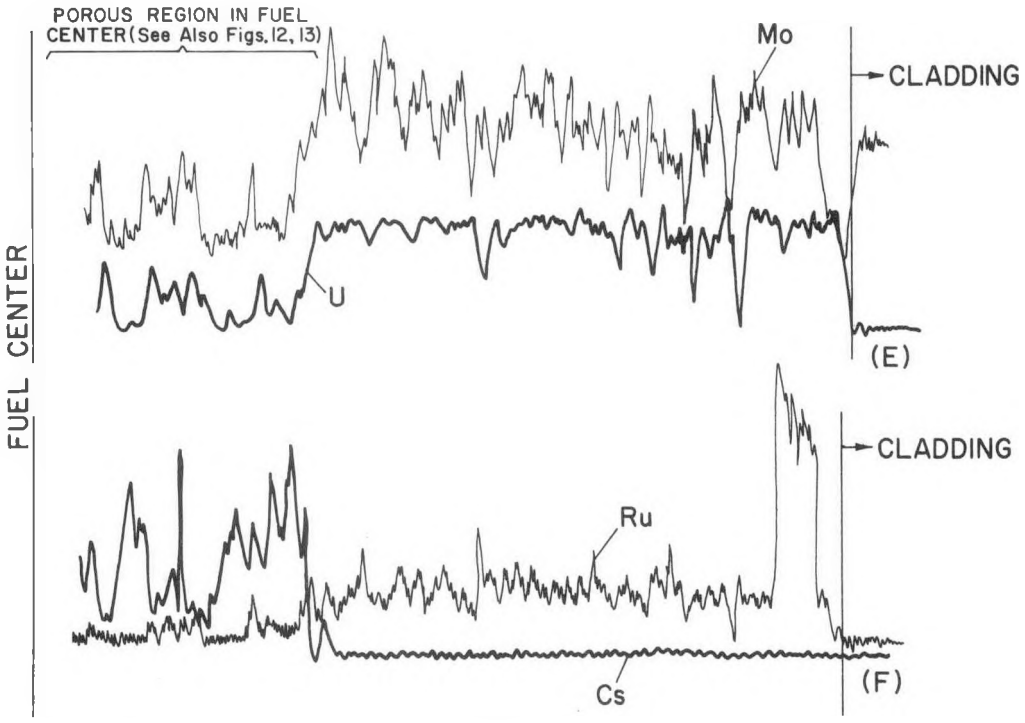
POROUS REGION IN FUEL
CENTER (See Also Figs. 12, 13)
FUEL CENTER
Mo
CLADDING
U
(E)
CLADDING
Ru
Cs
(F)

Fig. A.7 (Contd.)

APPENDIX B

Metallography

This appendix contains the results of the postirradiation metallography of the following elements:

Subassembly No.	Burnup, at. %	Element No.	SS Cladding	Fig. No.
C-2201S	~2	E-24	304L	B.1-B.13
		E-33	316	
C-2203S	~3	E-46	316	B.14-B.21
		E-73	316	
C-2234S	~4	E-1	316	B.22-B.37
		E-28	316	
		E-64	304L	
		E-74	304L	
C-2236S	~6	E-18	316	B.38-B.49
		E-24	304L	

1. Subassembly C-2201S; ~2 at. % Burnup

Element E-24--Type 304L Stainless Steel Cladding
Element E-33--Type 316 Stainless Steel Cladding

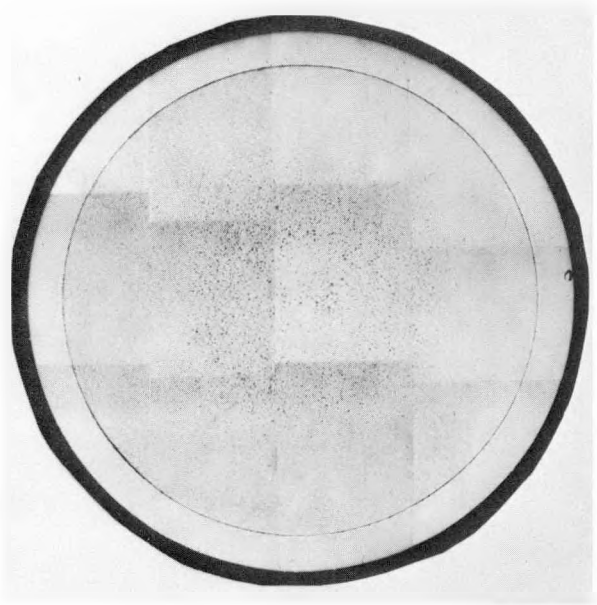

Fig. B.1. Cross Section of Element E-24, Subassembly C-2201S: 1 in. from Bottom of Fuel; ~2 at. % Burnup. As polished. Mag. 16.5X.

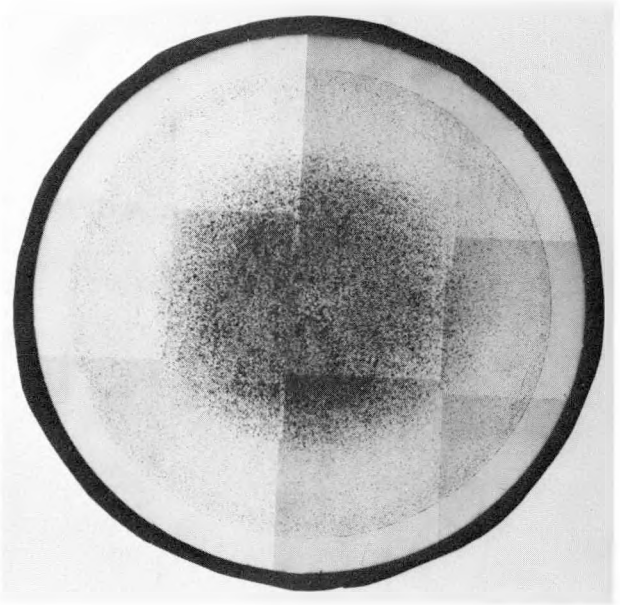

Fig. B.2. Cross Section of Element E-24, Subassembly C-2201S: 7 in. from Bottom of Fuel; ~2 at. % Burnup. As polished. Mag. 16.5X.

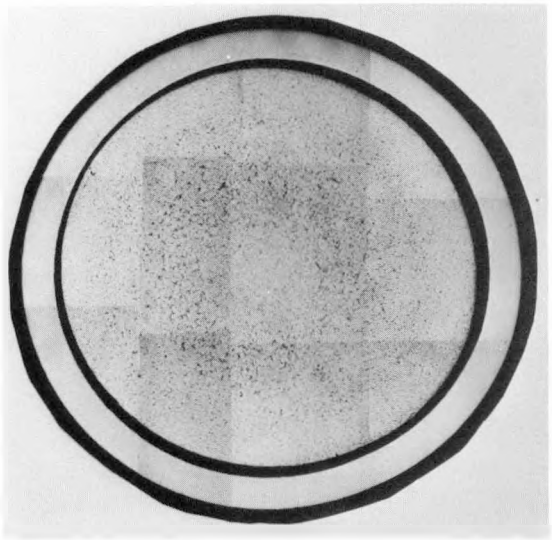

Fig. B.3

Cross Section of Element E-24, Subassembly C-2201S: 14 in. from Bottom of Fuel; ~2 at. % Burnup. As polished. Mag. 15X.

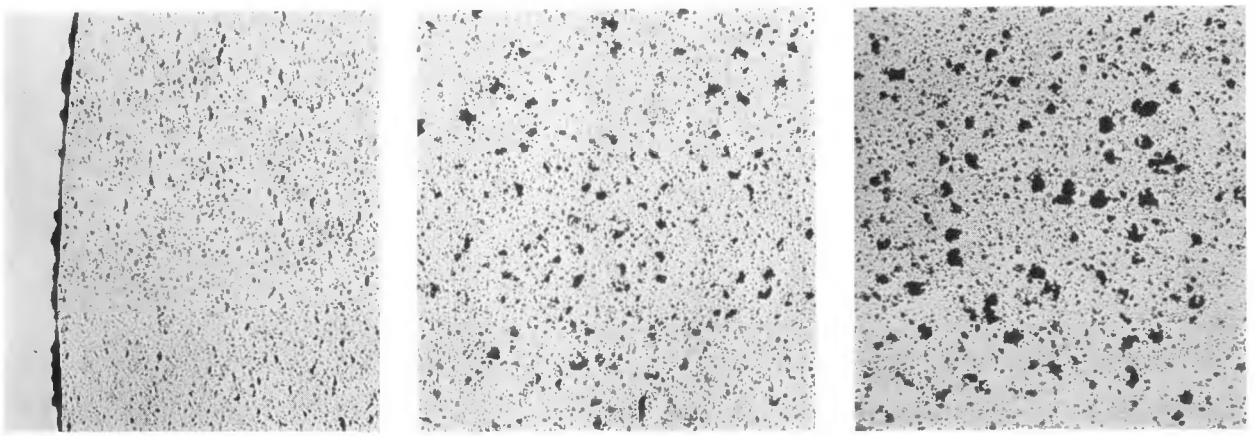

OD OF FUEL R/2 OF FUEL CENTER OF FUEL

Fig. B.4. Micrographs of Fuel of Element E-24, Subassembly C-2201S: 3 in. from Bottom of Fuel; ~2 at. % Burnup. As polished. Mag. 150X.

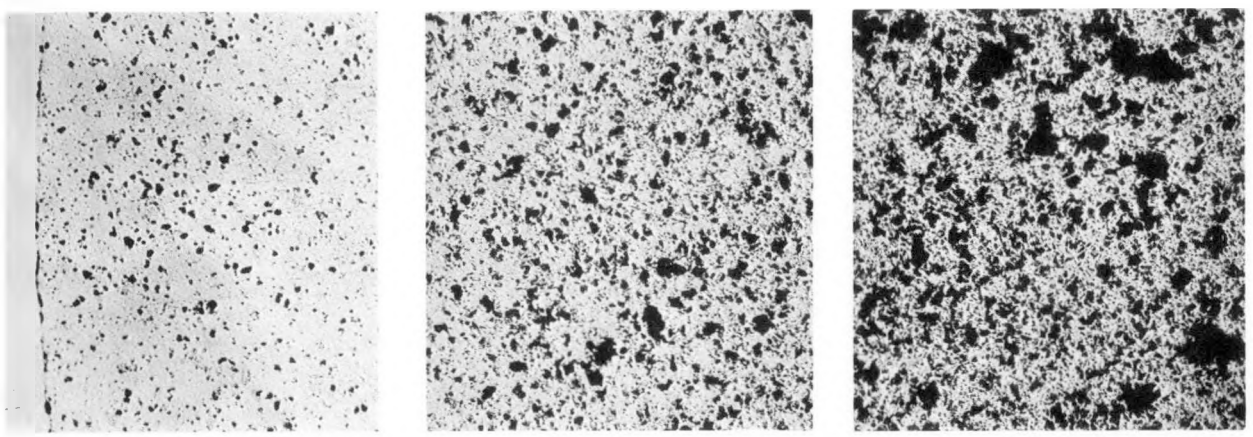

OD OF FUEL R/2 OF FUEL CENTER OF FUEL

Fig. B.5. Micrographs of Fuel of Element E-24, Subassembly C-2201S: 7 in. from Bottom of Fuel; ~2 at. % Burnup. As polished. Mag. 150X.

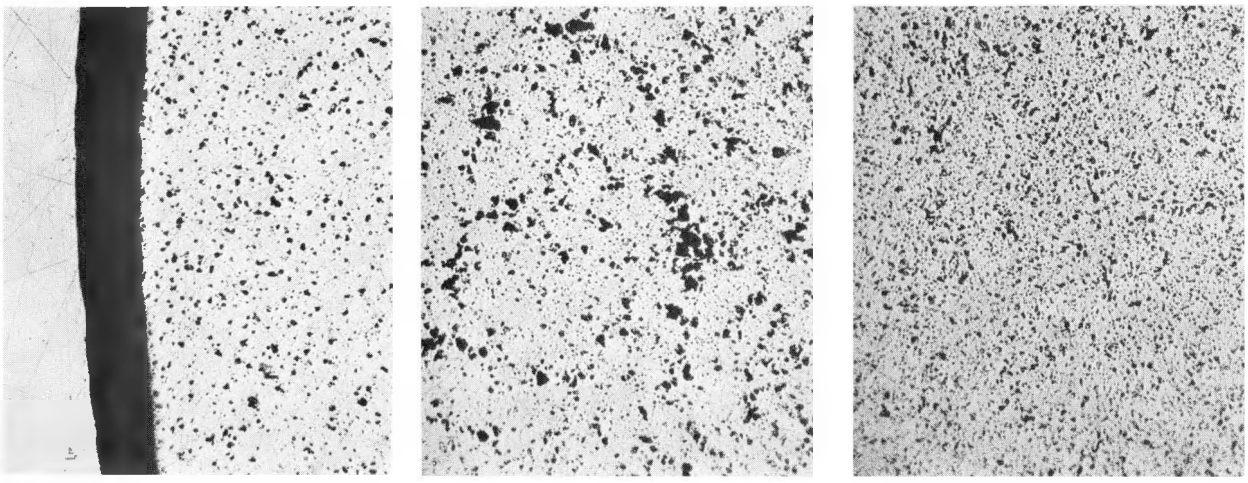

Fig. B.6. Micrographs of Fuel of Element E-24, Subassembly C-2201S: 11 in. from Bottom of Fuel; ~2 at. % Burnup. As polished. Mag. 150X.

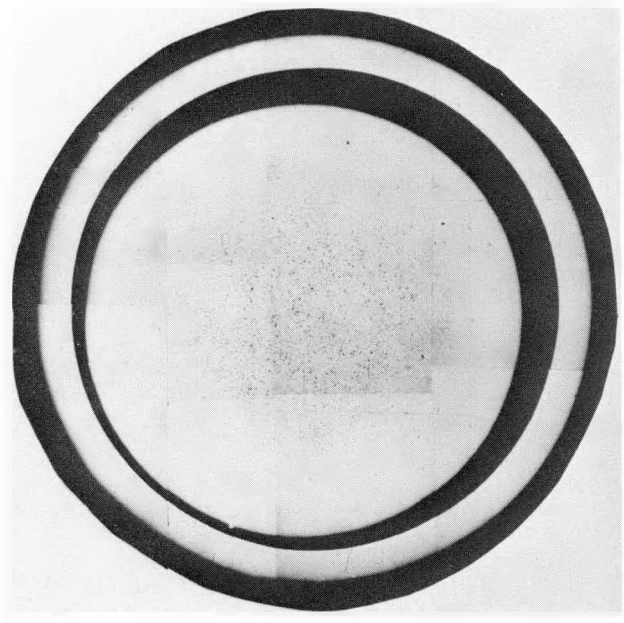

Fig. B.7. Cross Section of Element E-33, Subassembly C-2201S: 1 in. from Bottom of Fuel; ~2 at. % Burnup. As polished. Mag. 16.5X.

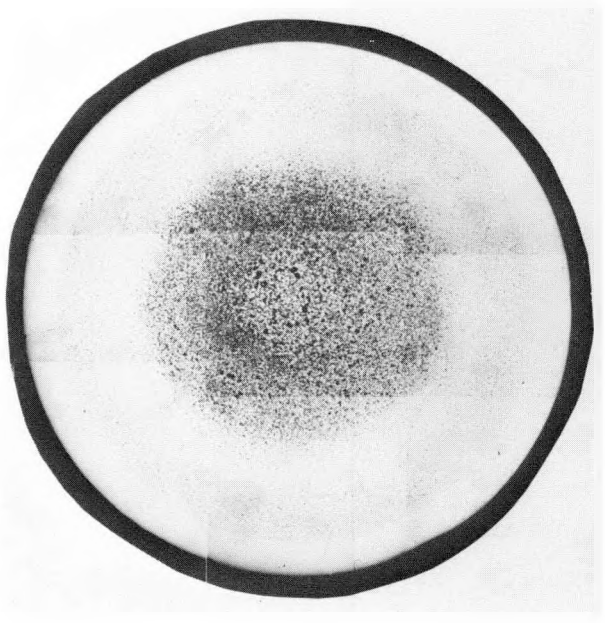

Fig. B.8. Cross Section of Element E-33, Subassembly C-2201S: 7 in. from Bottom of Fuel; ~2 at. % Burnup. As polished. Mag. 16.5X.

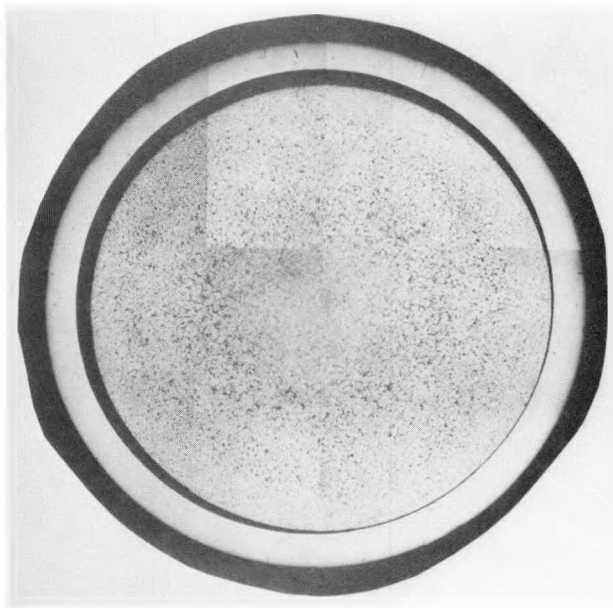

Fig. B.9. Cross Section of Element E-33, Subassembly C-2201S: 14 in. from Bottom of Fuel; ~2 at. % Burnup. As polished. Mag. 16.5X.

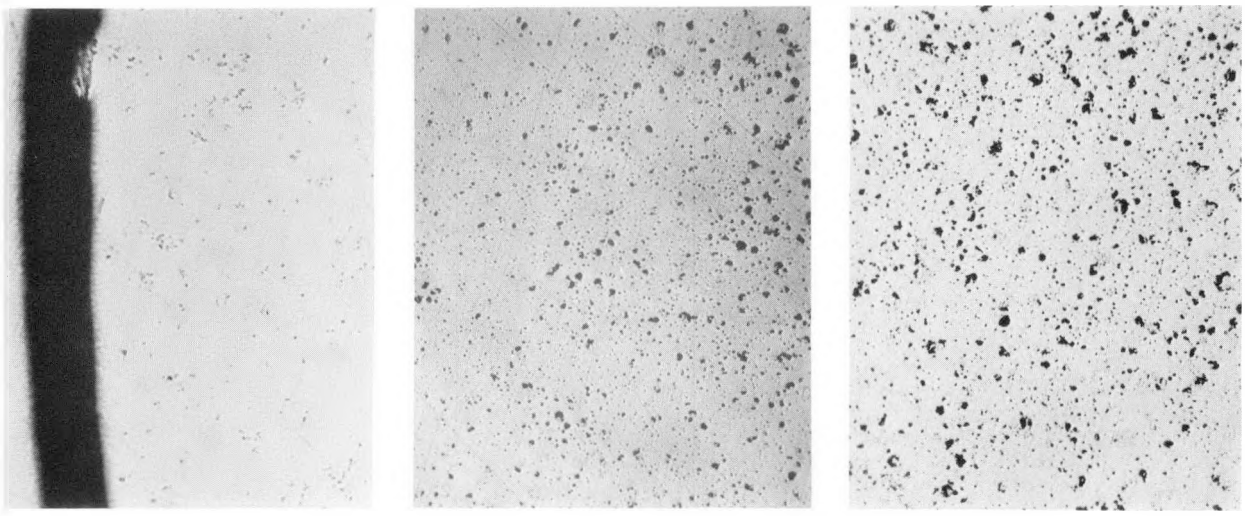

Fig. B.10. Micrographs of Fuel of Element E-33, Subassembly C-2201S: 3 in. from Bottom of Fuel; ~2 at. % Burnup. As polished. Mag. 150X.

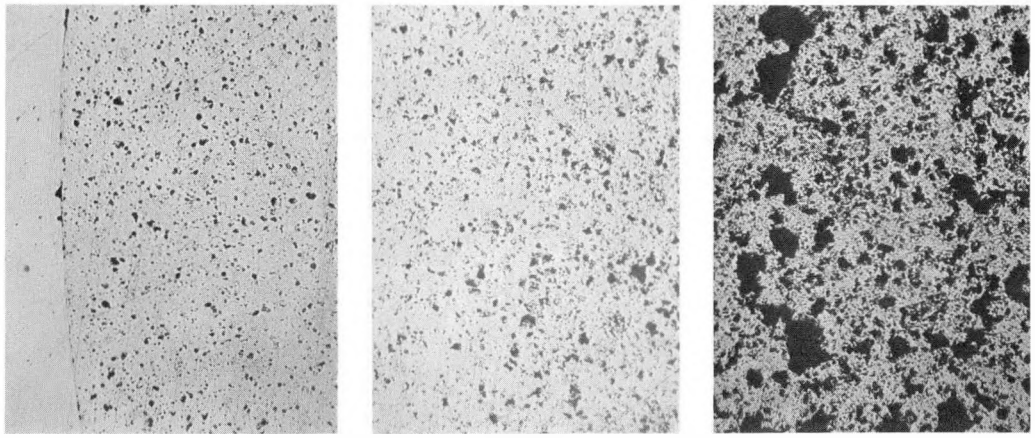

Fig. B.11. Micrographs of Fuel of Element E-33, Subassembly C-2201S: 7 in. from Bottom of Fuel; ~2 at. % Burnup. As polished. Mag. 125X.

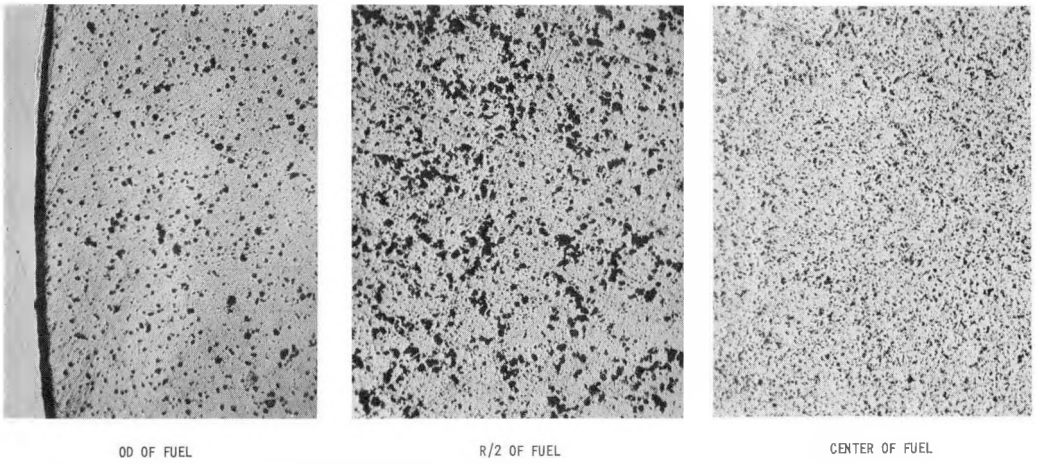

Fig. B.12. Micrographs of Fuel of Element E-33, Subassembly C-2201S: 11 in. from Bottom of Fuel; ~2 at. % Burnup. As polished. Mag. 125X.

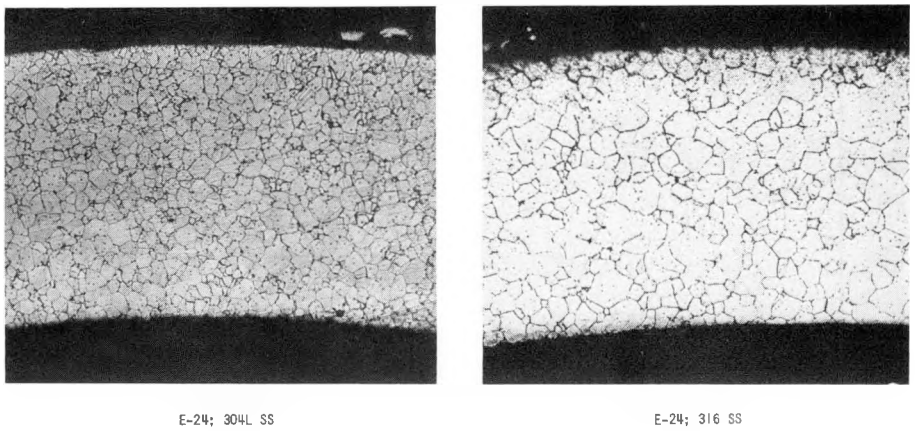

Fig. B.13. Cladding of Elements E-24 and -33, Subassembly C-2201S: 7 in. from Bottom of Fuel; ~2 at. % Burnup. Etched. Mag. 125X.

2. Subassembly C-2203S; ~3 at. % Burnup

Element E-46--Type 316 Stainless Steel Cladding
Element E-73--Type 316 Stainless Steel Cladding

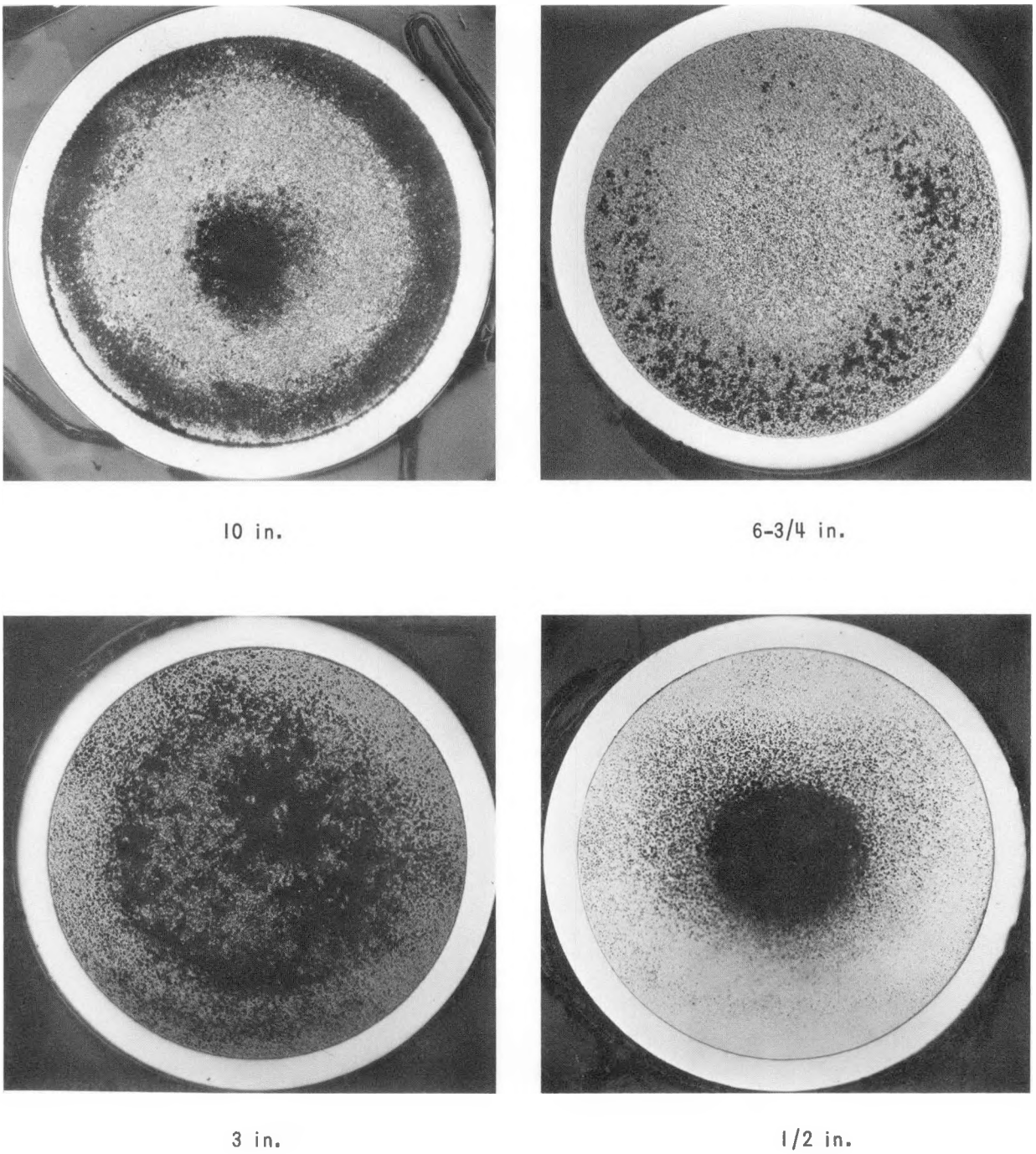

Fig. B.14. Cross Sections of Element E-46, Subassembly C-2203S, at 1/2, 3, 6-3/4, and 10 in. from Bottom of Fuel; ~3 at. % Burnup. Large darkened areas are caused by sodium residue on specimen surface. As polished. Mag. 17X. HFEF Met. Lab. Neg. Nos. 85C4-1, 85C3-1, 85C2-1, and 85C1-1.

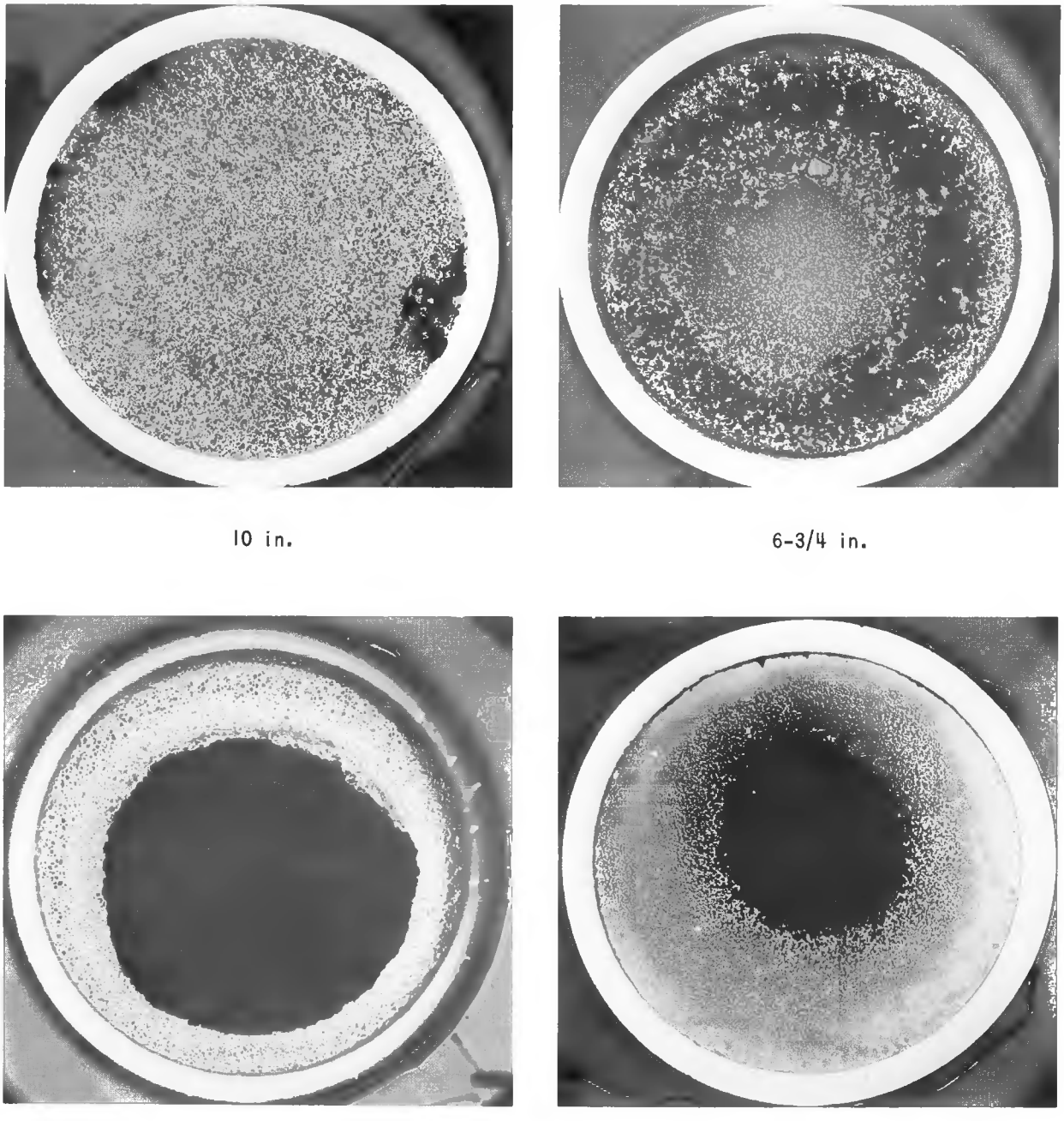

Fig. B.15. Cross Sections of Element E-73, Subassembly C-2203S, at 1/2, 3, 6-3/4, and 10 in. from Bottom of Fuel; ~3 at. % Burnup. Large darkened areas are caused by sodium residue on specimen surface except for the 3-in. section, where the dark center is a casting void. As polished. Mag. 17X. HFEF Met. Lab. Neg. Nos. 85C10-1, 85C9-1, 85C8-1, and 85C7-1.

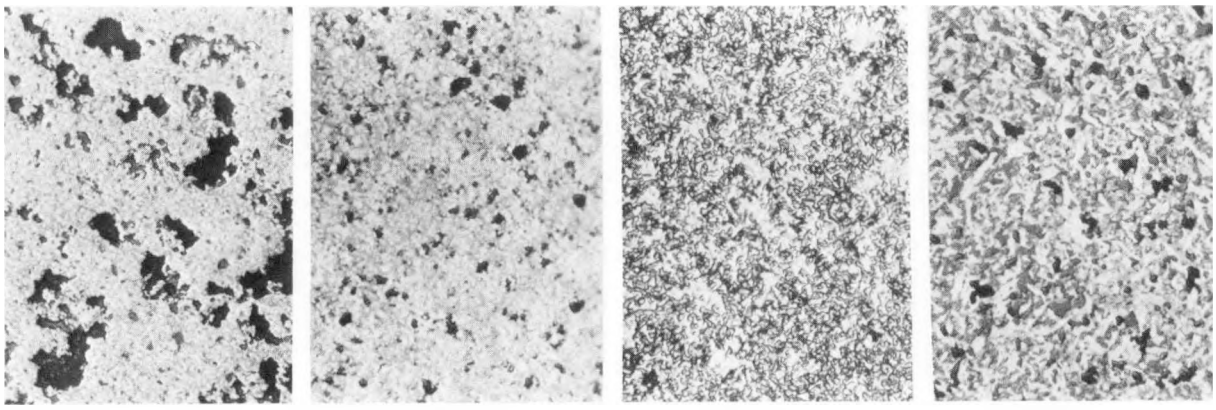

Fig. B.16. Microstructure of Fuel at Various Elevations near the Centerline of Fuel Pin in Element E–46, Subassembly C–2203S; ~3 at. % Burnup. As polished. Mag. 300X. HFEF Met. Lab. Neg. Nos. 85C1–3, 85C2–4, 85C3–3, and 85C4–3.

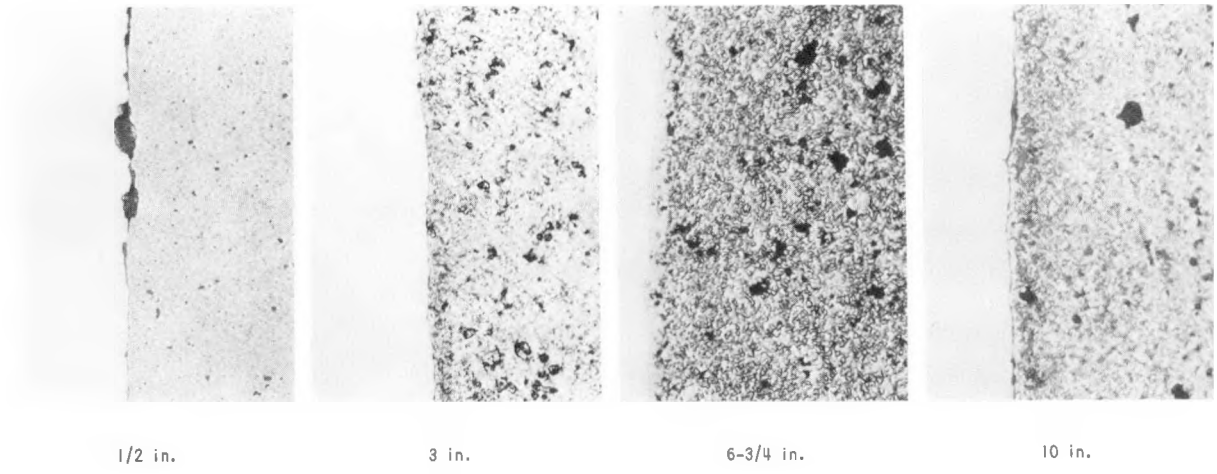

Fig. B.17. Microstructure at Various Elevations of Fuel/Cladding Interface of Element E–46, Subassembly C–2203S; ~3 at. % Burnup. As polished. Mag. 300X. HFEF Neg. Nos. 85C1–2, 85C2–3, 85C3–2, and 85C4–2.

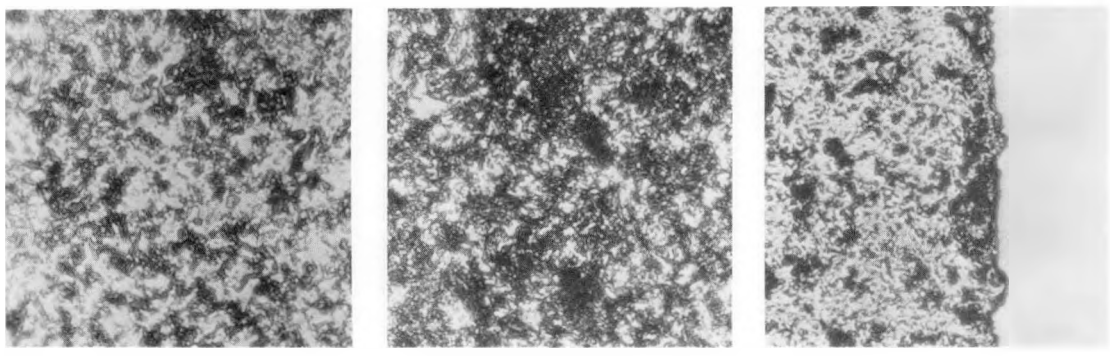

Fig. B.18. Microstructure of Fuel at (left to right) Fuel Centerline, Half the Fuel Radius, and at Fuel/Cladding Interface for Sample 6–3/4 in. from Bottom of Fuel of Element E–46, Subassembly C–2203S; ~3 at. % Burnup. Electroetched with solution of 65 ml lactic acid, 45 ml H_3PO_4, 30 ml H_2O, and 10 ml dioxane. Mag. 600X. HFEF Neg. Nos. 85C3–9, –8, and –7.

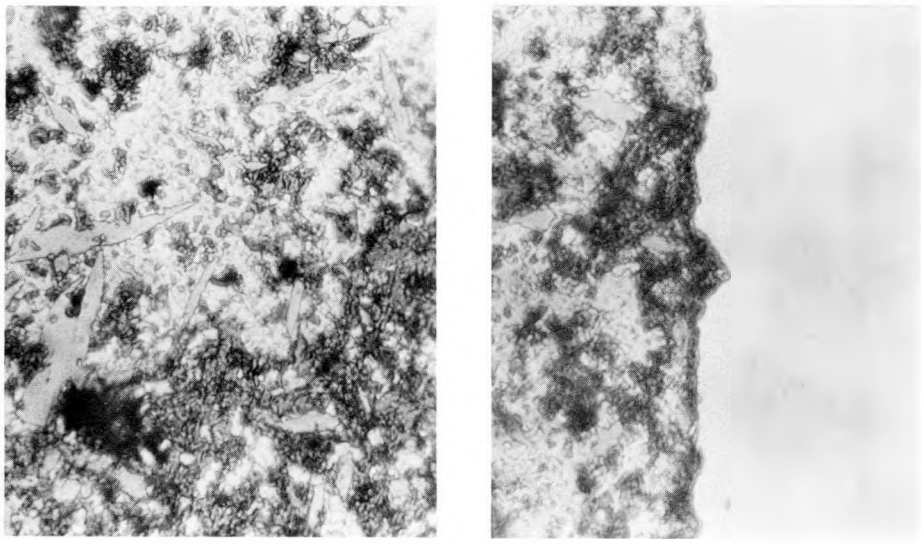

Fig. B.19. Microstructure of Fuel at Fuel Centerline (left) and Fuel/Cladding Interface for Sample 10 in. from Bottom of Fuel of Element E-73, Subassembly C-2203S; ~3 at. % Burnup. Same etch as in Fig. B.18. Mag. 700X. HFEF Met. Lab. Neg. Nos. 85C10-7 and -5.

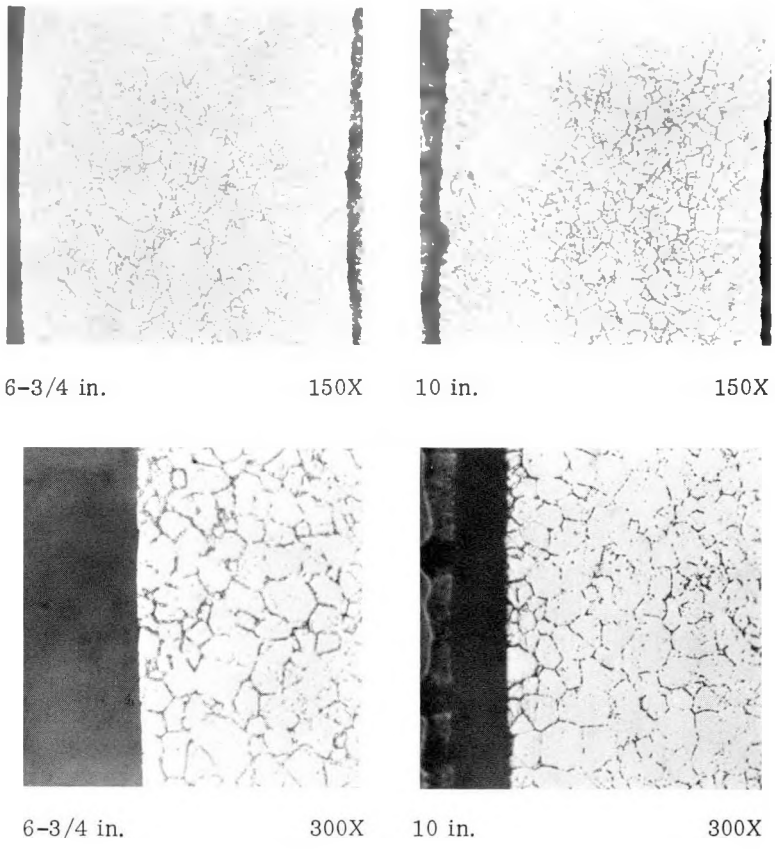

Fig. B.20. Microstructure of Type 316 Stainless Steel Cladding from High-fluence Region of Element E-46, Subassembly C-2203S; ~3 at. % Burnup. Lower micrographs show outer surface of cladding. Electroetched. HFEF Met. Lab. Neg. Nos. 85C3-4, 85C4-4, 85C3-5, and 85C4-6.

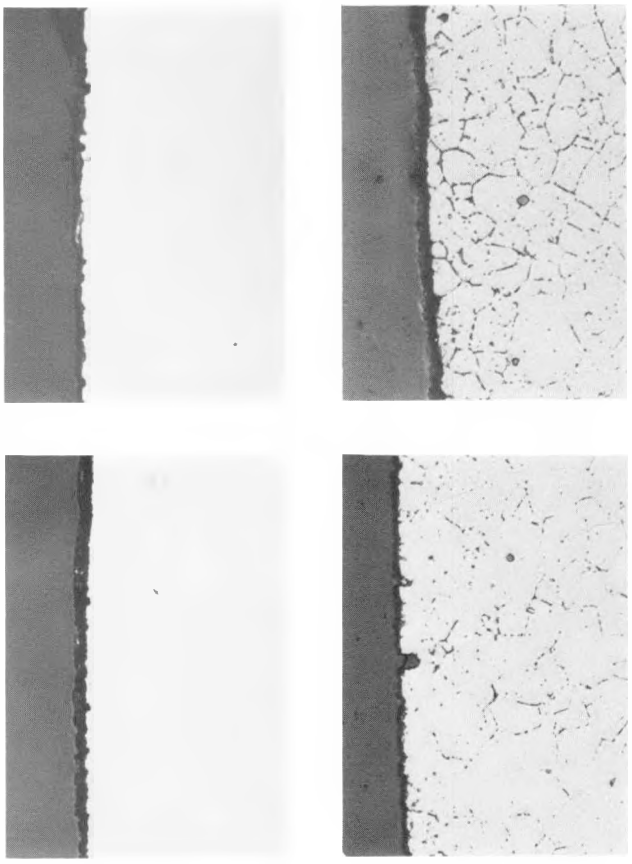

Fig. B.21

Micrographs of Typical Areas at Outer Surface of Cladding of Element E-46, Subassembly C-2203S, 15 (*top*) and 17 in. from Bottom of Fuel; ~3 at. % Burnup. Left, as polished; right, electroetched. HFEF Met. Lab. Neg. Nos. 85C11-1, 85C11-2, 85C12-1, and 85C12-2.

3. Subassembly C-2234S; ~4 at. % Burnup

Element E-1--Type 316 Stainless Steel Cladding
Element E-28--Type 316 Stainless Steel Cladding
Element E-64--Type 304L Stainless Steel Cladding
Element E-74--Type 304L Stainless Steel Cladding

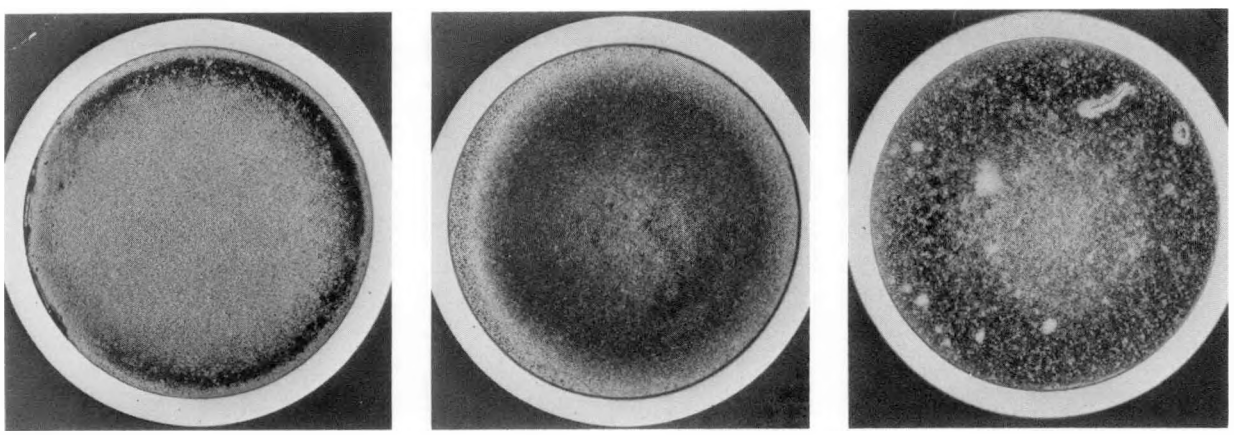

Fig. B.22. Cross Sections of Element E-1, Subassembly C-2234S, at (left to right) 1/2, 8, and 14 in. above Bottom of Fuel; ~4 at. % Burnup. As polished. Mag. 12X. HFEF Met. Lab. Neg. Nos. 37D2-1, 37D3-1, and 37D4-1.

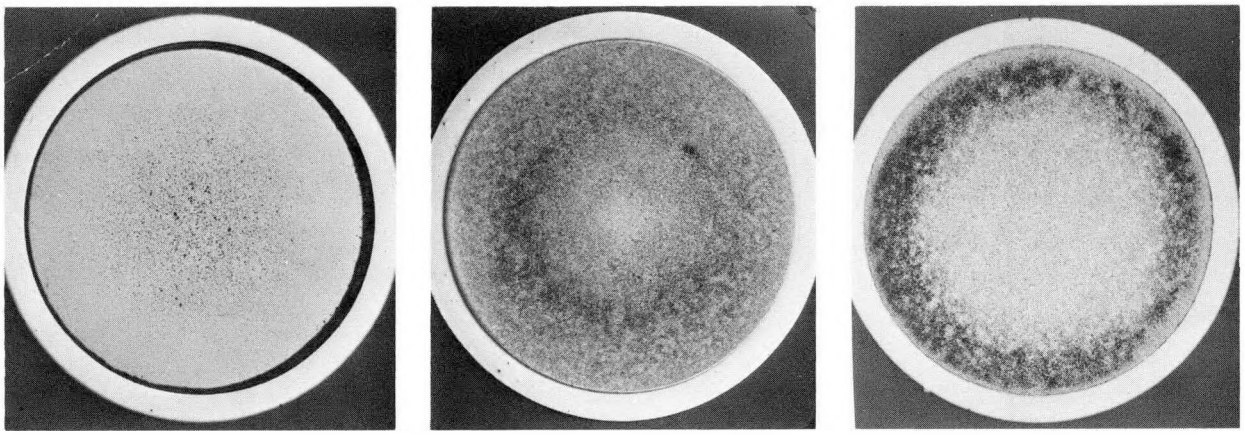

Fig. B.23. Cross Sections of Element E-28, Subassembly C-2234S, at (left to right) 1/2, 8, and 14 in. above Bottom of Fuel; ~4 at. % Burnup. As polished. Mag. 12X. HFEF Met. Lab. Neg. Nos. 38D2-1, 38D3-1, and 38D4-1.

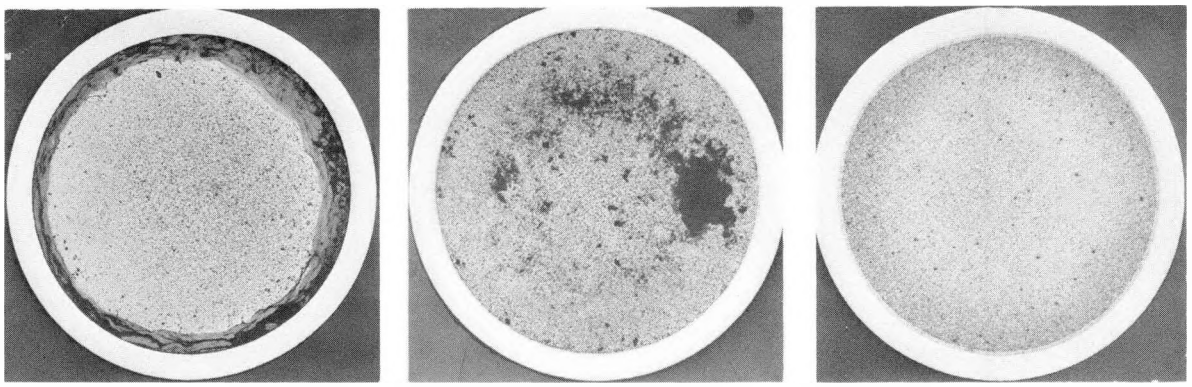

Fig. B.24. Cross Sections of Element E-64, Subassembly C-2234S, at (left to right) 1/2, 8, and 14 in. above Bottom of Fuel; ~4 at. % Burnup. As polished. Mag. 11X. HFEF Met. Lab. Neg. Nos. 44D2-1, 44D3-1, and 44D4-1.

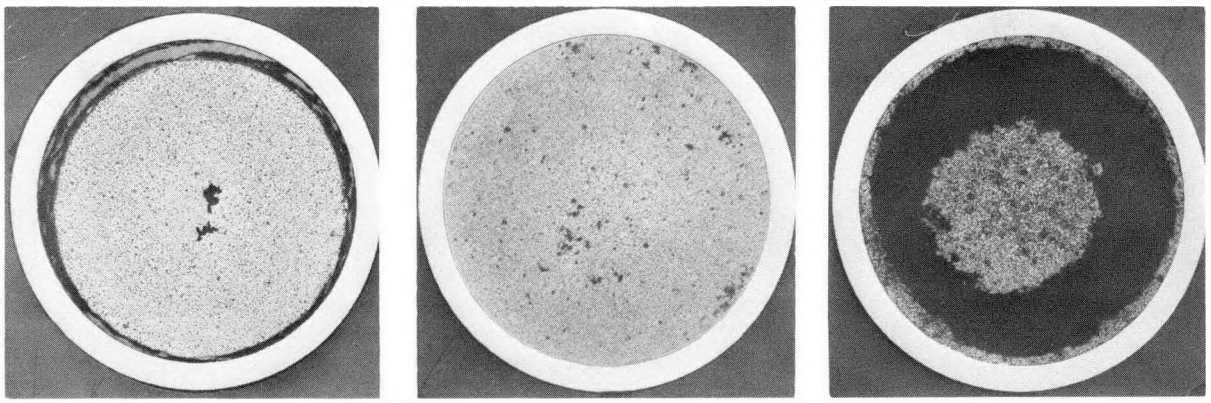

Fig. B.25. Cross Sections of Element E-74, Subassembly C-2234S, at (left to right) 1/2, 8, and 14 in. above Bottom of Fuel; ~4 at. % Burnup. As polished. Mag. 11X. HFEF Met. Lab. Neg. Nos. 45D2-1, 45D3-1, and 45D4-1.

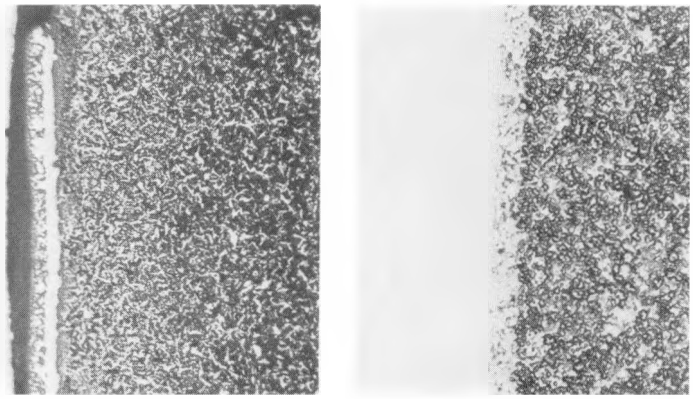

Fig. B.26

Typical Areas of Fuel/Cladding Interface at 1/2 (left) and 8 in. above Bottom of Fuel in Element E-1, Subassembly C-2234S; ~4 at.% Burnup. As polished. Mag. 300X. HFEF Met. Lab. Neg. Nos. 37D2-3 and 37D3-4.

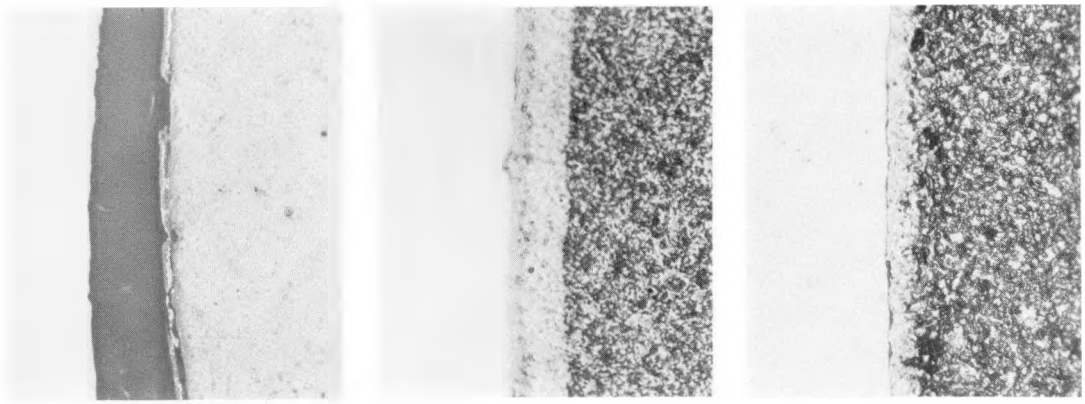

Fig. B.27. Typical Areas of Fuel/Cladding Interface at (left to right) 1/2, 8, and 14 in. above Bottom of Fuel in Element E-28, Subassembly C-2234S; ~4 at. % Burnup. As polished. HFEF Met. Lab. Neg. Nos. 38D2-3, 38D3-3, and 38D4-3.

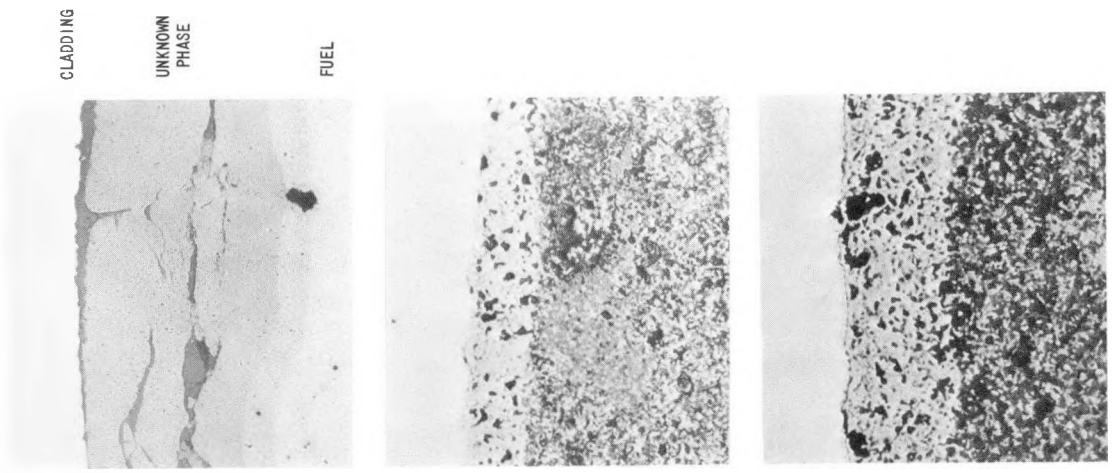

Fig. B.28. Typical Areas of Fuel/Cladding Interface at (left to right) 1/2, 8, and 14 in. above Bottom of Fuel in Element E-64, Subassembly C-2234S; ~4 at. % Burnup. A phase similar to the unknown phase 1/2 in. above the fuel bottom has also been observed in Mark-IA fuel and was found to contain carbon, hydrogen, and oxygen. The hydrogen was believed to have come from a carbohydride contaminant. As polished. Mag. 300X. HFEF Met. Lab. Neg. Nos. 44D2-2, 44D3-3, and 44D4-3.

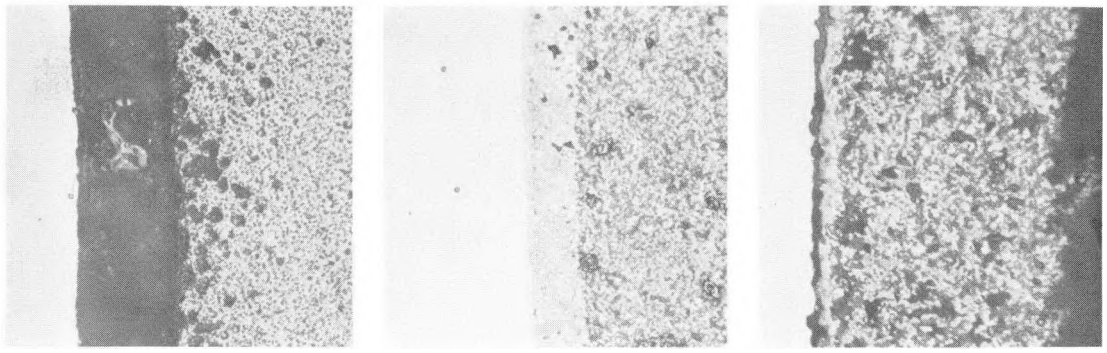

Fig. B.29. Typical Areas of Fuel/Cladding Interface at (left to right) 1/2, 8, and 14 in. above Bottom of Fuel in Element E-74, Subassembly C-2234S; ~4 at. % Burnup. As polished. Mag. 300X. HFEF Met. Lab. Neg. Nos. 45D2-6, 45D3-3, and 45D4-3.

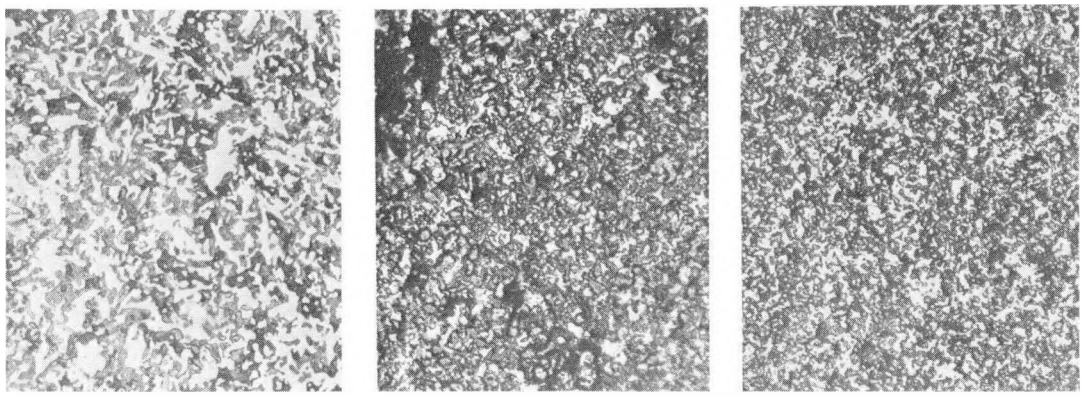

Fig. B.30. Typical Areas near Centerline of Fuel Pin at (left to right) 1/2, 8, and 14 in. above Bottom of Pin in Element E-1, Subassembly C-2234S; ~4 at. % Burnup. As polished. Mag. 300X. HFEF Met. Lab. Neg. Nos. 37D2-2, 37D3-6, and 37D4-2.

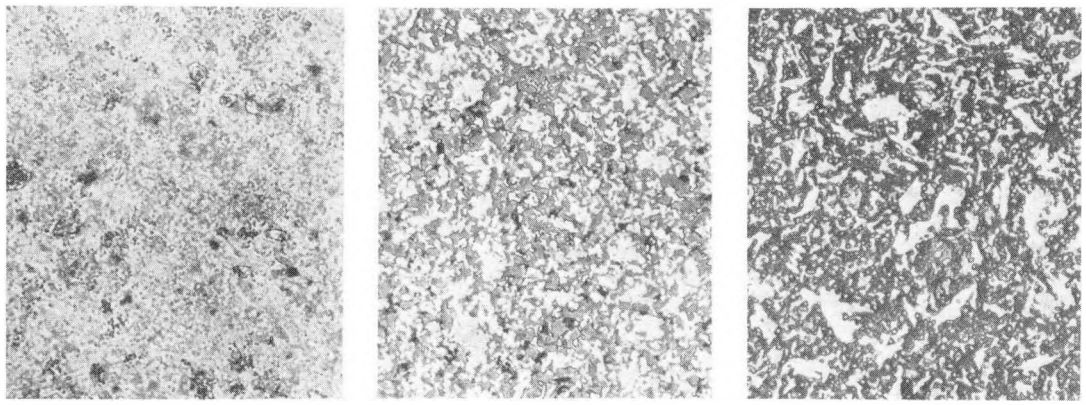

Fig. B.31. Typical Areas near Centerline of Fuel Pin at (left to right) 1/2, 8, and 14 in. above Bottom of Pin in Element E-28, Subassembly C-2234S; ~4 at. % Burnup. As polished. Mag. 300X. HFEF Met. Lab. Neg. Nos. 38D2-5, 38D3-4, and 38D4-2.

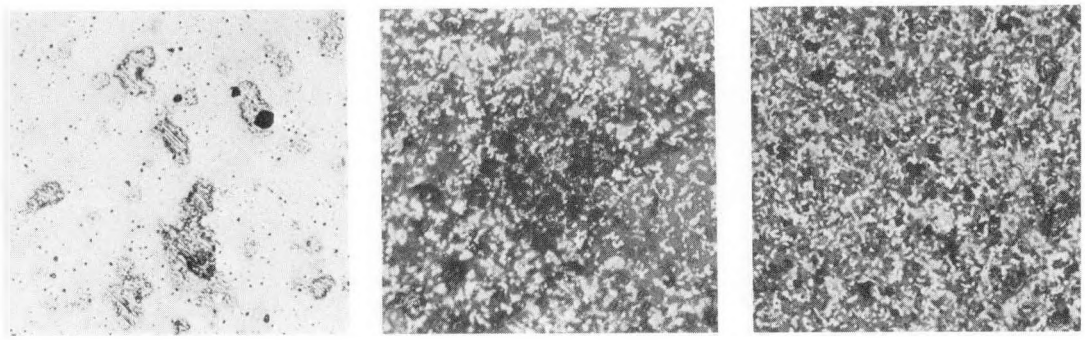

Fig. B.32. Typical Areas near Centerline of Fuel Pin at (left to right) 1/2, 8, and 14 in. above Bottom of Pin in Element E-64, Subassembly C-2234S; ~4 at. % Burnup. As polished. Mag. 300X. HFEF Met. Lab. Neg. Nos. 44D2-4, 44D3-4, and 44D4-5.

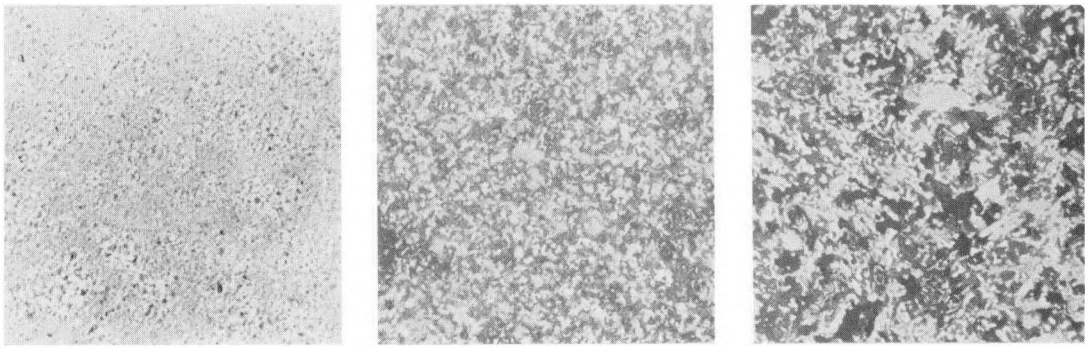

Fig. B.33. Typical Areas at Center of the Fuel Pin at (left to right) 1/2, 8, and 14 in. above Bottom of Pin in Element E-74, Subassembly C-2234S; ~4 at. % Burnup. As polished. Mag. 300X. HFEF Met. Lab. Neg. Nos. 45D2-4, 45D3-5, and 45D4-5.

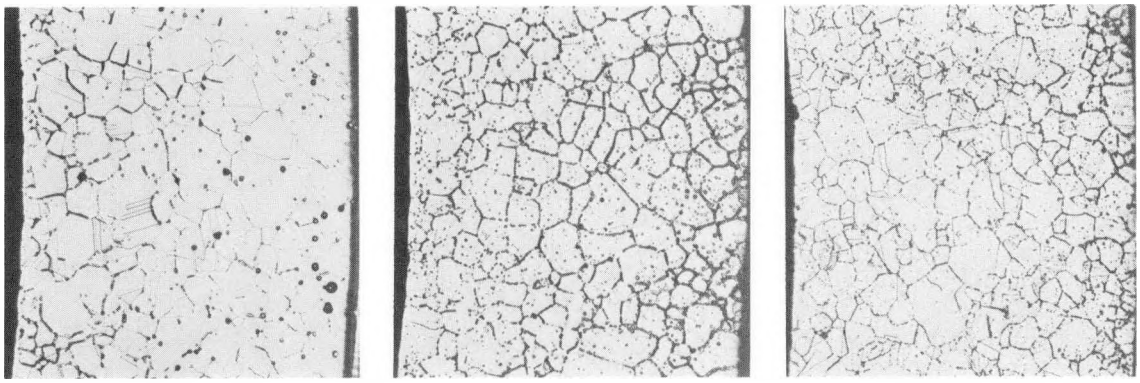

Fig. B.34. Typical Cross Sections of Cladding at (left to right) 1/2, 8, and 14 in. above Bottom of Fuel in Element E-1, Subassembly C-2234S; ~4 at. % Burnup. There is no evidence of an interaction band in the cladding. Electroetched. Mag. 150X. HFEF Neg. Nos. 37D2-5, 37D3-7, and 37D4-3.

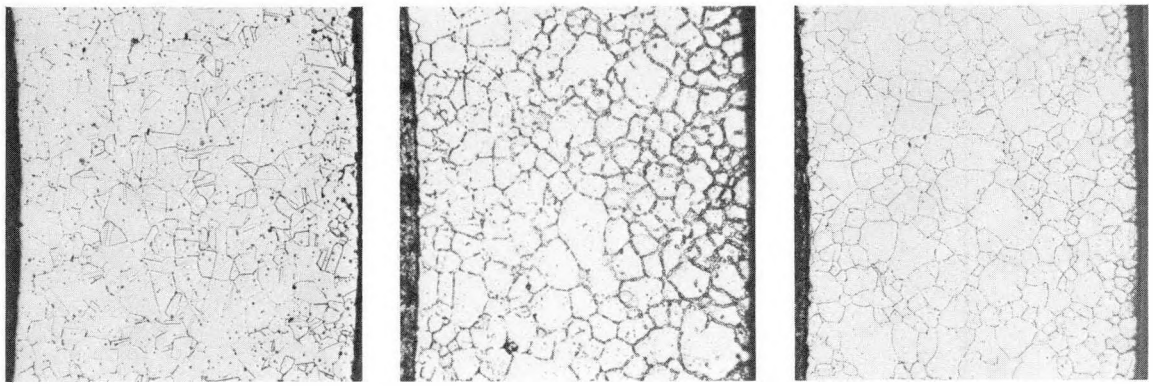

Fig. B.35. Typical Cross Sections of Cladding at (left to right) 1/2, 8, and 14 in. above Bottom of Fuel in Element E-28, Subassembly C-2234S; ~4 at. % Burnup. There is no evidence of an interaction band in the cladding. Electroetched. Mag. 150X. HFEF Neg. Nos. 38D2-5, 38D3-5, and 38D4-4.

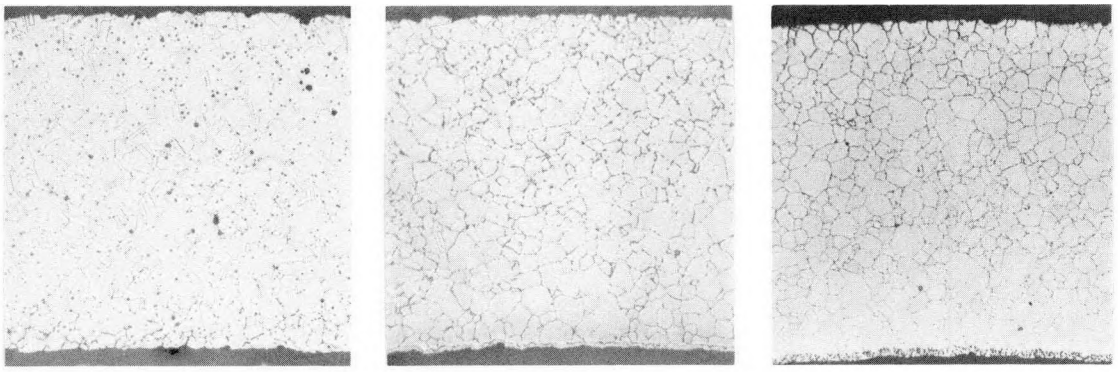

Fig. B.36. Typical Cross Sections of Cladding at (left to right) 1/2, 8, and 14 in. above Bottom of Fuel in Element E-64, Subassembly C-2234S; ~4 at. % Burnup. Interaction band at ID of cladding is obvious in two micrographs at right. Electroetched. Mag. 150X. HFEF Met. Lab. Neg. Nos. 44D2-3, 44D3-2, and 44D4-2.

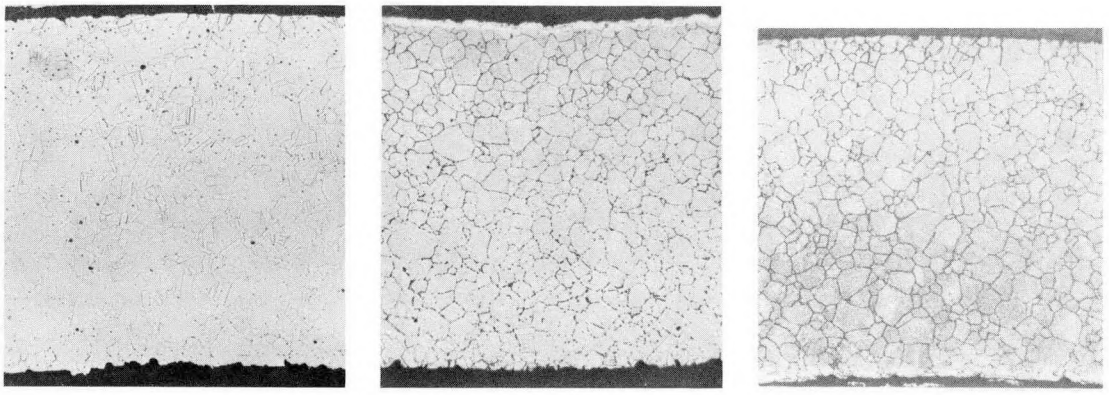

Fig. B.37. Typical Cross Sections of Cladding at (left to right) 1/2, 8, and 14 in. above Bottom of Fuel in Element E-74, Subassembly C-2234S; ~4 at. % Burnup. Interaction band in cladding is obvious in two micrographs at right. Electroetched. Mag. 150X. HFEF Met. Lab. Neg. Nos. 45D2-3, 45D3-2, and 45D4-2.

4. Subassembly C-2236S; ~6 at. % Burnup

Element E-18--Type 316 Stainless Steel Cladding
Element E-24--Type 304L Stainless Steel Cladding

Fig. B.38. Cross Section of Element E-18, Subassembly C-2236S: 1 in. from Bottom of Fuel; ~6 at. % Burnup. As polished. Mag. 15X. Neg. No. MSD-163602.

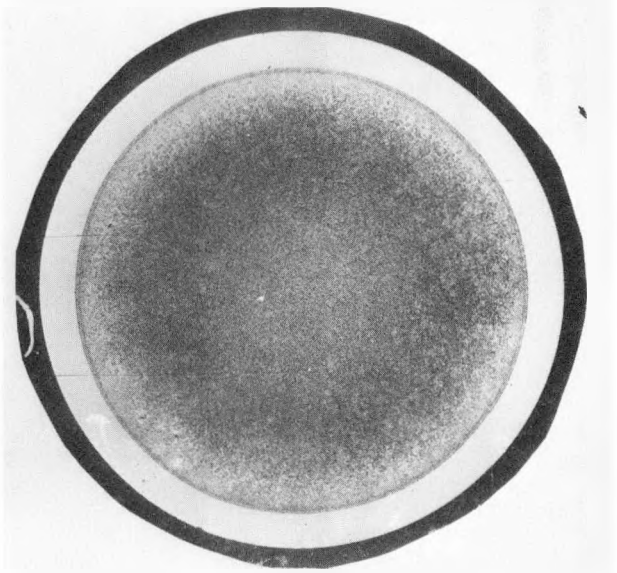

Fig. B.39. Cross Section of Element E-18, Subassembly C-2236S: 7 in. from Bottom of Fuel; ~6 at. % Burnup. As polished. Mag. 15X. Neg. No. MSD-163603.

Fig. B.40

Cross Section of Element E-18, Subassembly C-2236S: 14 in. from Bottom of Fuel; ~6 at. % Burnup. As polished. Mag. 15X. Neg. No. MSD-163604.

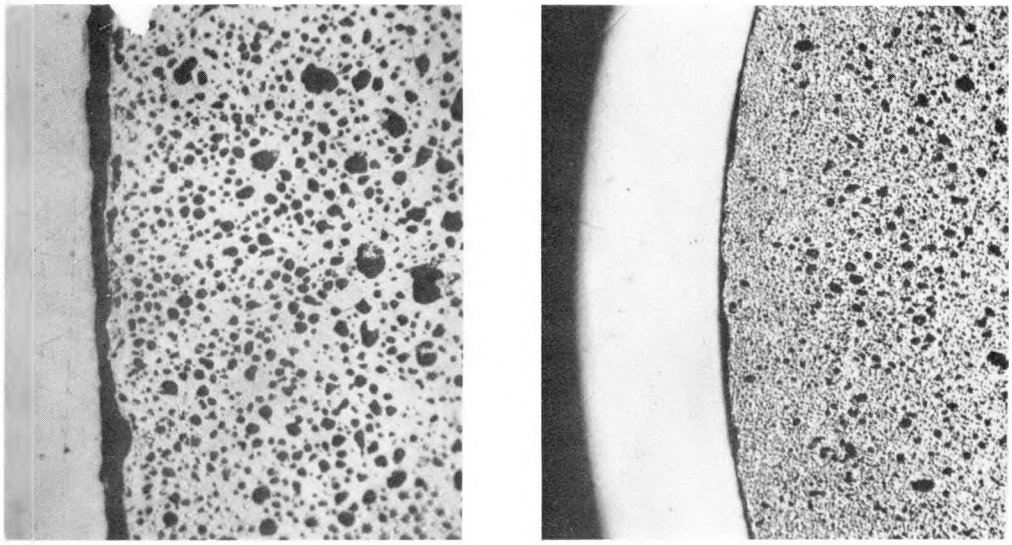

350X 70X

Fig. B.41. Microstructure at OD of Fuel in Element E-18, Subassembly C-2236S: 1 in. from Bottom of Fuel; ~6 at. % Burnup. As polished.

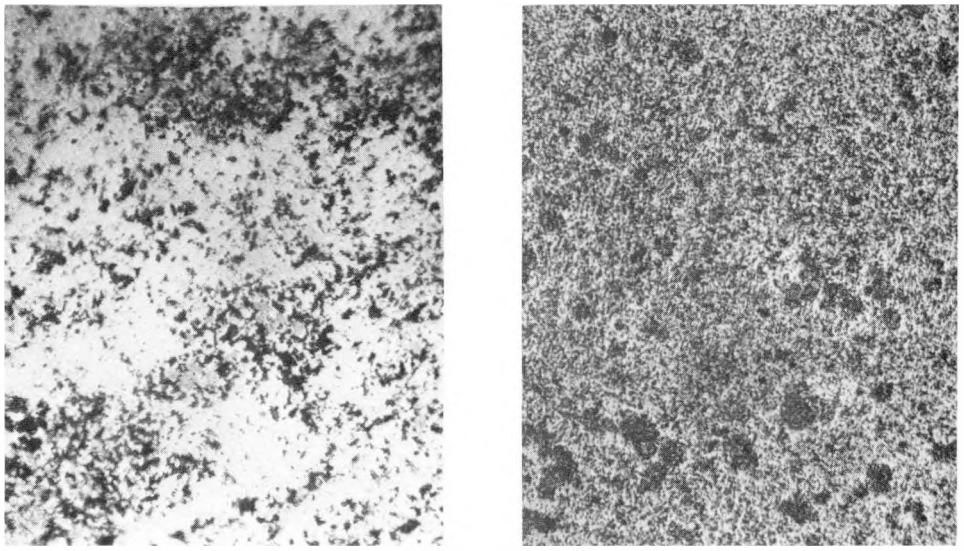

350X 70X

Fig. B.42. Microstructure at Center of Fuel in Element E-18, Subassembly C-2236S: 1 in. from Bottom of Fuel; ~6 at. % Burnup. As polished.

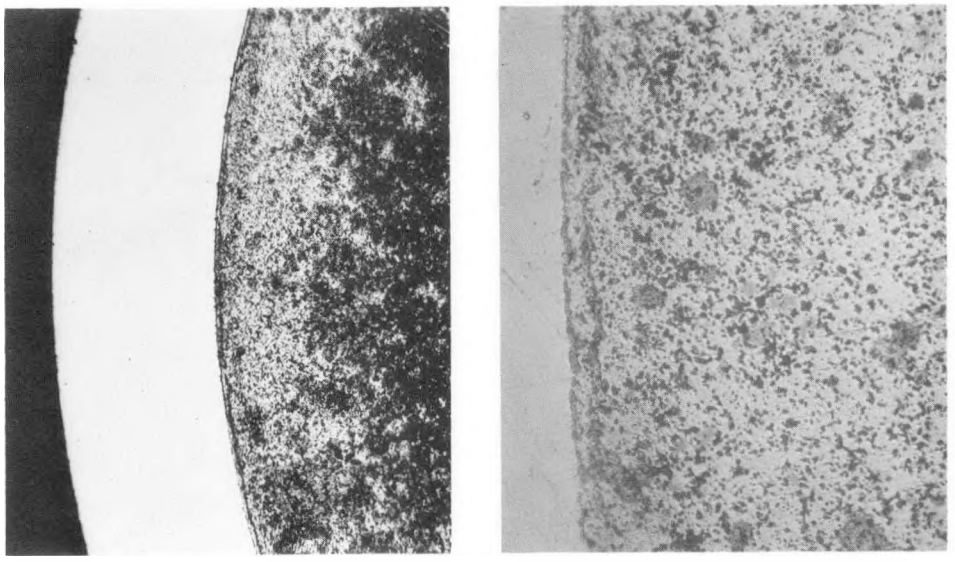

70X 350X

Fig. B.43. Microstructure at OD of Fuel in Element E-18, Subassembly C-2236S: 7 in. from Bottom of Fuel; ~6 at. % Burnup. As polished.

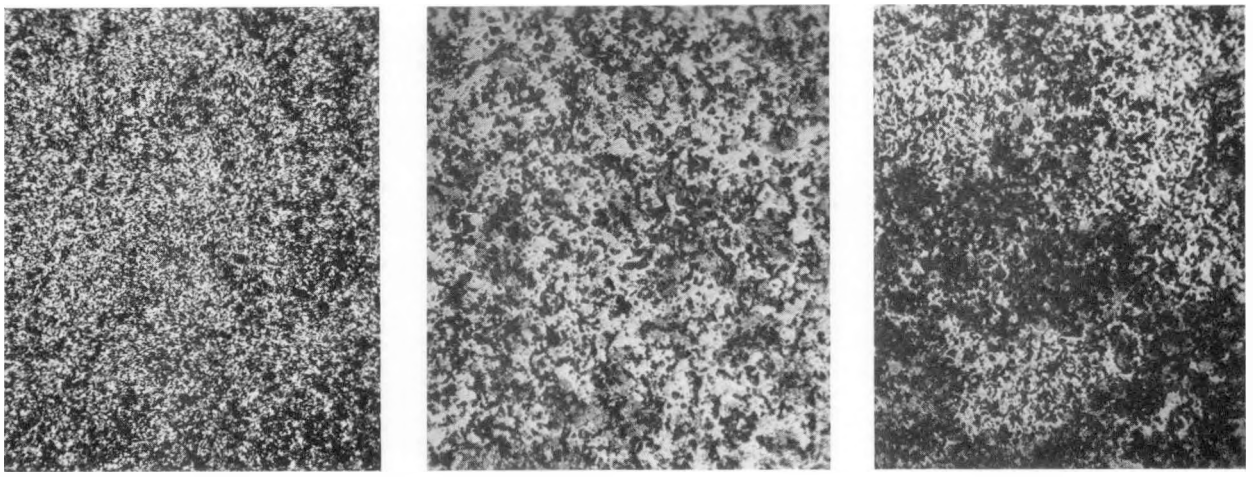

60X 300X 300X

Fig. B.44. Microstructure at Center of Fuel (two left micrographs) and at Half the Fuel Radius in Element E-18, Subassembly C-2236S: 7 in. from Bottom of Fuel; ~6 at. % Burnup. As polished.

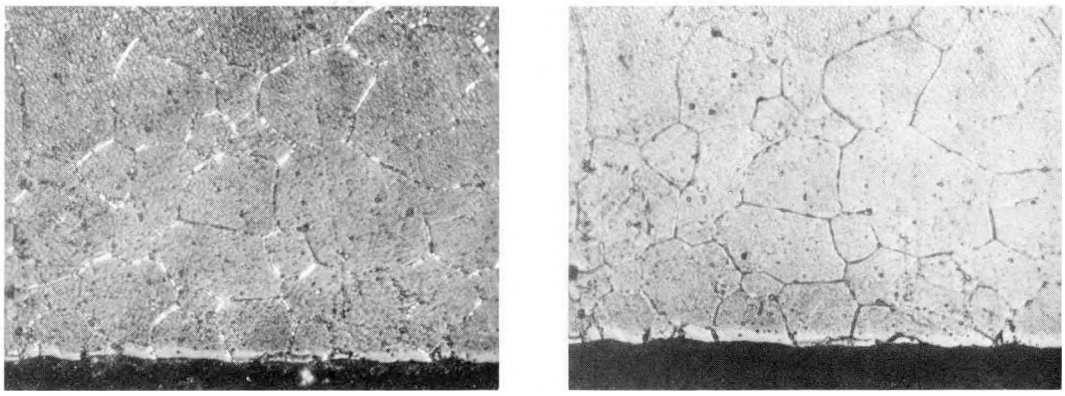

POLARIZED LIGHT BRIGHT FIELD

Fig. B.45. Micrographs at Cladding ID of Element E-18, Subassembly C-2236S: 7 in. from Bottom of Fuel; ~6 at. % Burnup. Electroetched. Mag. ~480X.

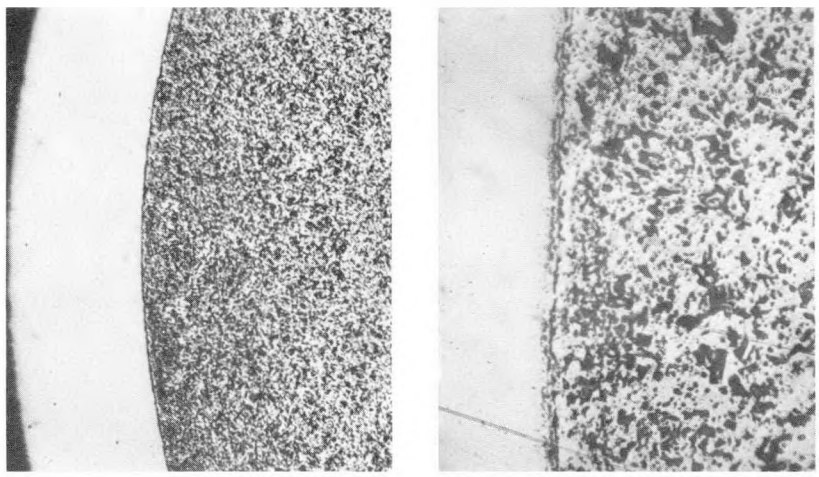

60X 300X

Fig. B.46

Microstructure at OD of Fuel in Element E-18, Subassembly C-2236S: 14 in. from Bottom of Fuel; ~6 at. % Burnup. As polished.

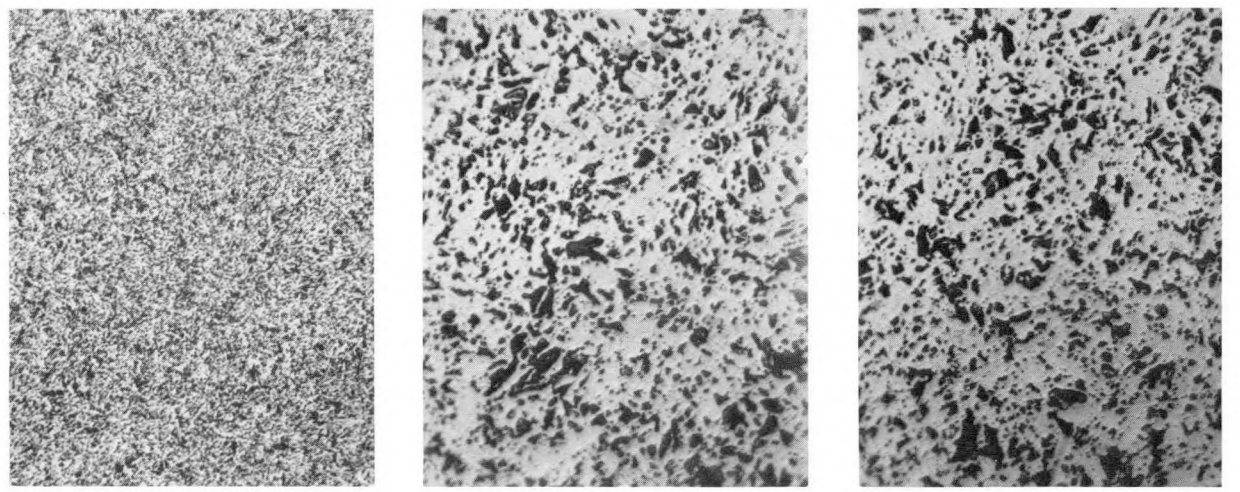

60X 300X 300X

Fig. B.47. Microstructure at Center of Fuel (two left micrographs) and at Half the Fuel Radius in Element E-18, Subassembly C-2236S: 14 in. from Bottom of Fuel; ~6 at. % Burnup. As polished.

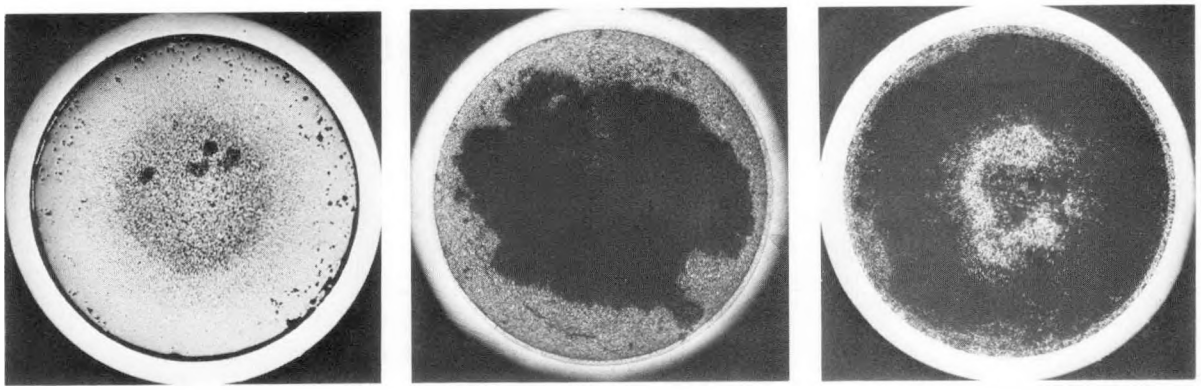

Fig. B.48. Cross Sections at (left to right) Bottom, Midplane, and Top of Element E-24, Subassembly C-2236S; ~6 at. % Burnup. Large darkened areas are caused by sodium residue on specimen surface. As polished. Mag. 13X.

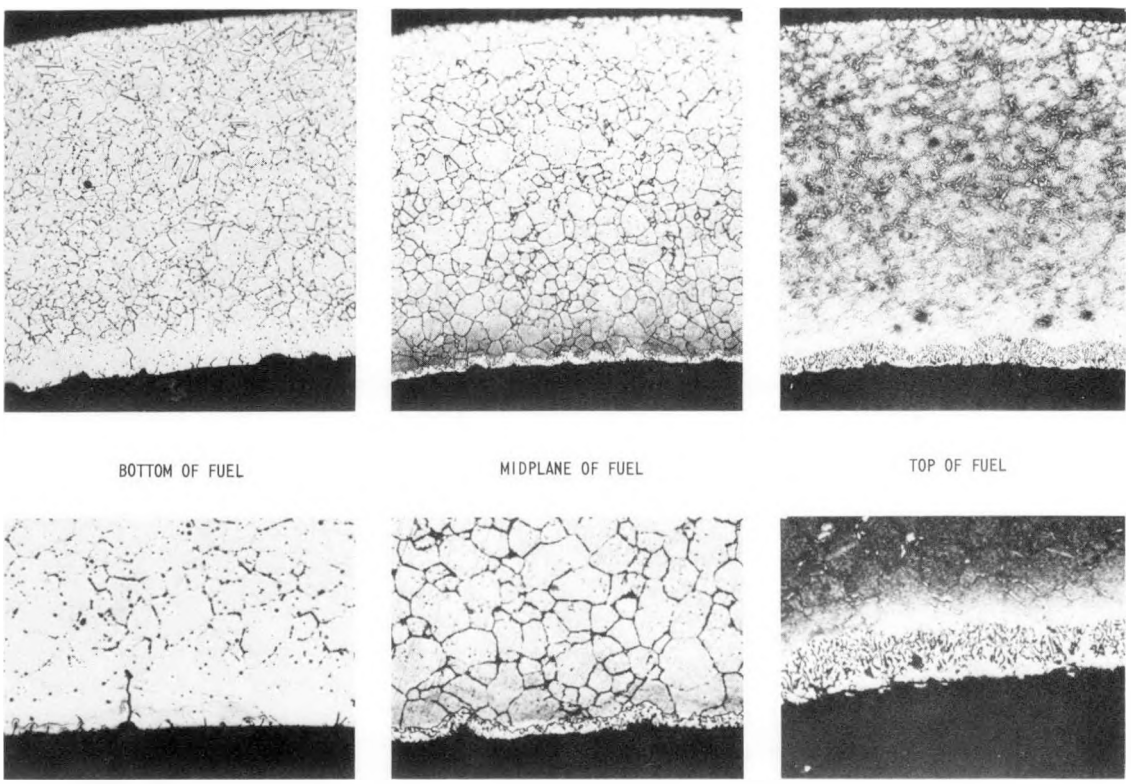

Fig. B.49. Microstructure of Cladding of Element E-24, Subassembly C-2236S, at Bottom, Midplane, and Top of Fuel; ~6 at. % Burnup. Bottom micrographs are 300X enlargements of cladding ID shown at 150X in top micrographs. Electroetched.

ACKNOWLEDGMENTS

We are grateful for the services of the Analytical Department under E. Ebersole at ANL-West, of the hot-cell personnel under J. P. Bacca and N. J. Grant at ANL-West and L. Neimark at ANL-MSD, of the EBR-II Analysis Department under G. H. Golden, and of the Central Shops at ANL-East.

REFERENCES

1. W. N. Beck, R. J. Fousek, and J. H. Kittel, *The Irradiation Behavior of High Burnup Uranium-Plutonium Alloy Prototype Fuel Elements*, ANL-7388, p. 33 (May 1968).
2. N. Kattchee and W. C. Reynolds, *HECTIC-II, An IBM 7090 FORTRAN Computer Program for Heat Transfer Analysis of Gas or Liquid Cooled Reactor Passages*, IDO-28595 (Dec 1962, revised Dec 1965).
3. J. P. Bacca, M. J. Feldman, and D. E. Mahagin, *EBR-II Driver-Fuel Surveillance*, Trans. Am. Nucl. Soc. *9*(2), 417 (1966).
4. L. C. Walters, G. L. Hofman, and R. H. Rohde, *Texture Studies on EBR-II Mark II Driver Fuel*, Trans. Am. Nucl. Soc. 17, 217 (1973).
5. V. Z. Jankus, *BEMOD, A Code for the Lifetime of Metallic Fuel Elements*, ANL-7586 (July 1969).
6. T. B. Fowler and D. R. Vondy, *Nuclear Core Analysis Code: CITATION*, ORNL-Tm-2496, Rev. 2 (July 1971).
7. W. E. Ruther, ANL, personal communication (Mar 29, 1974).
8. W. K. Appleby, *Evaluation of Cladding Alloy Swelling at High Fluences*, GEAP-13737 (Feb 1972).
9. T. T. Claudson et al., *The Effects of Fast Flux Irradiation on the Mechanical Properties and Dimensional Stability of Stainless Steel*, Nucl. Appl. and Tech. *9*(1), 10 (July 1970).
10. J. E. Flinn and G. L. Hofman, *Swelling Behavior of Type 304L Stainless Steel EBR-II Driver Fuel Capsules, Part I* (to be published as ANL topical report).
11. C. M. Walter, *Interdiffusion between U-5 w/o Fissium Alloy and Type 304 Stainless Steel*, ANL-6816 (Mar 1964).
12. S. T. Zegler, H. V. Rhude, Jr., and J. A. Lahti, *Compatibility of Uranium 5 w/o Fissium Alloy with Types 304L and 316 Stainless Steel*, ANL-7596 (Sept 1969).
13. C. M. Walter and L. R. Kelman, *The Interaction of Iron with Molten Uranium*, J. Nucl. Mater. *20*, 314 (1966).